EXPLORATION OF ROOM TEMPERATURE IONIC LIQUIDS AS MEDIA FOR STUDYING PHOTOPHYSICAL PROCESSES

A Thesis
Submitted for the Degree of

DOCTOR OF PHILOSOPHY

by

Aniruddha Paul

School of Chemistry
University of Hyderabad
Hyderabad 500 046
INDIA

March 2008

To
My parents

STATEMENT

I hereby declare that the matter embodied in the thesis entitled "***Exploration of Room Temperature Ionic Liquids as Media for Studying Photophysical Processes***" is the result of investigations carried out by me in the School of Chemistry, University of Hyderabad, Hyderabad, India under the supervision of **Prof. Anunay Samanta**.

In keeping with the general practice of reporting scientific investigations, due acknowledgements have been made wherever the work described is based on the findings of other investigators. Any omission or error that might have crept in is regretted.

March 2008 **Aniruddha Paul**

SCHOOL OF CHEMISTRY
UNIVERSITY OF HYDERABAD
HYDERABAD-500 046, INDIA

Phone: +91-40-2313 4813 (O)
+91-40-2313 0715 (R)
Fax: +91 40 2550 1532
Email: assc@uohyd.ernet.in
anunay_s@yahoo.com

Anunay Samanta, F.A.Sc., F.N.A.Sc.
Professor

CERTIFICATE

Certified that the work embodied in the thesis entitled ***"Exploration of Room Temperature Ionic Liquids as Media for Studying Photophysical Processes"*** has been carried out by **Mr. Aniruddha Paul** under my supervision and that the same has not been submitted elsewhere for any degree.

Anunay Samanta
(Thesis Supervisor)

Dean
School of Chemistry
University of Hyderabad

Acknowledgement

I express my sincere gratitude to Prof. Anunay Samanta, my research supervisor, for his constant cooperation, encouragement and kind guidance. He has been quite helpful to me in both academic and personal fronts.

I would like to thank the former and present Dean, School of Chemistry, for their constant inspiration and for the available facilities. I am extremely thankful individually to all the faculty members of the school for their kind help and cooperation at various stages of my stay in the campus. I am also grateful to all my former teachers for their help.

I value my association with my former lab-mates: Sankaran, Rana, Sandip, Tamal and Prasun from whom I have learned many valuable aspects of research. I am extremely thankful to Moloy for not only helping me academically but also in other quarters. I acknowledge my junior friends, Bhaswati, Ravi, Dinesh and Santhosh for maintaining the friendly and cooperative atmosphere in the lab. I am really lucky to have them as my juniors.

I also thank all non-teaching staff for their timely help, Mr. Shetty in particular.

I am thankful to all my colleagues in the school of chemistry for helping me with various things.

I would also like express my sincere thank to all my big brothers-Satyada, Dinuda, Binoyda and Rahulda. I am also thankful to my near and dear dadas, that include Archan, Abhik, Subhash, Manab, Suni, Sandy, Moloy, Saikat, Bishu and Masum, with whom I have shared many unforgettable moments in this campus and who were never really like 'dada' to me.

I am really lucky for my close association with 'the gang' of HCU Bongs which include Pradip, Sandip, Tanmoy, Arindam, Tapta, Abhijit, Prashant, Ghana, Utpal, Ghanta, Pati, Susruto, Rishi, Dinesh and so many others. Without their cheerful company, the campus life

would have been a trifle easier but a lot boring and even worn-out. I am also thankful to Tejender, Balaraman, Bipul, Sanjib, Ranjit, Naba, Tridib, Palash, Rakesh, Arun, Murli, Jagadish, Jaichander for their help and cooperation. I must not forget Shatabdi di, Rumpa, Anindita, Suparna, Tulika, Vasudhara, Joya, Sriparna di and so many others for various reasons.

I am also grateful for the valuable friendship of Bappai, Mintu, Laltu, Kaku, Bapi, Samrat who are still my buddies. I value the association of Sumanta, Rahul, Biplab, Rimi, and many other old-day friends with best regards. Finally, I must acknowledge my two 'Scottish Musketeers', Shahed and Surajit, for the valued friendship they offered and still maintained.

Without my parents' and sister's relentless support and love I would have not reached at this stage of life. I owe everything to them.

Financial assistance from CSIR, New Delhi is greatly acknowledged.

.

Aniruddha

List of Publications

1. "How transparent are the imidazolium ionic liquids? A case study with 1-methyl-3-butylimidazolium hexafluorophosphate, [bmim][PF_6]." **A. Paul**, P. K. Mandal and A. Samanta *Chem. Phys. Lett.* **2005**, 402, 375-379.
2. "On the optical properties of the imidazolium ionic liquids." **A. Paul**, P. K. Mandal and A. Samanta *J. Phys. Chem. B* **2005,** 109, 9148-9153.
3. "Fluorescence studies in environmentally benign solvents: Solvation dynamics of Coumarin 102 in [bmim][BF_4]." P. K. Mandal, **A. Paul** and A. Samanta *Res. Chem. Intermed.* **2005**, 31, 575-583.
4. "N-Butyl-4-butylamino-1,8-naphthalimide." S. Banthia and **A. Paul** *Acta Cryst. E.* **2005**, E61, o3474-o3475.
5. "Excitation wavelength dependent fluorescence behavior of the room temperature ionic liquids and dissolved dipolar solutes." P. K. Mandal, **A. Paul** and A. Samanta *J. Photochem. Photobiol. A: Chemistry* **2006**, 182, 113-120.
6. "Optical Absorption and Fluorescence Studies on Imidazolium Ionic Liquids Comprising the bis(trifluoromethanesulphonyl)imide anion." **A. Paul** and A. Samanta *J. Chem. Sci.* **2006**, 118, 335-340.
7. "Photoinduced Electron Transfer Reaction in Room Temperature Ionic Liquids: A Combined Laser Flash Photolysis and Fluorescence Study." **A. Paul** and A. Samanta *J. Phys. Chem. B* **2007**, 111, 1957-1962.
8. "Solute Rotation and Solvation Dynamics in an Alcohol-Functionalized Room Temperature Ionic Liquid." **A. Paul** and A. Samanta *J. Phys. Chem. B* **2007**, 111, 4724-4731.

9. "Effect of Nonpolar Solvents on the Solute Rotation and Solvation Dynamics in an Imidazolium Ionic Liquid." **A. Paul** and A. Samanta *J. Phys. Chem. B* **2008**, 112, 947-953.
10. "Interaction of the Major Protein from Bovine Seminal Plasma, PDC-109 with Phospholipid Membranes and Soluble Ligands Investigated by Fluorescence Approaches." V. Anbazhagan, R. S. Damai, **A. Paul** and M. J. Swamy *Biochim. Biophys. Acta* **2008** (In Press).
11. "Photophysical Behavior of a Microviscosity Probe in Room Temperature Ionic Liquids." **A. Paul** and A. Samanta (in preparation).

Conference presentations

1. An Unusual Excitation Wavelength Dependent Fluorescence of Imidazolium Ionic Liquids. **Aniruddha Paul**, P. K. Mandal, A. Samanta. – 7th National Symposium in Chemistry, 2005, organized by CRSI, IACS, Jadavpur, Kolkata, India, Feb. 2005 (Poster Presentation).
2. Photoinduced Electron Transfer Reaction in Room Temperature Ionic Liquids: A Combined Laser Flash Photolysis and Fluorescence Study. **Aniruddha Paul**, Anunay Samanta. – National Symposium on Radiation and Photochemistry, 2007, organized by BARC, NSUFP, Chennai, India, Jan. 2007 (Poster Presentation).
3. Influence of Hydrogen Bonding on the Solvation Dynamics in a Room Temperature Ionic Liquid: Realization of the Local Effect. **Aniruddha Paul**, Anunay Samanta. – 4th Annual In-house Symposium of School of Chemistry, ChemFest 2007, organized by School of Chemistry, University of Hyderabad, Hyderabad, India, Mar. 2007 (Oral Presentation).

Thesis Layout

The thesis has been divided into eight chapters. ***Chapter 1*** provides a brief introduction on room temperature ionic liquids (RTILs), the fundamentals of photoinduced electron transfer (PET) reaction, solvation dynamics study in various media including RTILs and a short note on microviscosity measurement of various organized assemblies using fluorescence techniques. Motivation behind the present work has also been briefly discussed. ***Chapter 2*** provides the details of the experimental procedures and methodologies adopted in this investigation. The instrumental details and methods for different calculations have also been discussed in this chapter**.** ***Chapter 3*** describes the investigation on the optical properties of some imidazolium ionic liquids. ***Chapter 4*** deals with the study of a PET reaction between pyrene and N,N-dimethylaniline in different RTILs. ***Chapter 5*** presents the rotational and solvation dynamics study of some dipolar probes in an alcohol-functionalized RTIL based on imidazolium moiety. ***Chapter 6*** describes the rotational and solvation dynamics study in the mixtures of an RTIL with the nonpolar solvents. ***Chapter 7*** delineates the photophysical behavior of a 'molecular rotor' probe in RTILs of varying viscosity with an emphasis on the relationship between bulk and microviscosity of the media. ***Chapter 8*** summarizes the findings of the present investigations by touching upon the achievements and looking into the future scope and upcoming challenges.

Chapter 1

Introduction

This chapter provides a brief introduction of room temperature ionic liquids (RTILs), highlighting their crucial physical and chemical properties, structural features and versatile applications. Fundamentals of intermolecular photoinduced electron transfer process, focusing mainly on the physical aspects, have been outlined in this chapter. The molecular basis of dynamic Stokes shift and salient features of solvation dynamics in various media, with an emphasis on the studies carried out in RTILs, have also been discussed in this chapter. The basic methods for microviscosity measurements exploiting the fluorescence behavior of suitable probe molecules have been briefly introduced. The chapter is concluded by describing the motivation of the thesis and introducing the systems studied in this work.

1.1. Room temperature ionic liquids

In the recent years, a significant effort has been directed towards the design and development of environmentally benign media to substitute the traditional solvents, most of which are volatile organic compounds (VOCs), usually employed for laboratory and industrial purposes. These VOCs are major source for environmental pollution, especially when employed in bulk scale for industrial purposes. Therefore, the quest for ***green chemistry***[1] has began and this has led to the realization of the importance of a number of alternatives, such as, solvent-free synthesis,[2] use of water as a solvent,[3] use of supercritical carbon dioxide[4] and ionic liquids as the reaction media.[5-16] The ionic liquids have been invoked as

environmentally benign solvents due to a number of suitable properties, but mainly because of their *negligible vapor pressure*, which prevents air and water pollution through emission of VOCs.

The ionic liquids are simply low melting organic salts, composed entirely of ions (i.e., cation and anion). The term '***ionic liquid***' has replaced the older phrase 'molten salt' as the latter suggests a high-temperature, highly corrosive, overtly viscous media, cf. NaCl at and above its melting point 803°C.[6] In the academic literature, the term '***ionic liquid***' usually refers to liquids composed entirely of ions that are fluid at around or below 100°C.[5] However, ***room temperature ionic liquids*** (RTILs) are the class of ionic liquids which are free-flowing liquid at ambient temperature (*ca*. 20-30°C) and pressure (1 bar), usually having melting point near 0°C or less. The lowest melting point for RTILs reported so far is as low as −96°C.[7]

RTILs are not new; ethyl ammonium nitrate, which is liquid at room temperature, was first described in 1914.[8] The modern chemistry of RTILs was introduced in the early 1980s by the use of the salts based on chloroaluminate anions ($AlCl_4^-$ or $Al_2Cl_7^-$) by Wilkes and his co-workers.[9] However, as these salts were extremely hygroscopic and highly reactive towards water their use was quite limited. So, they were soon replaced by air and water stable RTILs based on less reactive anions such as BF_4^-, PF_6^-, $CF_3CO_2^-$, $CH_3CO_2^-$, $CF_3SO_3^-$, $(CF_3SO_2)_2N^-$ etc.[10] The research employing the ionic liquids as reaction media received a boost in 1992 after the invention of air and water stable ionic liquids based on 1-ethyl-3-methylimidazolium cation and tetrafluoroborate anion, abbv. [emim][BF_4].[11] In subsequent years, RTILs based on a number of cationic moieties like (a)

imidazolium, (b) pyridinium, (c) pyrrolidinium, (d) ammonium, (e) phosphonium etc (Chart 1.1) have been synthesized.[12,13] Recently, even RTILs based on natural amino acids have been prepared.[14] Since these basic cationic moieties can be functionalized in numerous ways and anions can be introduced through metathetic exchange, a large number of RTILs can be synthesized with the desired physical and chemical properties. Most common RTILs are based on unsymmetrically substituted imidazolium cations and BF_4^-, PF_6^-, $(CF_3SO_2)_2N^-$ (commonly known as Tf_2N^-) anions, though alkylsulfate[15] and dicyanimde[16] anions are also becoming popular.

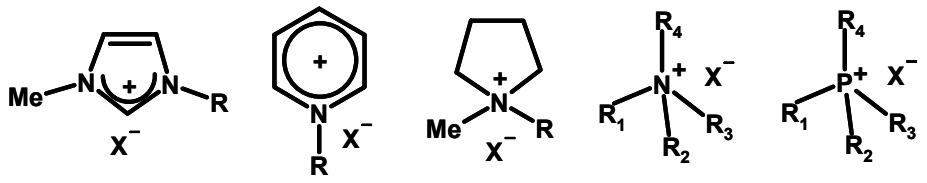

(a) (b) (c) (d) (e)

X = BF_4, PF_6, $EtSO_4$, $(CF_3SO_2)_2N$; R = alkyl group

Chart 1.1. Basic structure of some RTILs based on different cationic moieties.

1.1.1. Properties of room temperature ionic liquids

Though nonvolatility (negligible vapor pressure) is the main reason for the choice of RTILs as alternative media, there are a number of useful properties of these substances that make them suitable for diverse application. Among them, wide liquidus, high thermal and chemical stability, moderate to high polarity, high viscosity, non-toxicity and non-flammable nature etc are noteworthy. Moreover,

RTILs can dissolve a large variety of organic/inorganic substances and possess high electrical conductivity and wide electrochemical window.[17] Since the properties of ionic liquids are largely dependent on the constituent ions, it is possible to obtain a RTIL with desired properties by proper choice of the two ionic components, and thus, they are considered as "designer solvent".[18]

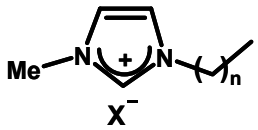

n =	1	3	5
X = BF_4,	[emim][BF_4]	[bmim][BF_4]	[hmim][BF_4]
= PF_6,		[bmim][PF_6]	[hmim][PF_6]
= $(CF_3SO_2)_2N$,	[emim][Tf_2N]	[bmim][Tf_2N]	
= $EtSO_4$,	[emim][$EtSO_4$]	[bmim][$EtSO_4$]	

Chart 1.2. Structure and abbreviation of some common imidazolium RTILs.

Melting Point: Most RTILs have melting point much below the room temperature (25°C). However, in many RTILs the exact melting point is difficult to determine as they undergo considerable supercooling, which implies that the temperature of phase change may differ considerably depending on whether the sample is heated or cooled.[19] Whence some correlation has been found in terms of the influence of cations, especially for those based on imidazolium salts,[19] the anion effect remains quite uncertain. It has been established that the melting point decreases with increasing size and asymmetry of the cation and increases with increasing branching in the alkyl chain.[20] The effect of hydrogen bonding and delocalization of charge has been invoked to explain the influence of anion, but only a rough

correlation can be drawn.[19] For example, low charge density and lack of hydrogen bonding interaction is the main reason for lower melting point of Tf_2N^- salts, whereas more spherical anions like BF_4^-, PF_6^- with potential hydrogen bonding ability result in higher melting point.

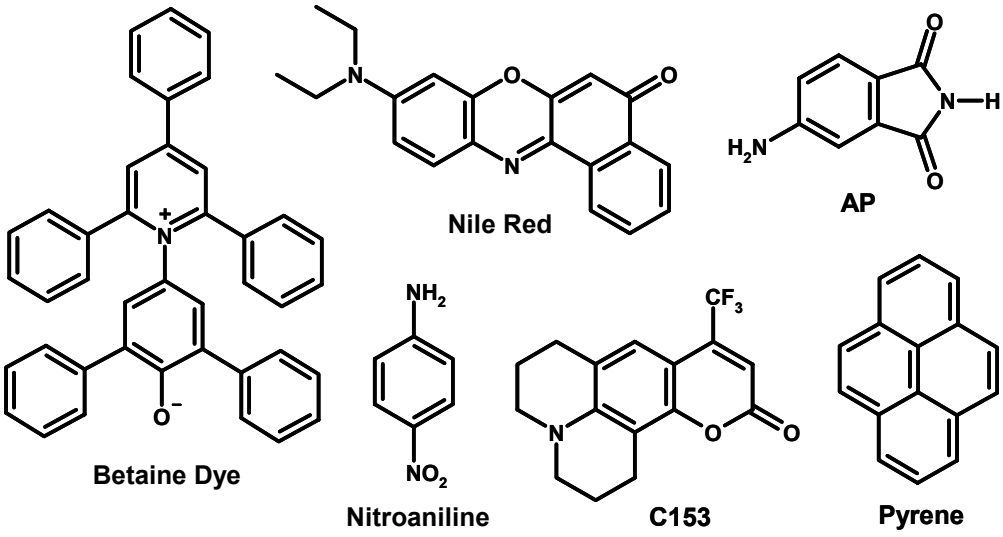

Chart 1.3. Structure of some probe molecules used for determination of polarity of RTILs.

Polarity: The microscopic polarity of the RTILs has been determined by using a number of solvatochromic probes and different polarity parameters.[21-27] The $E_T(30)$ or E_T^N values for most of the common RTILs have been determined.[23,24] Other polarity parameters like Kamlet-Taft parameters[25] and multiple polarity parameters[26] have also been employed to review the polarity criteria of RTILs. Most of these studies indicate that polarity of common RTILs (i.e., those having alkyl side-chains) is greater than acetonitrile but less than methanol. $E_T(30)$ values

indicate that these RTILs are as polar as short-chain alcohols (cf. butanol). However, recent measurement of static dielectric constant (ε) of a few RTILs indicates that RTILs have very low dielectric constant (in the range of 9-13) which is similar to that of pyridine (ε = 12.3).[27] The reason for such large difference in the polarity estimates of the RTILs is unclear at this moment.

Viscosity and Density: Viscosity of the RTILs is much higher compared to normal solvents like water or alcohols. Even the least viscous RTIL is ~30 times viscous than water and follow Newtonian-fluid behavior.[19] Generally, RTIL viscosity is sensitive to moisture content and impurities like chloride etc salts.[7,28] Often non-Arrhenius behavior is apparent in the temperature dependence of viscosity,[19,29] especially when measured for a long temperature-range.[29] Examining various anion-cation combinations, the increase in viscosity observed on changing selectively the anion or cation has been primarily attributed to an increase in the van der Waals forces.[30] Hydrogen bonding is always an important parameter and the effect is distinct in the case of alcohol-functionalized RTILs, which are found to be more viscous than their alkyl counterparts.[31] The symmetry of the anion contributes as an additional parameter. Considering the symmetry and hydrogen bonding parameters, the following order of viscosity decrease can be realized: $Cl^- > PF_6^- > BF_4^- > Tf_2N^-$.[20]

The density of RTILs is also much higher than that of the conventional molecular solvents and the density tends to decrease with increasing anionic volume.[20,30] It is also highly dependent on the molar mass of anions.[32]

Conductivity: The electrical conductivities of RTILs are similar to those of organic solvents with added inorganic electrolytes. The conductivity generally

decreases in the following order: 1-alkyl-3-methylimidazolium > N,N-dialkylpyrrolydinium > tetraalkylammonium.[17] This order has been attributed to the decrease in planarity of the cationic component. Among same cationic series with different anions, the conductivity values do not to change much.[33] The heat conductivities of the RTILs are also very high. Thus the RTILs permit a very rapid dispersal of the heat of reaction.[19]

Other properties: RTILs usually show high thermal stability, say upto 400°C, though prolonged heating at comparatively lower temperatures, say 200°C, may lead to appreciable thermal degradation. It has been shown that the stability dependence is PF_6^- > Tf_2N^- ~ BF_4^- > halides,[34] and the cation size does not have much effect.[19] Due to extremely low vapor pressure the RTILs cannot be distilled in normal condition. But, recently the distillation of some RTILs has been achieved at low pressure.[35] Analysis of the vapor by mass spectroscopic method has shown the existence of neutral ion pairs in vapor state.[35b]

Depending upon the miscibility of RTILs with water they are classified as hydrophobic or hydrophilic. The anion has a dominant role in controlling this property. The PF_6^-, Tf_2N^- etc salts are hydrophobic, while halides, BF_4^-, alkylsulfates are mostly hydrophilic.[19] However, increasing alkyl chain length reduces water solubility, while polar side-chains (those with OH, NH_2) enhance the same. Generally hydrophobic RTILs show more nonpolar behavior in terms of solubility and are readily miscible with the weakly polar organic solvents. However, the solubility of RTILs in aliphatic hydrocarbons is scarce.

1.1.2. Structural features and heterogeneity

Structural features of the ionic liquids have been investigated in the solid state (mainly by crystallography) as well as in the liquid state using various techniques. Even the crystal structure of some RTILs has been determined by in situ crystallization at low temperatures.[36] For imidazolium-based ionic liquids, extensive cation-anion hydrogen bonding network is revealed in the crystal structures, but for the liquid salts presence of such interaction is still not clear.[11,37] Though the hydrogen bonding interaction in some BF_4^- salts[38,39] and its absence in Tf_2N^- salts are revealed in liquid state,[40] the case of the PF_6^- salts is doubtful.[38] Again, some IR studies have revealed that the C–H---X hydrogen bonding remains intact in the liquid state in many cases.[39,41,42]

Many simulation studies have been carried out to obtain an insight into the liquid structure of the RTILs. Molecular dynamics simulations using both atomistic and coarse-grained methods demonstrated the interaction between hydrophobic alkyl tails on the cations, providing local liquid structures reminiscent of membranes and worm-like micelles.[43,44] The heterogeneity in the liquid structure of RTILs and the presence of '*local structure*' have been indicated in many studies. While some experimental studies have indirectly indicated the heterogeneity or local structures,[45,46] recent X-ray diffraction[47] and Raman scattering[48] studies have shown the evidence of nanoscale ordering and mesoscopic local structure. Using experimental tools like neutron scattering,[49] XAFS,[50] optical Kerr effect[51] etc many aspects of the nanoscale local structure of the RTILs have been revealed. The presence of cation-cation, cation-anion local association has been conclusively shown by NOE and ROESY experiments.[39,42,52]

A different variety and level of modeling and simulation studies have also predicted a nanostructured feature of RTILs.[53-55] All simulations confirm a pronounced long-range charge order in RTILs.

1.1.3. RTILs in mixed solvents

The scope of applications of the RTILs is broadened by addition of conventional solvents as this allows fine-tuning of the solvent properties of RTILs. This is why a growing number of researches focus on the study of the physicochemical properties of mixtures of RTIL and conventional molecular solvent. It is found that the addition of a cosolvent significantly changes a number of physical properties of the RTILs such as the viscosity,[7,28,56] polarity,[57-59] solvation[58,59] and electrochemical[60,61] behavior. In case of some RTILs, even traces of water or moisture drastically reduce the viscosity.[28] The microscopic polarity parameters of binary and ternary RTIL-molecular solvent mixtures, measured from the solvatochromic behavior of various probe molecules,[57,58] indicate that these molecules are preferentially solvated within the RTIL core in most RTIL-cosolvent mixtures. However, highly polar and protic cosolvent can also enrich the cybotactic region of the probe.[58] Electrochemical studies in RTIL-cosolvent mixtures have addressed the influence of added solvents on the ionic association/dissociation phenomenon.[60,61] It has been shown that the organic solvents with low dielectric constants promote ionic association in RTILs. However, solvents having high dielectric constants and strong hydrogen bonding ability (such as water) effectively promote dissociation.[61]

1.1.4. Application of RTILs

The early usage of RTILs was mostly confined to their role as alternative solvent system for a large number of organic and inorganic synthesis,[12,62-64] catalysis,[6,10] electrochemical[17,65] and separation processes.[66] In recent days, RTILs are emerging as versatile media with potential applicability ranging from synthesis of nanomaterials[67,68] to development of lunar telescope.[69] The RTILs have also been found to be useful in mass spectroscopy,[70] enzyme stabilization,[73] as biocatalysis,[71] gas sensor,[72] and supporting electrolyte for solar[74] and fuel cells.[75] The biphasic acid scavenging utilizing ionic liquids (BASIL) has even met the industrial requirement.[5]

Because functionalization of the RTILs by covalently tethering a functional group to the cation or anion (or both) imparts a particular capability to the ionic liquids, there is considerable current interest in designing and development of various types of functionalized ionic liquids, categorized as "task-specific" ionic liquids (TSILs).[76,77] These TSILs serve specific purposes such as catalysis, organic synthesis, separation of specific materials, as well as construction of nanostructured materials and ion conductive materials etc.[77]

1.2. Photoinduced electron transfer

Photoinduced electron transfer (PET) reactions play quite an important role in numerous chemical[78] and biological systems.[79] The application of PET ranges from photosensitized catalysis to solar energy conversion.[80] In case of PET, the transfer of an electron occurs between the photoexcited state (singlet or triplet) and ground state molecule to generate a charge transfer species, which may either be an excited state charge transfer complex or a charge separated radical ion

pair.[81] The initial species then may undergo a variety of secondary processes like back electron transfer leading to the ground state of the molecule, ionic dissociation to free, solvent-separated ions, triplet recombination to generate an excited state of one of the reactants, or other charge transfer intermediates and/or stable products (Scheme 1.1).[78,81]

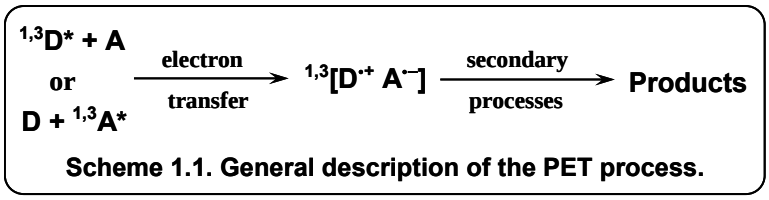

Scheme 1.1. General description of the PET process.

In case of PET reaction involving singlet excited species, the electron transfer leads to quenching of fluorescence and formation of either an exciplex, often a fluorescent species, formed especially in nonpolar solvents, or a charge separated ion pair, usually called geminate or contact ion pair, which is normally realized in polar solvents. These species then undergo a number of secondary reactions and one most common route is shown in Scheme 1.2.[82,83]

The thermodynamic driving force, ΔG_{ET} of the overall PET process, i.e. formation of the solvent separated species from the photoexcited species (see Scheme 1.2), is given by[83,84]

$$\Delta G = E_D^{ox} - E_A^{red} - E_{0,0} - e^2/\varepsilon r_q \qquad (1.1)$$

where, E_D^{ox} and E_A^{red} are the oxidation and reduction potentials of the donor and the acceptor, respectively. $E_{0,0}$ is the energy corresponding to the 0-0 transition of the photoexcited molecule (donor or acceptor) and $e^2/\varepsilon r_q$ is the coulombic energy of interaction of the ion pair at the effective encounter distance of the donor and

acceptor ($r_q = r_d + r_a$). The coulombic energy term depends on solvent polarity and becomes negligible when the solvent is highly polar, cf. acetonitrile.

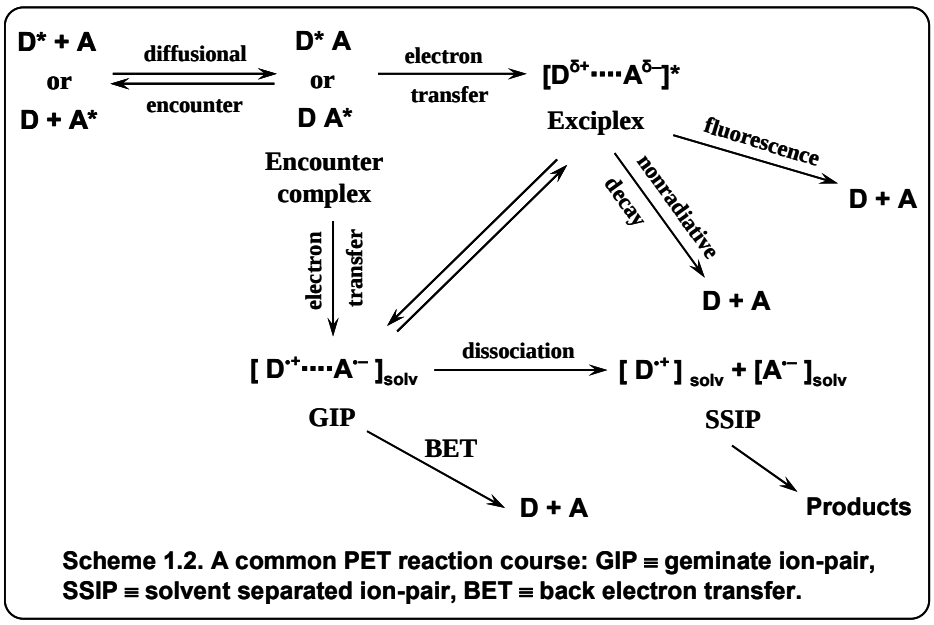

Scheme 1.2. A common PET reaction course: GIP ≡ geminate ion-pair, SSIP ≡ solvent separated ion-pair, BET ≡ back electron transfer.

The exothermicity ($\Delta G_{ET} < 0$) is the primary condition for an efficient PET process and it is shown by Rehm and Weller that the rate of PET process (determined by fluorescence quenching constant, k_q) increases sharply with decrease of ΔG_{ET} and it attains the diffusion controlled limited value (~2×10^{10} M^{-1} s^{-1} in acetonitrile) when $\Delta G_{ET} \leq -10$ kcal (~ –0.43 eV).[84] In this context it is important to note that the Marcus theory of outer sphere electron transfer predicts a bell-shaped free energy dependence of the PET rate constant,[85,86] i.e., when ΔG_{ET} is highly negative, the PET rate constant (k_{ET}) will decrease with decreasing ΔG_{ET}. However, this phenomenon, known as electron transfer in the Marcus

inverted region, is not realized experimentally in case of intermolecular PET reaction, due to the masking effect of the diffusion-controlled quenching process (i.e., $k_q \approx k_{diff}$, where k_{diff} is the diffusion constant).[87,88] Other factors like efficient nuclear tunneling through large free energy barrier,[88] or electron transfer from electronically or vibrationally excited states[84] have also been invoked to explain the lack of an observable inverted region. Nevertheless, evidence of the inverted region has been demonstrated for intramolecular electron transfer between donor-acceptor pairs held by rigid spacer,[89] and in case of back electron transfer (BET) occurring in geminate ion pair (Scheme 1.2).[90,91]

The kinetic criterion of a PET process correlates the free energy of activation for a PET reaction ($\Delta G_{ET}^{\neq}$) with the free energy changes due to nuclear motion and that induced by solvent motion, and thus for uncharged reactants, we have[78,86]

$$\Delta G_{ET}^{\neq} = \frac{\lambda}{4}\left(1+\frac{\Delta G_{ET}}{\lambda}\right)^2 \qquad (1.2)$$

where, $\lambda = \lambda_i + \lambda_0$. λ_i and λ_0 are intrinsic barriers corresponding to bond length changes and solvent reorganization energy, respectively. However, in most electron transfer reactions λ_i is quite small and therefore, solvent reorganization energy (λ_0) becomes the dominant factor. According to Marcus theory, solvent reorganization energy is given by[85,86]

$$\lambda_0 = \frac{e^2}{2}\left(\frac{1}{r_d}+\frac{1}{r_a}-\frac{2}{r}\right)\left(\frac{1}{n^2}-\frac{1}{\varepsilon}\right) \qquad (1.3)$$

where, donor-acceptor distance, r is given by, $r = r_d + r_a$, n and ε represent solvent refractive index and dielectric constant, respectively. Eqn. 1.3 reveals that solvent polarity is the governing factor in determining the barrier of the electron transfer

process. In a subsequent semi-empirical treatment, Rehm and Weller connected the rate constant for electron transfer fluorescence quenching (k_q) with $\Delta G_{ET}^{\neq}$ by the following relationship,[84]

$$k_q = \frac{2\times10^{10}\ M^{-1}\ s^{-1}}{1+0.25[\exp(\Delta G_{ET}^{\neq}/RT)+\exp(\Delta G_{ET}/RT)]} \qquad (1.4)$$

which agrees well with the experiments for PET reactions featured with high negative ΔG_{ET} values.

The PET reaction is monitored using a number of experimental techniques. Since energy transfer mechanism is another dominating pathway of fluorescence quenching, it is often required to distinguish the PET quenching from quenching due to energy transfer. Feasibility of the PET reaction for a particular donor-acceptor pair can be evaluated by calculating ΔG_{ET} using eqn. 1.1. Again energy transfer can be excluded if the energy of acceptor exceeds that of the donor by 3 kcal $mole^{-1}$, as energy transfer then becomes inefficient.[92] But, probably the best evidence of PET and subsequent reaction comes out of the detection of intermediates, like those described in Scheme 1.2. Among the various tools, laser flash photolysis (LFP) detection is most popular as it offers direct determination of the radical ions and other transient species resulted in PET reaction.[81,82,93] Other techniques like ESR or spin trapping,[94] chemically induced nuclear polarization (CIDNP),[95] transient photocurrent measurement,[96] scavenging or trapping the intermediates[97] etc have also been employed to elucidate the PET reaction course.

1.3. Solvation dynamics

Solvation dynamics is generally understood as the reorientation of the solvent dipoles around an instantly created solute dipole originating from photoexcitation. In the fluorescence probe study, the solute refers to the fluorescent molecules which undergoes a significant change in dipole moment due to photoexcitation and becomes strongly polar in the excited state (Chart 1.4). Instantaneous excitation with an ultra-short laser pulse triggers an electronic redistribution in the

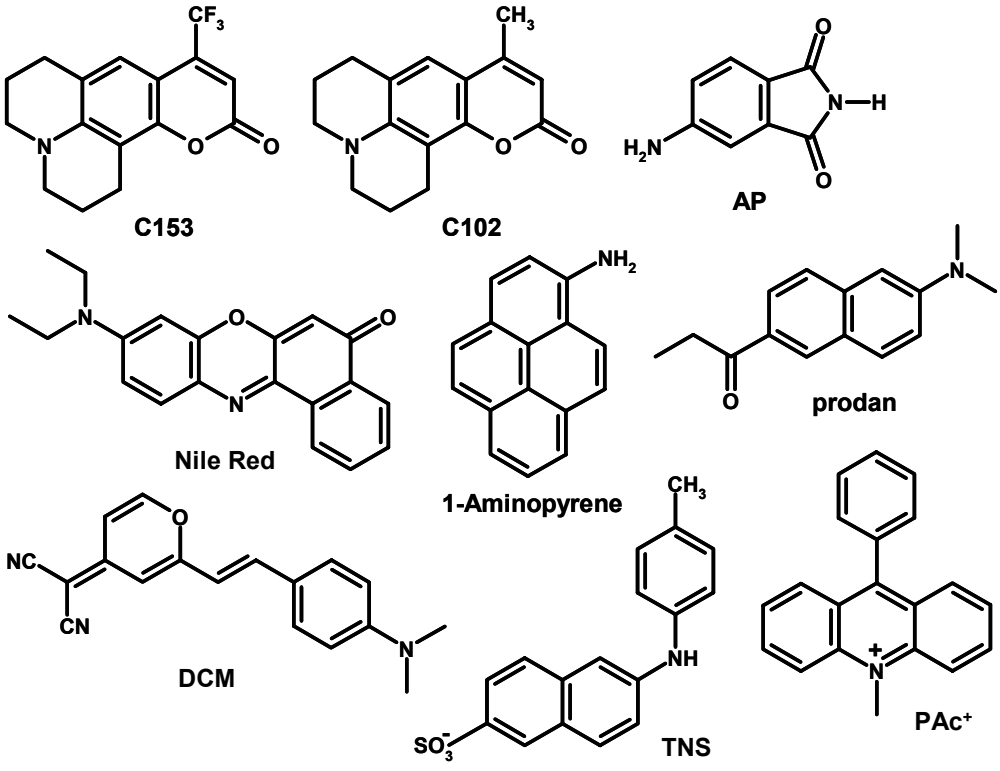

Chart 1.4. Typical fluorescence probe molecules used for the study of solvation dynamics.

probe molecule, thereby creating a strong instantaneous dipole, which in turn, perturbs the equilibrium arrangement of the solvent dipoles surrounding the probe. The solvent molecules then reorient themselves around the newly created dipole in order to attain a further equilibrium and the time required for this rearrangement is known as the relaxation time of the solvent. This solvent relaxation time, popularly called *solvation time*, depends on the viscosity, molecular structure and temperature of the medium. In conventional molecular solvents, the solvation time is typically less than 100 ps at room temperature whereas the excited state lifetimes of the probes are in the order of a few nanoseconds.[98] This indicates the attainment of excited state equilibrium prior to fluorescence, but, the entire scenario may change in viscous solvents and organized assemblies like micelles, proteins or membranes. In these cases, emission from various stages of solvent relaxation can be monitored and thus a time-dependent shift in the emission spectra, known as dynamic Stokes shift, can be observed (Scheme 1.3). The method of studying the solvation dynamics using dynamic Stokes shift technique has been elaborated in Chapter 2.

1.3.1. Solvation dynamics in conventional solvents

The solvation dynamics is extremely fast in conventional molecular solvents. The ultrafast time-resolved studies indicate that in the absence of specific solute-solvent interactions, ca. hydrogen bonding, the solvent relaxation in most solvents occurs in the sub-picosecond time scale at room temperature.[99,100] The results can be explained using nonspecific theory of solvation dynamics. The linear correlation between the average solvation time and longitudinal relaxation time, as predicted by simple continuum theory, depends primarily on the nature of

solute-solvent interaction and temperature of the medium. Deviation from the above can be accounted for considering the translational contribution to the solvent relaxation, specific hydrogen bonding ability of the protic solvents etc.[101,102]

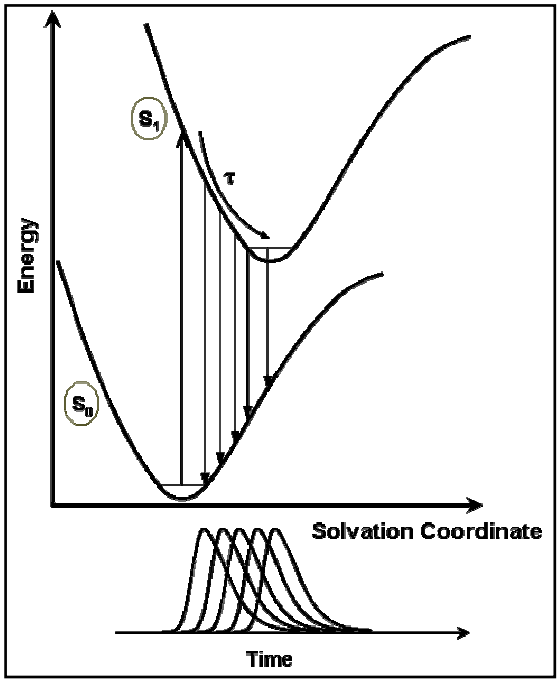

Scheme. 1.3. Schematic representation of the dynamic Stokes shift.

However, an excellent correlation between the average solvation time and the longest longitudinal relaxation time can be observed when solvation dynamics in alcoholic solvents is studied at high pressures.[103] For high pressure solvation dynamics in ethanol, the solvent relaxation is found to become biphasic (i.e., biexponential relaxation) though in normal condition the dynamics is

monoexponential.[104] The slow, biphasic dynamics has been explained by the liquid-solid phase transition of ethanol at high pressure.

In case of dynamic solvation in solutions of ionic salts (metal perchlorates and halide) in nonaqueous solvents, the solvation time is found to be quite high and it shows excitation wavelength dependence.[105] Also, the solvation rate is found to decrease with solvent polarity and charge to size ratio of the cation.

1.3.2. Solvation dynamics in confined environment

The relaxation in pure water is biexponential with solvation times 126 fs and 880 fs, respectively.[106] According to Fleming et. al., the faster component is the result of vibration relaxation, whereas the slower one is due to librational motion.[106] However, a large number of dynamical studies in water confined in organized assemblies like micelles,[107] microemulsions,[108] cyclodextrins,[109] vesicles,[110] proteins[111] etc have revealed the presence of a much slower component in the relaxation of water in such media.[112] The dynamics of 'confined water' is found to be biphasic where the ultrafast sub-picosecond component is associated with a slow component, which can be as large as hundreds of picoseconds. The observation has been attributed to the dynamic exchange of free and bound water molecules in such media.[112]

1.3.3. Solvation dynamics in RTILs

Since the RTILs are sufficiently polar, it is possible to obtain useful information on the time scale of reorganization of the constituent ions around the photoexcited probe by probing the time-resolved fluorescence behavior of the dipolar molecules. Ever since the early work of Karmakar and Samanta,[113] many

researchers have contributed to the solvation dynamics study in RTILs with a view to elucidating various aspects of this phenomenon. These studies have indicated that the solvation dynamics in RTILs is a rather slow process, much slower than that observed in conventional molecular solvents. Also, the slow dynamics is mostly accompanied by an ultrafast component, usually called missing component as this is missed in most experimental setups having a finite time-resolution (typically 25 ps). In as much as 30-50% of the total dynamics has been found to be ultrafast depending upon the nature of RTILs employed, but generally, the ultrafast (or missing) component is independent of the viscosity of the media.[113-116] Although the exact time scale or the physical origin of the ultrafast component is still under considerable speculation and doubt,[115-121] it is generally believed that the planar ring system and polarizability of cation, small amplitude motion of ions in the first solvation shell contribute to the missing dynamics.[117-120] The time scale of the ultrafast dynamics was earlier conjectured to be 5 ps or < 1 ps.[116,117] Recent studies based on optical Kerr-gated emission spectroscopy have indicated that this dynamics is of the order of 300-700 fs at room temperature,[119] whereas another recent work based on the femtosecond upconversion technique has shown that only 10-20% of the total dynamics is ultrafast and it occurs within 10 ps.[120]

The slow observable dynamics is biphasic in nature with the two components typically in the picosecond and nanosecond time scale.[113,114,122] Again, some authors prefers a nonexponential description for this slow dynamics with the emphasis on the contribution of collective motion of the cation and anion to the slow relaxation process.[115-118] In both cases, the average solvation time has been

found to be roughly correlated with the viscosity of the media, at least for less viscous RTILs (< 100 cP). The solvation dynamics in RTILs has also been found to be probe-dependent.[121-122]

Due to the complex characteristics of the solvation dynamics in RTILs, many simulation studies have been carried out to investigate the dynamical properties of the RTILs.[55,123-126] While in their earlier studies Shim et. al. attributed the fast component to the translation of anions,[123] Kobrak and Znamenskiy[124] assigned the ultrafast component of the dynamics to the collective cation-anion motion. The model of Shim et. al.[123] was probably unrealistic as it emphasized on the small molecule dynamics, which is an untrue picture of RTILs. Later, Shim et al. suggested that ultrafast dynamics is dependent on the local density of the ions near the probe molecules.[125] In the case of high local density the ultrafast component is governed by the motion of a few ions close to the probe molecule, whereas, for low initial density, the contribution of ions from the further region becomes significant. The solvation dynamics has also been studied in the mixtures of RTILs and conventional solvents and in ionic liquid-based micelle, microemulsion etc.[127,128] Recent femtosecond time-resolved ultrafast dynamical studies based on the Kerr effect have also revealed the intermolecular dynamics and the time scales of the different relaxation processes in imidazolium and pyrrolidinium ionic liquids.[129]

1.4. Fluorescent viscosity probes: measurement of microviscosity

Fluorescence technique has often been found useful for the measurement of microviscosity of a variety of microheterogeneous systems, e.g., model systems like micelles, reverse micelles or microemulsions, lipid bilayers or vesicles, as

well as polymers, proteins and membranes. An early application of steady-state fluorescence anisotropy measurements has been the determination of microviscosity in the miceller interior.[130-132] Weber et. al.[130] have shown that microviscosity (η_m) can be derived from the steady-state anisotropy using Perrin's relation:

$$\frac{r_0}{r} = 1 + \frac{kT\tau}{\eta_m V_0} \qquad (1.5)$$

where, r and r_0 are the measured and limiting fluorescence anisotropies, respectively, τ is the excited state lifetime and V_0 is the hydrodynamic volume of the probe. The common probes used for this kind of measurements are shown in Chart 1.5. Microviscosities of many other confined systems like microemulsions,[133] vesicles or lipid bilayers,[134] proteins,[135] and membranes[136] have also been determined using this technique. However, it has been pointed out that for restricted systems like lipid bilayers, the probe movement becomes anisotropic and thus rotational movements are constrained, often leading to 'wobbling in a cone motion' as observed for DPH (l,6-diphenyl-l,3,5-hexatriene).[137] On this basis, it was suggested that the steady state measurement may give erroneously overestimated microviscosity of certain confined systems.[137]

Excimer fluorescence of intramolecular excimer-forming probes, mostly based on pyrene derivatives (cf. dipyrenylalkanes), has been used to probe the microviscosity of organized assemblies like micelles, lipid bilayers and membranes as well as the free volume parameters for different polymer oils.[138-140] However, the measured ratio of monomer to excimer intensities, which is required

for microviscosity calculations, is also found to be solvent polarity dependent and thus complication may arise during the estimation of absolute local viscosity.[138,139]

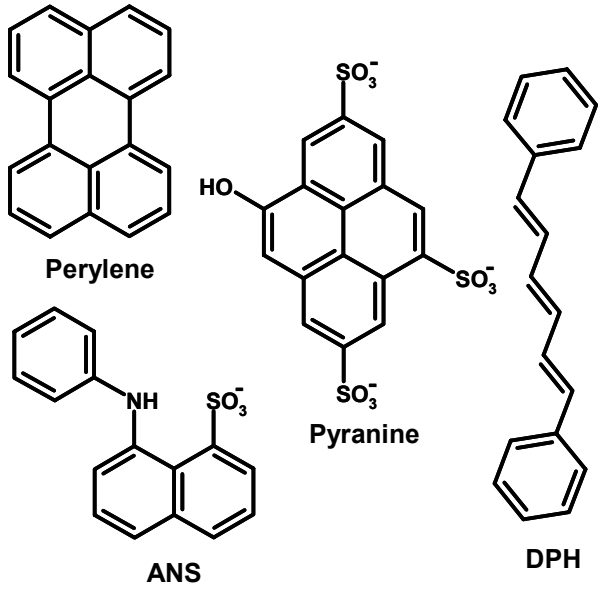

Chart 1.5. Structure of some probe molecules used for microviscosity measurement using fluorescence technique.

Fluorescent dyes which undergo rapid internal torsional relaxation leading to a very fast nonradiative decay of the photoexcited state, often exhibit viscosity-dependent fluorescence quantum yield (Φ_f) due to the hindrance of the twisting motion in viscous media. These molecules are popularly known as "*molecular rotors*" (Chart 1.6) and they have long been used as microviscosity probes for various microheterogeneous media.[141] Though the early use of the malonitrile derivatives (e.g., DCVJ, see Chart 1.6) was to serve as a free volume probe for

monitoring the degree of polymerization during polymerization reaction,[142] these and other derivatives have been used later for measuring microviscosity of different biological systems[143] as well as model confined media like lipid bilayers, micelles and inverse micelles etc.[144,145]

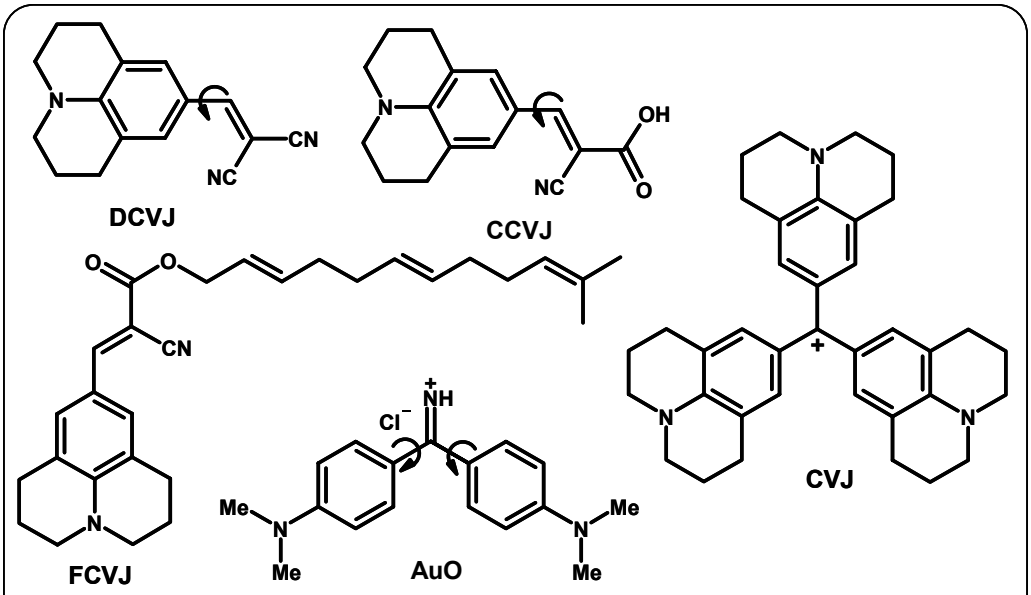

Chart 1.6. Structure of some fluorescent 'molecular rotor' probes for microviscosity measurement. The arrow indicates the internal rotation contributing to rapid nonradiative process.

As mentioned earlier, these molecules posses very short excited state lifetime, typically a few picoseconds in conventional less viscous solvents, and are characterized by a very rapid nonradiative decay, which is directly associated with the internal twisting or torsional motion around certain single bond.[146,,147] Viscosity-governed hindrance inhibits the twisting motion and thus the fluorescence quantum yield is enhanced. According to Förster and Hoffmann the

relationship between solvent viscosity (η) and fluorescence quantum yield (Φ_f) is as follows:[148]

$$\log \Phi_f = C + x \log \eta \quad (1.6)$$

where, C is a constant and x is a term that depends on the structural properties of the rotor and represents a fraction of the total critical volume for solvent motion that is required for the molecular rotor to undergo torsional rearrangement.[147] Eqn. 1.6 holds good for a range of high viscosity solvents or solvent mixtures (5-1000 cP) when malonitriles like DCVJ, CCVJ etc (Chart 1.6) are used as probes. Therefore, the microviscosity can be measured for a large variety of biological assemblies using a calibration curve following eqn. 1.6.

1.5. Motivation behind the thesis

The work embodied in this thesis has been primarily undertaken with a two-dimensional objective: firstly, to understand the UV-visible absorption and fluorescence behavior of neat RTILs based on imidazolium salts. This is considered necessary as it imposes certain limitations on the systems to be studied in these media. Secondly, to study the photophysical processes like photoinduced electron transfer, solvation dynamics etc in RTILs in order to get an insight into the mechanistic details of these processes, such as, to what extent these phenomena differ from those in normal solvents and what is the specific role of the RTILs, if any, in such differential characteristics of the aforementioned photoprocesses.

In the recent years, many photophysical studies have been carried out in imidazolium RTILs, though optical properties of the RTILs themselves remained largely unexplored. In some current literatures an impression is given that the

imidazolium salts are optically transparent liquids possessing no absorption in the UV–vis region (above 250 or 300 nm) and that any absorption beyond this wavelength is probably due to the presence of impurity.[149] In order to have a definite understanding, we have carried out a detailed investigation on the absorption and emission properties of a few carefully prepared and rigorously purified imidazolium RTILs (RTILs **1**-**4**, in Chart 1.7).

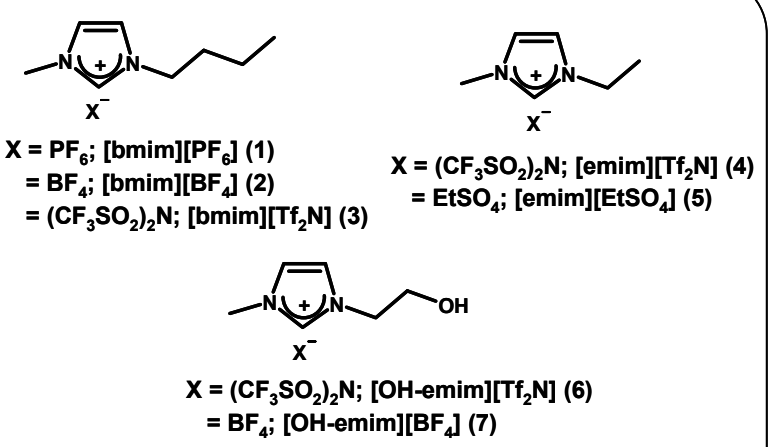

Chart 1.7. Structure and abbreviation of the RTILs employed in the present study.

Photoinduced electron transfer (PET) reaction has been quite an interesting phenomenon with the potentiality of diverse application. Though various mechanistic aspects of the overall PET process are intimately related to solvent polarity and viscosity, very little effort has been made to examine the PET reaction in RTILs. The handful of studies made in this direction have largely been confined to determining the effect of viscosity and/or polarity on the rate constant

of such processes.[150] How the *course* of a PET reaction is influenced by the viscosity, polarity and ionic constituents of the RTILs is still an open question. Therefore, we have studied a common PET reaction occurring between pyrene and N,N-dimethylaniline in RTILs of varying viscosity (RTILs **1-4**, in Chart 1.7) in order to understand the influence of viscosity and polarity on the reaction course.

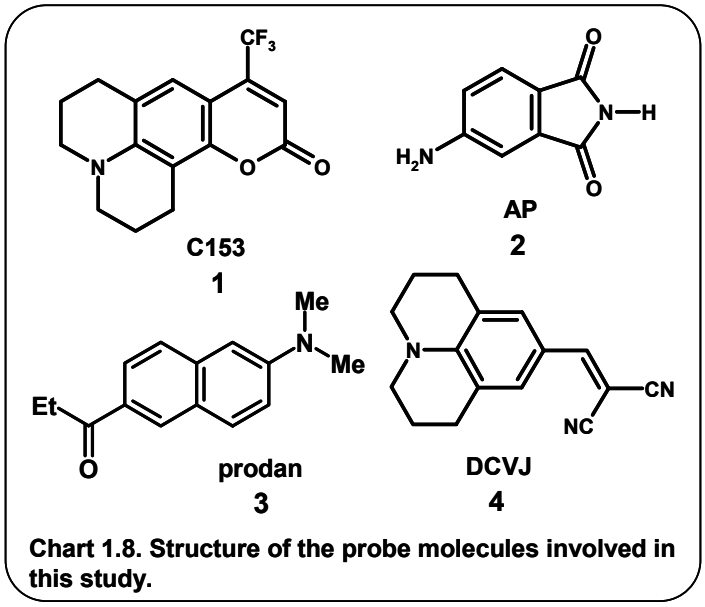

Chart 1.8. Structure of the probe molecules involved in this study.

In recent days, the dynamic solvation in RTILs has stimulated a great variety of experimental as well as theoretical/simulation studies.[113-115,123-126] However, many features of solvation dynamics in RTILs are not well-understood so far. There remains considerable speculation and debate regarding the physical nature and exact time scale of the early dynamics, called the ultrafast dynamics, which '*missed*' in most dynamical studies.[115-121] Therefore, we have aimed at

determining the factors that might affect this ultrafast dynamics and probed the influence of hydrogen bonding interaction on the missing and observable components of the dynamics by using an alcohol-functionalized RTIL, [OH-emim][Tf_2N] (Chart 1.7) and three solvation probes (probes **1-3**, in Chart 1.8).

Since addition of conventional solvent broadens the scope of applications of the RTILs by allowing fine-tuning of the solvent properties, a growing number of recent studies focus on the physicochemical properties of mixtures of RTIL and conventional molecular solvent. These studies are mostly confined to the use of medium-to-high polarity solvents as the second constituent in RTIL-cosolvent mixtures.[56-61] The few solvation dynamics studies in the RTIL-molecular solvent mixtures reported so far have only focused on the polar solvents like water or methanol as cosolvent.[127] Hence, we thought it would be interesting to follow the dynamical course in a mixture of RTIL ([bmim][PF_6], Chart 1.7) with nonpolar solvents like toluene and 1,4-dioxane.

Recently, the liquid structure and heterogeneous nature of RTILs have been probed by many experimental and simulation studies, although a clear picture is yet to emerge.[45-55] To understand the heterogeneous character of RTILs, the microviscosity of RTILs is needed to be probed. However, a little effort has been made in this context.[151] Therefore, we have undertaken the photophysical study of a molecular rotor probe, namely 9-(dicyanovinyl)julolidine (DCVJ, Chart 1.8),[146] in a series of RTILs of varying viscosity (RTILs **1-7**, in Chart 1.7), to understand the free volume parameters and microviscosity of the RTILs.

References

1. Nelson, W. M. In *Green Chemistry*; Anastas, P. T., Williamson, T. C., Eds.; Oxford University Press: Oxford, 1998.
2. Tanaka, K.; Toda, F. *Chem. Rev*. **2000**, *100*, 1025.
3. Hang, C. T.; Lianhai, L.; Yang, Y.; Wenshuo, L. Developing green chemistry: Organometallic reactions in aqueous media. In *Clean Solvents: Alternative Media for Chemical Reactions and Processing*; Abraham, M., Moens, L., Eds.; ACS Symposium Series 819; American Chemical Society: Washington, DC, 2002; p 166.
4. Kajimoto, O. *Chem. Rev.* **1999**, *99*, 355.
5. (a) Seddon, K. R. *Nature (Materials)* **2003**, *2*, 363. (b) Rogers, R. D.; Seddon, K. R. *Science* **2003**, *302*, 792.
6. Wasserscheid, P.; Keim, W. *Angew. Chem., Int. Ed.* **2000**, *39*, 3772.
7. Seddon, K. R.; Stark, A.; Torres, M. J. *Pure Appl. Chem.* **2000**, *72*, 2275.
8. Walden, P. *Bull. Acad. Imper. Sci. (St. Petersberg)* **1914**, 1800.
9. (a) Wilkes, J. S.; Levinsky, J. A.; Wilson, R. A.; Hussey, C. L. *Inorg. Chem*. **1982**, *21*, 1263. (b) Boon, J. A.; Levinsky, J. A.; Pflug, J. L.; Wilkes, J. S. *J. Org. Chem*. **1986**, *51*, 480.
10. Sheldon, R. *Chem. Commun.* **2001**, 2399.
11. Wilkes, J. S.; Zaworotko, M. J. *Chem. Commun*. **1992**, 965.
12. Welton, T. *Chem. Rev.* **1999**, *99*, 2071.
13. (a) MacFarlane, D. R.; Meakin, P.; Sun, J.; Amini, N.; Forsyth, M. *J. Phys. Chem. B* **1999**, *103*, 4164. (b) Henderson, W. A.; Passerini, S. *Chem. Mater.* **2004**, *16*, 2881.
14. (a) Tao, G.; He, L.; Sun, N.; Kou, Y. *Chem. Commun.* **2005**, 3562. (b) Fukumoto, K.; Yoshizawa, M.; Ohno, H. *J. Am. Chem. Soc.* **2005**, *127*, 2398. (c) Ohno, H.; Fukumoto, K. *Acc. Chem. Res.* **2007,** *40,* 1122.
15. Holbrey, J. D.; Reichert, W. M.; Swatloski, R. P.; Broker, G. A.; Pitner, W. R.; Seddon, K. R.; Rogers, R. D. *Green Chem.* **2002**, *4*, 407.
16. (a) McFarlane, D. R.; Golding, J.; Forsyth, S.; Forsyth, M.; Deacon, G. B. *Chem. Commun.* **2001**, 1430. (b) McFarlane, D. R.; Forsyth, S. A.; Golding, J.; Deacon, G. B. *Green Chem.* **2002**, *4*, 444.
17. Buzzeo, M. C.; Evans, R. G.; Compton, R. G. *Chem. Phys. Chem.* **2004**, *5*, 1106.
18. Freemantle, M. *Chem. Eng. News* **1998**, *76*, 32.
19. Chiappe, C; Pieraccini, D. *J. Phys. Org. Chem.* **2005**, *18*, 275.
20. (a) Huddleston, J. G.; Visser, A. E.; Reichert, W. M.; Willauer, H. D.; Broker G. A.; Rogers, R. D. *Green Chem.* **2001**, *3*, 156. (b) Dzyuba, S.; Bartsch, R. A. *Chem. Phys. Chem.* **2002**, *3*, 161. (c) Carda-Broch, S.; Berthold, A.; Armstrong, D. W. *Anal. Bioanal. Chem.* **2003**, *375*, 191.
21. Carmichael, A. J.; Seddon, K. R. *J. Phys. Org. Chem.* **2000**, *13*, 591.
22. Aki, S N. V. K.; Brennecke, J. F.; Samanta, A. *Chem. Commun.* **2001**, 413.

23. Muldoon, M. J.; Gordon, C. M.; Dunkin, I. R. *J. Chem. Soc., Perkin Trans. 2* **2001**, 433.
24. Reichardt, C. *Green Chemistry* **2005**, *7*, 339.
25. Crowhurst, L.; Mawdsley, P. R.; Perez-Arlandis, J. M.; Salter, P. A.; Welton, T. *Phys. Chem. Chem. Phys.* **2003**, *5*, 2790.
26. Anderson, J. L.; Ding, J.; Welton, T.; Armstrong, D. W. *J. Am. Chem. Soc.* **2002**, *124*, 14247.
27. (a) Wakai, C.; Oleinikova, A.; Ott, M.; Weingartner, H. *J. Phys. Chem. B.* **2005**, *109*, 17028. (b) Daguenet, C.; Dyson, P. J.; Krossing, I.; Oleinikova, A.; Slattery, J.; Wakai, C.; Weingartner, H. *J. Phys. Chem. B.* **2006**, *110*, 12682.
28. Widegren, J. A.; Laesecke, A.; Magee, J. W. *Chem. Commun.* **2005**, 1610.
29. Seddon, K. R.; Stark, A.; Torres, M. J. In *Clean Solvents: Alternative Media for Chemical Reactions and Processing*; Abraham, M., Moens, L., Eds.; ACS Symposium Series 819; American Chemical Society: Washington, DC, 2002; p 34.
30. Xu, W.; Wang, L.-M.; Nieman, R. A.; Angell C. A. *J. Phys. Chem. B* **2003**, *107*, 11749.
31. (a) Holbrey, J. D.; Turner, M. B.; Reichert, W. M.; Rogers, R. D. *Green Chem.* **2003**, *5*, 731. (b) Branco, L. C.; Rosa, J. N.; Ramos, J. J. M.; Afonso, C. A. M. *Chem. Eur. J.* **2002**, *8*, 3671.
32. Pringle, J. M.; Golding, J.; Baranyai, K.; Forsyth, C. M.; Deacon, G. B.; Scott, J. L.; MacFarlane, D. R. *New J. Chem.* **2003**, *27*, 1504.
33. Every, H. A.; Bisop, A. G.; MacFarlane, D. R.; Oradd, G.; Forsyth, M. *Phys. Chem. Chem. Phys.* **2004**, *6*, 1758.
34. Ngo, H. L.; LeCompte, K.; Hargens, L.; McEwen, A. B. *Thermochim. Acta* **2000**, *357*, 97.
35. (a) Earle, M.; Esperanca, J. M. S. S.; Gilea, M. A.; Lopes, J. N. C.; Rebelo, N. P. L.; Magee, J. W.; Seddon, K. R.; Widegren, *Nature* **2006**, *439*, 831. (b) Armstromg, J. P.; Hurst, C.; Jones, R. G.; Licence, P.; Lovelock, K. R. J.; Satterley, J.; Villar-Garcia, I. J. *Chem. Phys. Chem.* **2007**, *9*, 982.
36. Choudhury, A. R.; Winterton, N.; Steiner, A.; Cooper, A. I.; Johnson, K. A. *J. Am. Chem. Soc.* **2005**, *127*, 16792.
37. (a) Kölle, P.; Dronskowski, R. *Inorg. Chem.* **2004**, *43*, 2803. (b) van de Broeke, J.; Stam, M.; Lutz, M.; Kooijman, H.; Spek, A. L.; Deelman, B.-J.; van Koten, G. *Eur. J. Inorg. Chem.* **2003**, *26*, 2798. (c) Gordon, G. M.; Holbrey, D. M.; Kennedy, A. R.; Seddon, K. R. *J. Mater. Chem.* **1998**, *8*, 2627.
38. Suarez, P. A. Z.; Dullius, J. E. L.; de Souza, R. F.; Dupont, J. *J. Chim. Phys. Phys.-Chim. Biol.* **1998**, *95*, 1626.
39. Mele, A.; Tran, C. D.; De Paoli Lacerda, S. H. *Angew. Chem. Int. Ed.* **2003**, *42*, 4364.

40. Bonhote, P.; Dias, A. P.; Papageorgiou, N.; Kalyanasundaram, K.; Gratzel, M. *Inorg. Chem.* **1996**, *35*, 1168.
41. Avent, A. G.; Charloner, P. A.; Day, M. P.; Seddon K. R.; Welton, T. *J. Chem. Soc., Dalton Trans.* **1994**, *23*, 3405.
42. Mele, A.; Romano, G.; Giannone, M.; Ragg, E.; Fronza, G.; Raos, G.; Marcon, V. *Angew. Chem. Int. Ed.* **2006**, *45*, 1123.
43. (a) Wang, Y.; Voth, G. A. *J. Am. Chem. Soc.* **2005**, *127*, 12192. (b) Lopes, J. N. C.; Padua, A. A. H. *J. Phys. Chem. B* **2006**, *110*, 3330. (c) Jiang, W.; Wang, Y.; Voth, G. A. *J. Phys. Chem. B* **2007**, *111*, 4812.
44. Wang, Y.; Jiang, W.; Yan, T.; Voth, G. A. *Acc. Chem. Res.* **2007**, *40*, 1193.
45. Mandal, P. K.; Sarkar, M.; Samanta, A. *J. Phys. Chem. A* **2004**, *108*, 9048.
46. Funston, A. M.; Fadeeva, T. A.; Wishart, J. F.; Castner, E. W., Jr. *J. Phys. Chem. B* **2007**, *111*, 4963.
47. (a) Triolo, A.; Russina, O.; Bleif, H.-J.; Di Cola, E. *J. Phys. Chem. B* **2007**, *111*, 4641. (b) Moutiers, B. G.; Labet, A.; Azzi A. E.; Gaillard, C.; Mariet, C.; Lutzenkirchen, K. *Inorg. Chem.* **2003**, *42*, 1726. (c) Carmichael, A. J.; Hardacre, C.; Holbrey, J. D. *Mol. Phys.* **2001**, *99*, 795.
48. (a) Hayashi, S.;Ozawa, R.; Hamaguchi, H. *Chem. Lett.* **2003**, *32*, 498. (b) Ozawa, R.; Hayashi, S.; Saha, S.; Kobyashi, A.; Hamaguchi, H. *Chem. Lett.* **2003**, *32*, 948. (c) Iwata, K.; Okazima, H.; Saha, S.; Hamaguchi, H. *Acc. Chem. Res.* **2007,** *40,* 1174.
49. Hardacre, C.; Holbrey, J. D.; McMath, S. E. J.; Bowron, D. T.; Soper, A. K. *J. Chem. Phys.* **2003**, *118*, 273.
50. Carmichael, A. J.; Hardacre, C.; Holbrey, J. D.; Nieuwenhuyzen, M.; Seddon, K. R. *Anal. Chem.* **1999**, *71*, 4572.
51. (a) Xiao, D.; Rajian, J. R.; Li, S. F.; Bartsch, R. A.; Quitevis, E. L. *J. Phys. Chem. B* **2006**, *110*, 16174. (b) Xiao, D.; Rajian, J.; Cady, A.; Li, S.; Bartsch, R.; Quitevis, E. *J. Phys. Chem. B* **2007**, *111*, 4669.
52. Dupont, J.; Suarez, P. A. Z.; de Suza, R. F.; Burrow, R. A.; Kintzinger, J. *Chem. Eur. J.* **2000**, *6*, 2377.
53. (a) Hu, Z.; Margulis, C. J. *Proc. Natl. Acad. Sci.* **2006**, *103*, 831. (b) Hu, Z.; Margulis, C. J. *J. Phys. Chem. B* **2006**, *110*, 11025. (c) Hu, Z.; Margulis, C. J. *Acc. Chem. Res.* **2007**, *40*, 1097.
54. (a) Popolo, M.; Kohanoff, J.; Lynden-Bell, R. M.; Pinilla, C. *Acc. Chem. Res.* **2007**, 40, 1156. (b) Padua, A. A. H.; Costa Gomes, M. F.; Canongia Lopes, J. N. A. *Acc. Chem. Res.* **2007**, *40*, 1087.
55. (a) Hardacre, C.; Holbrey, J. D.; Nieuwenhuyzen, M.; Youngs, T. G. A. *Acc. Chem. Res.* **2007**, *40*, 1144. (b) Castner, E. W., Jr.; Wishert, J. F.; Shirota, H. *Acc. Chem. Res.* **2007**, *40*, 1144.

56. (a) Wang, J. J.; Tian, Y.; Zhao, Y.; Zhou, K. L. *Green Chem.* **2003**, *5*, 618. (b) Rodriguez, H.; Brennecke, J. F. *J. Chem. Engg. Data* **2006**, *51*, 2145.
57. (a) Baker, S. N.; Baker, G. A.; Bright, F. V. *Green Chem.* **2002**, *4*, 165. (b) Fletcher, K. A.; Pandey, S. *J. Phys. Chem. B* **2003**, *107*, 13532. (c) Fletcher, K. A.; Pandey, S. *Appl. Spectrosc.* **2002**, *56*, 1498. (d) Fletcher, K. A.; Baker, S. N.; Baker, G. A.; Pandey, S. *New J. Chem.* **2003**, *27*, 1706.
58. (a) Harifi-Mood, A. R.; Habibi-Yangjeh, A.; Gholami, M. R. *J. Phys. Chem. B* **2006**, *100*, 7073. (b) Mellein, B. R.; Aki, S. N. V. K.; Ladewski, R. L.; Brennecke, J. F. *J. Phys. Chem. B* **2007,** *111,* 6452.
59. (a) Chakrabarty, D.; Seth, D.; Chakraborty, A.; Sarkar, N. *J. Phys. Chem. B* **2005**, *109*, 5753. (b) Seth, D.; Chakraborty, A.; Setua, P.; Sarkar, N. *J. Phys. Chem. B* **2007**, *111*, 4781.
60. (a) Zhang, J.; Wu, W.; Jiang, T.; Gao, H.; Liu, Z.; He, J.; Han, B. *J. Chem. Engg. Data* **2003**, *48*, 1315. (b) Jarosik, A.; Krajewski, S. R.; Lewandowski, A.; Radzimski, P. *J. Mol. Liq.* **2006**, *123*, 43. (c) Comminges, C.; Barhdadi, R.; Laurent, M.; Troupel, M. *J. Chem. Engg. Data* **2006**, *51*, 680. (d) Tokuda, H.; Baek, S. J.; Watanabe, M. *Electrochemistry* **2005**, *73*, 620.
61. Li, W.; Zhang, Z.; Han, B.; Hu, S.; Xie, Y.; Yang G. *J. Phys. Chem. B* **2007,** *111,* 6452.
62. Dupont, J.; de Suza, R. F.; Suarez, P. A. Z. *Chem. Rev*. **2002**, *102*, 3667.
63. *Ionic Liquids in Synthesis*; Welton, T., Wasserscheid, P., Eds.; VCH-Wiley: Weinheim, Germany, 2002.
64. (a) Seddon, K. R.; Stark, A.; Torres, M. J. In *Clean Solvents: alternative Media for Chemical Reactions and Processing*; Abraham, M., Moens, L., Eds.; ACS Symposium Series 819; American Chemical Society: Washington, DC, 2002. (b) *Ionic Liquids, Industrial Applications for Green Chemistry*; Rodgers, R., Seddon, K. R., Eds.; ACS Symposium Series 818; American Chemical Society: Washington, DC, 2002.
65. (a) Abedin, S. Z. E.; Endres, F. *Acc. Chem. Res.* **2007**, *40*, 1106. (b) MacFarlane, D. R.; Forsyth, M.; Howlett, P. C.; Pringle, J. M.; Sun, J.; Annat, G.; Neil, W.; Izgorodina, E. I. *Acc. Chem. Res.* **2007**, *40*, 1165.
66. (a) Huddleston, J. G.; Willauer, H. D.; Swatlowski, R. P.; Visser, A. E.; Rodgers, R. D. *Chem. Commun.* **1998**, 1765. (b) Dai, S.; Ju, Y. H.; Barnes, C. E. *J. Chem. Soc., Dalton Trans.* **1999**, 63.
67. (a) Itoh, H.; Naka, K.; Chujo, Y. *J. Am. Chem. Soc.* **2004**, *126*, 3026. (b) Wei, G.-T.; Yang, Z.; Lee, C.-Y.; Yang, H.-Y.; Wang, C. R. C. *J. Am. Chem. Soc.* **2004**, *126*, 5036. (c) Tatumi, R.; Fujihara, H. *Chem. Commun.* **2005**, 83.
68. (a) Yu, B.; Zhou, F.; Liu, G.; Liang, Y.; Huck, W. T. S.; Liu, W. *Chem. Commun.* **2006**, 2356. (b) Wang, Y.; Yang, H. *Chem. Commun.* **2006**, 2545. (c) Zhao, D.; Fei,

Z.; Ang, W. H.; Dyson, P. J. *Small* **2006**, *7*, 879. (d) Green, M.; Rahmana, P.; Smyth-Boyle, D. *Chem. Commun.* **2007**, 574.
69. Borra, E. F.; Seddiki1, O.; Angel, R.; Eisenstein, D.; Hickson, P.; Seddon, K. R.; Worden, S. P. *Nature* **2007**, *447*, 979.
70. Armstromg, D. W.; Zhang, L. K.; He, L.; Gross, M. L. *Anal. Chem.* **2001**, *73*, 3679.
71. van Rantwijk, F.; Lau, R.; Sheldon, R. A. *Trends Biotechnol.* **2003**, *21*, 131.
72. (a) Bates, E. D.; Mayton, R. D.; Ntai, I.; Davis, J. H., Jr. *J. Am. Chem. Soc.* **2002**, *124*, 926. (b) Buzzeo, M. C.; Hardacre, C.; Compton, R. G. *Anal. Chem.* **2004**, *76*, 4583.
73. Park, S.; Kazlauskas, R. J. *Curr. Opin. Biotech.* **2003**, *14*, 432.
74. Wang, P.; Zakeeruddin, S. M.; Comte, P.; Exnar, I.; Gratzel, M. *J. Am. Chem. Soc.* **2003**, *125*, 1166.
75. Kimizuka, N.; Nakashima, T. *Langmuir* **2001**, *17*, 6759.
76. For review on this subject, see (a) Davis, J. H. *Chem. Lett.* **2004**, *33*, 1072. (b) Lee, S. *Chem. Commun.* **2006**, 1049.
77. Ref. 76 and references therein.
78. For a review, see Kavarnos, G. J.; Turro N. J. *Chem. Rev.* **1986**, *86*, 401.
79. Marcus, R. A.; Sutin, N. *Biochim. Biophys. Acta* **1985**, *811*, 265.
80. (a) Julliard, M.; Chanon, M. *Chem. Rev.* **1983**, *83*, 425. (b) Whitten, D. G. *Acc. Chem. Res.* **1980**, *84*, 981. (c) Balzani, V.; Scandola, F. In *Photochemical Conversion and Storage of Solar Energy*; Connolly, J. S., Ed.; Academic: New York, 1981; Chapter 4.
81. *The Exciplex*; Gordon, M., Ware, W. R., Eds.; Academic Press: New York, 1974.
82. (a) Mataga, N. *Pure & Appl. Chem.* **1984**, *56*, 1255. (b) Weller, A. *Pure & Appl. Chem.* **1984**, *56*, 1255.
83. (a) Rehm, D.; Weller, A. *Ber. Bunsen-Ges. Phys. Chem.* **1969**, *73*, 834. (b) Knibbe, H.; Rehm, D.; Weller, A. *Ber. Bunsen-Ges. Phys. Chem.* **1968**, *72*, 257.
84. Rehm, D.; Weller, A. *Isr. J. Chem.* **1970**, *8*, 259.
85. Marcus, R. A. *J. Chem. Phys.* **1956**, *24*, 966.
86. Marcus, R. A. *Annu. Rev. Phys. Chem.* **1964**, *15*, 155.
87. Kikuchi, K.; Takahasi, Y.; Katagiri, T.; Niwa, T.; Hoshi, M.; Miyashi, T. *Chem. Phys. Lett.* **1991**, *180*, 403.
88. Marcus, R. A.; Siders, P. *J. Phys. Chem.* **1982**, *86*, 622.
89. (a) Miller, J. R.; Calcaterra, L. T.; Closs, G. L. *J. Am. Chem. Soc.* **1984**, *106*, 3047. Closs, G. L.; (b) Calcaterra, L. T.; Green, N. J.; Penfield, K. W.; Miller, J. R. *J. Phys. Chem.* **1986**, *90*, 3673.
90. (a) Mataga, N.; Kanada, Y.; Asahi, T.; Miyasaka, T.; Okada, T.; Kakitani, T. *Chem. Phys.* **1988**, *127*, 239. (b) Mataga, N.; Asahi, T.; Kanada, Y.; Okada, T. *Chem. Phys.* **1988**, *127*, 249.

91. (a) Gould, I. R.; Ege, D.; Moser, J. E.; Farid, S. *J. Am. Chem. Soc.* **1990**, *112*, 4290. (b) Inada, T. N.; Miyazawa, C. S.; Kikuchi, K.; Yamauchi, M.; Nagata, T.; Takahashi, Y.; Ikeda, H.; Miyashi, T. *J. Am. Chem. Soc.* **1999**, *121*, 7211. (c) Inada, T.; Kikuchi, K.; Takahashi, Y.; Ikeda, H.; Miyashi, T. *J. Phys. Chem. A.* **2002**, *106*, 4345.
92. (a) Turro, N. J. In *Modern Molecular Photochemistry*; Benjamin/Cummings: Menlo Park, CA, 1978; Chapter 9. (b) Stryer, L.; Haugland, R. P. *Proc. Natl. Acad. Sci. U.S.A.* **1967**, *58*, 719. (c) Turro, N. J. *Pure Appl. Chem.* **1977**, *49*, 405.
93. (a) Hinto, T.; Akazawa, H.; Mashuhara, H.; Mataga N. *J. Phys. Chem.* **1976**, *80*, 33. (b) Hirata, Y.; Kanda Y.; Mataga, N. *J. Phys. Chem.* **1983**, *87*, 1659. (c) Mataga, N; Okada, T.; Kanda, Y.; Shioyama, H. *Tetrahedron* **1986**, *42*, 6143.
94. (a) Schaap, A. P.; Zaklika, K. A.; Kaskar, B.; Fung, L. V.-M. *J. Am. Chem. Soc.* **1980**, *102*, 389. (b) Sostero, S.; Traverso, O.; Bernardo, F. D.; Kemp, T. J. *J. Chem. Soc., Dalton Trans.* **1979**, 659. (c) Janzen, E. G. In *Creation and Detection of the Excited State*; Ware, W. R., Ed; Marcel Dekker, Inc.: New York, 1976; Chapter 3.
95. (a) Glarum, S. H. In *Chemically Induced Magnetic Polarization*; Lepley, A. R., Closs, G. L., Eds.; Wiley-Interscience: New York, 1973; Chapter 1. (b) Roth, H. D.; Schilling, M. L. M. *J. Am. Chem. Soc.* **1980**, *102*, 4303. (c) Closs, G. L.; Czeropski, M. S. *J. Am. Chem. Soc.* **1977**, *99*, 6126.
96. (a) Jarnigan, R. C. *Acc. Chem. Res.* **1971**, *4*, 420. (b) Taniguchi, Y.; Nishina, Y.; Mataga, N. *Bull. Chem. Soc. Jpn.* **1972**, *45*, 764.
97. (a) Gassman, P. G.; Olson, K. D. *J. Am. Chem. Soc.* **1982**, *104*, 3740. (b) Maioulis, A. J.; Shigemitsu, Y.; Arnold, D. R. *J. Am. Chem. Soc.* **1978**, *100*, 535.
98. Lakowicz, J. R. *Principles of Fluorescence Spectroscopy*; 2nd Ed.; Kluwer Academic/Plenum Press: New York, 1999; p 211.
99. Horng, M. L.; Gardecki, J. A.; Papazyan, A.; Maroncelli, M. *J. Phys. Chem.* **1995**, *99*, 17311.
100. Horng, M.-L.; Gardecki, J.; Maroncelli, M. *J. Phys. Chem.* **1997**, *101*, 1030.
101. (a) Castner, E.W., Jr.; Maroncelli, M.; Fleming, G. R. *J. Chem. Phys*. **1987**, *86*, 1090. (b) Chapman, C. F.; Fee, R. S.; Maroncelli, M. *J. Phys. Chem.* **1995**, *99*, 4811.
102. (a) Chapman, C. F.; Fee, R. S.; Maroncelli, M. *J. Phys. Chem.* **1990**, *94*, 4929. (b) Simon, J. D. *Acc. Chem. Res.* **1988**, *21*, 128.
103. Kometani, N.; Kajimoto, O.; Hara, K. *J. Phys. Chem. A* **1997**, *101*, 4916.
104. Molotsky, T. Koifman, N.; Huppert, D. *J. Phys. Chem. A* **2002**, *106*, 12185.
105. Chapman, C. F.; Maroncelli, M. *J. Phys. Chem.* **1991**, *95*, 9095.
106. Jimenez, R.; Fleming, G. R.; Kumar, P. V.; Maroncelli, M. *Nature* **1994**, *369*, 471.
107. (a) Hara, K.; Kuwabara, H.; Kajimoto, O. *J. Phys. Chem. A* **2001**, *105*, 7174. (b) Sarkar, N.; Dutta, A.; Das, S.; Bhattacharyya, K. *J. Phys. Chem.* **1996**, *100*, 15483.

108. (a) Dutta, A.; Mandal, D.; Pal, S. K.; Bhattacharyya, K. *J. Phys. Chem. B* **1997**, *101*, 10221. (b) Mandal, D.; Dutta, A.; Pal, S. K.; Bhattacharyya, K. *J. Phys. Chem. B* **1998**, *102*, 9070.
109. (a) Vajda, S.; Jimenez, R.; Rosenthal, S. J.; Fidler, V.; Fleming, G. R.; Castner, E.W., Jr. *J. Chem. Soc., Faraday Trans.* **1995**, *91*, 3405. (b) Sen, S.; Sukul, D.; Mandal, D.; Dutta, P.; Bhattacharyya, K. *J. Phys. Chem. A* **2001**, *105*, 10635.
110. Datta, A.; Pal, S. K.; Mandal, D.; Bhattacharyya, K. *J. Phys. Chem. B* **1998**, *102*, 6114.
111. (a) Pierce, D. W.; Boxer, S. G. *J. Phys. Chem.* **1992**, *96*, 5560. (b) Joo, T.; Jai, Y.; Yu, J.-Y.; Jonas, D. M.; Fleming, G. R. *J. Phys. Chem.* **1996**, *100*, 2399. (c) Pal, S. K.; Peon, J.; Zewail, A. H. *Proc. Natl. Acad. Sci.* **2002**, *99*, 1763.
112. (a) Bhattacharyya, K.; Bagchi, B. *J. Phys. Chem. A* **2000**, *104*, 10603. (b) Bhattacharyya, K. *Acc. Chem. Res.* **2003**, *36*, 95. (c) Nandi, N.; Bhattacharyya, K.; Bagchi, B. *Chem. Rev.* **2000**, *100*, 2013. (d) Bagchi, B. *Chem. Rev.* **2005**, *105*, 3197.
113. (a) Karmakar, R.; Samanta, A. *J. Phys. Chem. A* **2002**, *106*, 4447. (b) Karmakar, R.; Samanta, A. *J. Phys. Chem. A* **2002**, *106*, 6670. (c) Karmakar, R.; Samanta, A. *J. Phys. Chem. A* **2003**, *107*, 7340.
114. (a) Mandal, P. K.; Saha, S.; Karmakar, R.; Samanta, A. *Curr. Sci.* **2006**, *90*, 301. (b) Samanta, A. *J. Phys. Chem. B* **2006,** *110,* 13704.
115. Jin, H.; Baker, G. A.; Arzhantsev, S.; Dong, J.; Maroncelli, M. *J. Phys. Chem. B* **2007**, *111*, 7291.
116. Ingram, J. A.; Moog, R. S.; Ito, N.; Biswas, R.; Maroncelli, M. *J. Phys. Chem. B* **2003**, *107*, 5926.
117. (a) Arzhantsev, S.; Ito, N.; Heitz, M.; Maroncelli, M. *Chem. Phys. Lett.* **2003**, *381*, 278. (b) Ito, N.; Arzhantsev, S.; Heitz, M.; Maroncelli, M. *J. Phys. Chem. B* **2004**, *108*, 5771.
118. (a) Chowdhury, P. K.; Halder, M.; Sanders, L.; Calhoun, T.; Anderson, J. L.; Armstrong, D. W.; Song, X.; Petrich, J. W. *J. Phys. Chem. B* **2004**, *108*, 10245. (b) Headley, L. S.; Mukherjee, P.; Anderson, J. L.; Ding, R.; Halder, M.; Armstrong, D. W.; Song, X.; Petrich, J. W. *J. Phys. Chem. A*. **2006**, *110*, 9549.
119. Arzhantsev, S.; Jin, H.; Ito, N.; Maroncelli, M. *Chem. Phys. Lett.* **2006**, *417*, 524.
120. Lang, B.; Angulo, G.; Vauthey E. *J. Phys. Chem. A* **2006,** *110,* 7028.
121. Ito, N.; Arzhantsev, S.; Maroncelli, M. *Chem. Phys. Lett.* **2004**, *396*, 83.
122. (a) Mandal, P. K.; Paul, A.; Samanta, A. *Res. Chem. Intermed.* **2005**, *31*, 575. (b) Mandal, P. K.; Samanta, A. *J. Phys. Chem. B* **2005,** *109,* 15172.
123. Shim, Y.; Duan, J. S.; Choi, M. Y.; Kim, H. J. *J. Chem. Phys*. **2003**, *119*, 6411.
124. (a) Kobrak, M. N.; Znamenskiy, V. *Chem. Phys. Lett*. **2004**, *395*, 127. (b) Znamenskiy, V.; Kobrak, M. N. *J. Phys. Chem. B* **2004**, *108*, 1072.
125. Shim, Y.; Choi, M. Y.; Kim, H. J. *J. Chem. Phys*. **2005**, *122*, 044511.

126. Shim, Y.; Jeong, D.; Manjari, S.; Choi, M. Y.; Kim, H. J. *Acc. Chem. Res.* **2007**, *40*, 1130.
127. (a) Chakrabarty, D.; Chakraborty, A.; Seth, D.; Sarkar, N. *J. Phys. Chem. A* **2005**, *109*, 1764. (b) Chakrabarty, D.; Chakraborty, A.; Seth, D.; Hazra, P.; Sarkar, N. *Chem. Phys. Lett.* **2004**, *397*, 469. (c) Baker, S. N.; Baker, G. A.; Munson, C. A.; Chen, F.; Bukowski, E. J.; Cartwright, A. N.; Bright, F. V. *Ind. Eng. Chem. Res.* **2003**, *42*, 6457.
128. (a) Chakrabarty, D.; Seth, D.; Chakraborty, A.; Sarkar, N. *J. Phys. Chem. B* **2005**, *109*, 5753. (b) Seth, D.; Chakraborty, A.; Setua, P.; Sarkar, N. *J. Phys. Chem. B* **2007**, *111*, 4781.
129. (a) Giraud, G.; Gordon, C. M.; Dunkin, I. R.; Wynne, K. *J. Chem. Phys.* **2003**, *119*, 464. (b) Hyun, B-R.; Dzyuba, S. V.; Bartsch, R. A.; Quitevis, E. L. *J. Phys. Chem. A* **2002**, *106*, 7579. (c) Shirota, H.; Funston, A. M.; Wishart, J. F.; Castner, E. W., Jr. *J. Chem. Phys*. **2005**, *122*, 184512. (d) Cang H.; Li, J.; Fayer, M. D. *J. Chem. Phys.* **2003**, *119*, 13017.
130. Weber, G.; Shinitzky, M.; Dianoux, A. C.; Gitler, C. *Biochemistry* **1971**, *10*, 2106.
131. (a) Shinitzky, M. *Isr. J. Chem.* **1974**, *12*, 879. (b) Turro, N. J.; Tanimoto, Y. *Photochem. Photobiol.* **1981**, *34*, 157.
132. (a) Chen, M.; Grätzel, M.; Thomas, J. K. *J. Am. Chem. Soc.* **1975**, *97*, 2052. (b) Kalyansundaram, K.; Grätzel, M.; Thomas, J. K. *J. Am. Chem. Soc.* **1975**, *97*, 3915.
133. (a) Correll, G. D.; Cheser, R. N.; Nome, F., III; Fendler, J. H. *J. Am. Chem. Soc.* **1978**, *100*, 1254. (b) Zinsli, P. E. *J. Phys. Chem.* **1979**, *83*, 3223.
134. (a) Lentz, B. R.; Barenholz, Y.; Thompson, T. E. *Biochemistry* **1976**, *15*, 4521. (b) Andrich, M. P.; Vanderkooi, J. M. *Biochemistry* **1976**, *15*, 1257.
135. (a) Weber, G. *Biochem. J.* **1952**, *51*, 155. (b) Laurence, D. J. R. *Biochem. J.* **1952**, *51*, 168.
136. Yguerabide, J., Foster, M. C. In *Molecular Biology, Biochemistry and Biophysics: Membrane Spectroscopy*; Grell, E., Ed.; Springer-Verlag: New York, 1982; p 199.
137. (a) Kinosita, K., Jr.; Kataoka, R.; Kimura, Y.; Gotoh, O.; Ikegami, A. *Biochemistry* **1981**, *20,* 4270. (b) Kawato, S.; Kinosita, K., Jr.; Ikegami, A. *Biochemistry* **1977**, *16*, 2319. (c) Kinosita, K., Jr.; Ikegami, A.; Kawato, S. *Biophys. J.* **1982**, *37*, 461.
138. (a) Zachariasse, K. A. *Chem. Phys. Lett.* **1978**, *57*, 429. (b) Zachariasse, K. A.; Kuhnle, W.; Weller, A. *Chem. Phys. Lett.* **1980**, *73*, 6.
139. (a) Emert, J.; Behrens, C.; Goldenberg, M. *J. Am. Chem. Soc.* **1979**, *101*, 771. (b) Turro, N. J.; Aikawa, M.; Yekta, A. J. *J. Am. Chem. Soc.* **1979**, *101*, 772. (c) Viriot, M. L. ; Bouchy, M. ; Donner, M. ; Andri, J. C. *Photobiochem. Photobiophys.* **1983**, *5*, 293.

140. (a) Pajot-Augy, E.; Bokobza, L.; Monnerie, L.; Castellan, A.; Bouas-Laurent, H. *Macormolecules* **1984**, *17*, 1490. (b) Bokobza, L.; Pajot-Augy, E.; Monnerie, L.; Castellan, A.; Bouas-Laurent, H. *Polymer* **1988**, *29*, 251.
141. (a) Haidekker, M. A.; Brady, T. P.; Lichlyter, D.; Theodorakis, E. A. *Bioorg. Chem.* **2005**, *33*, 415. (b) Haidekker, M. A.; Theodorakis, E. A. *Org. Biomol. Chem.* **2007**, *5*, 1669.
142. Loutfy, R. O. *Pure Appl. Chem.* **1986**, *58*, 1239.
143. (a) Iwaki, T.; Torigoe, C.; Noji, M. Nakanishi, M. *Biochemistry* **1993**, *32*, 7589. (b) Haidekker, M. A.; Heureux, N. L.; Frangos, J. A. *Am. J. Physiol. Heart Circ. Physiol.* **2000**, *278*, H1401. (c) Haidekker, M. A.; Ling, T.; Anglo, M.; Steven, H. Y.; Frangos, J. A.; Theodorakis, E. A. *Chem. Biol.* **2001**, *8*, 123. (d) Haidekker, M. A.; Tsai, A. G.; Brady, T.; Stevens, H. Y.; Frangos, J. A.; Theodorakis, E.; Intaglietta, M. *Am. J. Physiol. Heart Circ. Physiol.* **2002**, *282*, H1609. (e) Gautam, P.; Harriman, A. *J. Chem. Soc., Faraday Trans.* **1994**, *90*, 697.
144. (a) Grieser, F.; Lay, M.; Thitlethwaite, P. J. *J. Phys. Chem.* **1985**, *89*, 2065. (b) Law, K. Y. *Photochem. Photobiol.* **1981**, *33,* 799. (c) Hasegawa, M.; Sugiura, T.; Shindo, Y.; Kitahara, A. *Colloids Surf., A* **1996**, *109*, 305.
145. (a) Kung, C. E.; Reed, J. K. *Biochemistry* **1986**, *25*, 6114. (b) Kung, C. E.; Reed, J. K. *Biochemistry* **1989**, *28*, 6678. (c) Lukac, S. *J. Am. Chem. Soc.* **1984**, *106*, 4386.
146. (a) Loutfy, R. O.; Law, K. Y. *J. Phys. Chem.* **1980**, *84*, 2803. (b) Loutfy, R. O.; Arnold, B. A. *J. Phys. Chem.* **1982**, *86*, 4205.
147. Law, K. Y. *Chem. Phys. Lett.* **1980**, *75*, 545.
148. Förster, Th.; Hoffmann, G. *Z. Phys. Chem. (Weisbaden)* **1971**, *75*, 63.
149. (a) Muldoon, M. J.; McLean, A. J.; Gordon, C. M.; Dunkin, I. R. *Chem. Commun.* **2001**, 2364. (b) Lancaster, N. L.; Salter, P. A.; Welton, T.; Young, G. B. *J. Org. Chem.* **2002**, *67*, 8855.
150. (a) Gordon, C. M.; McLean A. J. *Chem. Commun.* **2000**, 1395. (b) Alvaro, M.; Ferrer, B.; Garcia, H.; Narayana, M. *Chem. Phys. Lett.* **2002**, *362*, 435. (c) Marquis, S.; Ferrer, B.; Alvaro, M.; Garcia, H.; Roth, H. D. *J. Phys. Chem. B* **2006**, *110*, 14956.
151. (a) Gutkowski, K. I.; Japas, M. L.; Aramendia, P. F. *Chem. Phys. Lett.* **2006**, *426*, 329. (b) Lu, J.; Liotta, C. L.; Eckert, C. A. *J. Phys. Chem. A* **2003**, *107*, 3995.

Chapter 2

Materials, Instrumentation and Methods

This chapter lists the materials used in this study procured from various commercial sources followed by the methods of purification of reagents and solvents. Synthesis and purification of the RTILs employed in the present study have also been described. The instrumental details, especially the time-correlated single-photon counting technique (TCSPC) based picosecond setup and nanosecond laser flash photolysis setup have been outlined. Various methodologies employed in the present investigation, such as measurements of fluorescence quantum yield, analysis of TCSPC data, estimation of $E_T(30)$ values of RTILs have been discussed. The method of analysis of data for spectral reconstruction of the time-resolved emission spectra from the decay curves has also been discussed.

2.1. Materials

Laser grade C153 was procured from Eastman Kodak and used as received. Spectroscopic grade DCVJ and prodan were procured from Molecular probes and used without further purification. AP was obtained from TCI (Japan) and recrystallized twice from ethanol/water mixture prior to photophysical experiments. Pyrene was recrystallized twice from ethanol. The purity of all compounds was checked by single spot in thin layer chromatography (TLC), as well as by matching the absorption and emission spectra with literature.

The various drying agents such as calcium sulphate ($CaSO_4$), phosphorous pentoxide (P_2O_5), potassium hydroxide (KOH) and sodium metal, used at

different stages of the purification procedure, were purchased from local companies. Calcium hydride was obtained from Spectrochem (India). N,N-dimethylaniline was obtained from Aldrich. GR grade solvents were obtained from Merck (India) for spectroscopic and synthetic purposes and their purification procedures are given in the following section. Deuteriated solvents, chloroform-d, methanol-d_4 and acetone-d_6 used for NMR spectral measurements were obtained either from Aldrich or from Merck (India).

The reagents required for synthesis of various RTILs employed in different studies embodied in this thesis were obtained from various sources and carefully purified following standard procedure. The materials like 1-methyimidazole, sodium tertafluoroborate ($NaBF_4$), 1-chlorobutane, 1-bromoethane, 1-hydroxy-2-bromoethane, 1-hydroxy-2-chloroethane and 1,1,1-tricholoroethane were obtained from Acrös. Hexafluorophosphoric acid (65% solution in water) was procured from Lancaster, whereas sodium hexafluorophosphate ($NaPF_6$) and lithilum bis(trifluoromethanesulfonyl)imide ($LiTf_2N$) were obtained from Aldrich.

The ionic liquid, [emim][$EtSO_4$] was obtained as free sample from Wako Chemicals (Japan) and this liquid was rigorously dried under high vacuum before use.

2.2. Purification of conventional solvents and reagents

The solvents used at various stages of the study were purified using the procedures available in the literature.[1] We have adopted the following procedures for the purification of various solvents.

Toluene and 1,4-dioxane: The solvent was refluxed over metallic sodium for 3-4 hr and then benzophenone was added after cooling. The dark blue solution was

refluxed for another hour and distilled under dry condition. The purified solvents were optically transparent in the spectral region of interest.

Dichloromethane (DCM): The solvents were stirred with calcium hydride for 5-6 hr and then distilled. The distilled solvent was collected and stored under dry condition.

Ethyl acetate: After stirring with P_2O_5 for some hours, the solvent was distilled out.

Acetone: At first it is refluxed for some hours with anhydrous $CaSO_4$ and then the solvent was distilled out.

Water: Water was initially distilled using potassium permanganate and potassium hydroxide. This was subsequently distilled twice before taken to study.

N,N-dimethylaniline (DMA): This reagent was procured from Aldrich and was dried for 12 hrs with anhydrous KOH beads. Then the amine was distilled under reduced pressure in a reagent bottle wrapped with aluminium foil. For experimental purposes, only freshly distilled DMA was used.

2.3. Synthesis and purification of RTILs

Methods for preparation of imidazolium RTILs have been depicted in Scheme 2.1. A brief description of synthesis of individual RTIL is outlined in the following discussion.

2.3.1. [bmim][BF_4]

[bmim][BF_4] was prepared from its chloride salt, [bmim]Cl, following a standard procedure.[2] The latter was first prepared by treating a mixture of 1-methylimidazole (distilled from KOH under reduced pressure) and 1-chlorobutane

(distilled from P_2O_5), taken in 1:2 mole ratio, at 65°C for 48-60 hrs under nitrogen.[3] It should be noted that the addition of 1-chlorobutane has to be slow and under cooling condition. The reaction mixture was then cooled down to room temperature and kept overnight in an ice-acetone bath in tightly sealed condition. The white solid salt so obtained was washed several times with dry warm ethyl acetate until the washings were free from unreacted 1-methylimidazole. The halide salt was then rigorously dried under high vacuum before proceeding to the next reaction step.

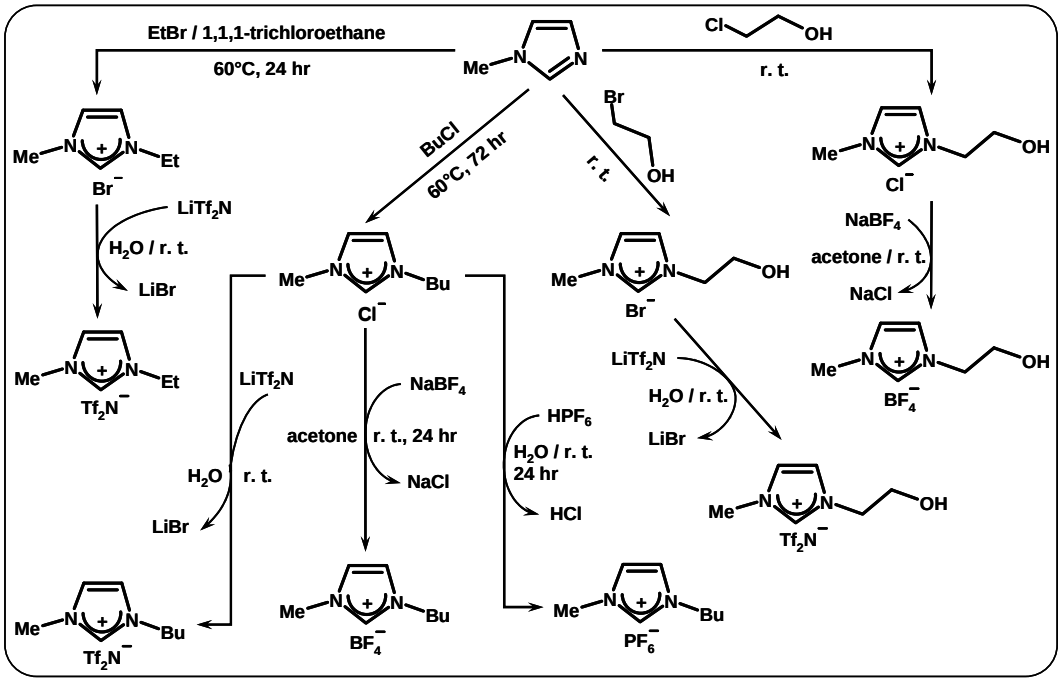

Scheme 2.1. Synthetic steps of various RTILs employed in the present study.

The solid [bmim]Cl was then taken in dry-distilled acetone and to it $NaBF_4$ (in 1:1.2 mole ratio) was added under inert atmosphere. The resulting mixture was then stirred for 24 hrs at room temperature under nitrogen. The resulting solution of [bmim][BF_4] was then filtered through a plug of celite and the volatiles were removed under reduced pressure.

2.3.2. [bmim][PF_6]

[bmim][PF_6] was prepared from [bmim]Cl using the following procedure.[4] A dilute aqueous solution of [bmim]Cl was prepared in a plastic box and cooled to 0-4°C in an ice bath. To this ice-cold solution was added ice-cooled HPF_6 (65% solution in water), maintaining 1:1.5 molar proportion, dropwise over an hour or so with constant vigorous stirring. This slow addition prevented significant rise of the temperature and avoided rapid exothermic reaction. The reaction mixture was then stirred for 24 hrs at room temperature. After decanting the upper acidic layer, the lower viscous ionic liquid portion was washed with excess water until it was free from acid (checked by a pH paper).

2.3.3. [bmim][Tf_2N] and [emim][Tf_2N]

[bmim][Tf_2N] was prepared from [bmim]Cl in the following way.[5] The chloride salt and $LiTf_2N$ were dissolved in equimolar amount in doubly distilled de-ionized water and the mixture was stirred for at least 18 hrs, first in room temperature and then at 50-60°C, but always under nitrogen atmosphere. After cooling the mixture, the viscous lower part (hydrophobic) was separated and washed with water for 4-5 times, until and unless no trace of halide was detected in the wash-liquid by $AgNO_3$ test.

Using a similar procedure [emim][Tf_2N] was synthesized from the corresponding bromide salt, [emim]Br. [emim]Br, was prepared in a very similar procedure as that of [bmim]Cl.[5] A mixture of 1-methylimidazole and 1-bromoethane, taken in 1:2 mole ratio in 1,1,1-trichloroethane, was stirred at 60-65°C for 24 hrs under nitrogen. Subsequent treatment of the resulting mixture was the same as in [bmim]Cl and the resulting white solid was then used in the next step. The bromide salt and $LiTf_2N$, taken 1:1 mole ratio in water, was stirred for 12 hrs at room temperature and the resulting hydrophobic liquid was then separated and washed with water quite a few times to remove the precursors.

2.3.4. [OH-emim][Tf_2N] and [OH-emim][BF_4]

[OH-emim][Tf_2N] was synthesized according to a published procedure.[6] In brief, 1-methylimidazole and 2-bromoethanol were stirred for 24 hrs in an inert atmosphere under room temperature to obtain 1-(2-hydroxyethyl)-3-methylimidazolium bromide ([OH-emim]Br) as a supercooled liquid, which when treated with ethyl acetate, yielded white solid at room temperature. It was washed further with ethyl acetate and then dried.

This bromide salt was then treated with $LiTf_2N$ in water at room temperature to yield the desired ionic liquid. The ionic liquid was washed 3-4 times with de-ionized distilled water until it was free from halide (confirmed by the $AgNO_3$ test on the wash-liquid).

The other salt, [OH-emim][BF_4] was prepared from the corresponding chloride salt, [OH-emim]Cl.[7] The latter was synthesized from 1-methylimidazole and 2-chloroethanol using the same procedure described for [OH-emim]Br. This chloride salt, obtained as a white solid, was then treated with $NaBF_4$ in dry

acetone at room temperature to yield the desired ionic liquid. Acetone was removed under reduced pressure to obtain the neat RTIL.

2.3.5. Purification of the RTILs

The purification of RTILs is the most crucial step as these liquids are used as solvents for spectroscopic purposes. Care was taken to ensure that these liquids are free from impurities, particularly those which might contribute to the absorption/fluorescence in the wavelength region of interest. For hydrophobic RTILs like [bmim][PF_6], [bmim][Tf_2N], [emim][Tf_2N] and [OH-emim][Tf_2N], the freshly prepared liquids were washed many times with water to remove the unreacted precursors and halides. The removal of the halide impurities was ensured by the fact that the ionic liquids or the washings did not form any precipitate of silver halide when treated with aqueous $AgNO_3$ solution. For hydrophilic RTILs like [bmim][BF_4] and [OH-emim][BF_4], the halide content was minimized by using dry organics solvent like acetone for reaction, as it is reported that the solubility of halides in acetone is very low.[8] Typically, for NaCl, the solubility in acetone is 5.5×10^{-6} M.[9] For further purification, [bmim][BF_4] was diluted with dry DCM (freshly distilled), quickly filtered through small celite plug and then DCM was evaporated under reduced pressure to furnish neat RTIL. This process is repeated 2-3 times for effective removal of precursors and residual halides. The same procedure was adopted for [OH-emim][BF_4], but it was found to be less effective as the miscibility of this RTIL with DCM is very less.

All the RTILs were then dried under high vacuum (pressure 10^{-2}-10^{-3} mbar), sometimes with heating at 50-60°C, for at least 10-12 hrs to minimize the water

content and for the removal of the traces of organic impurities, if any, present in these liquids.[10] In this way effectively dry ionic liquid was obtained. The RTILs thus prepared were characterized by NMR and IR spectroscopic techniques (compared with the literature data)[2-7] and then stored in vacuum desiccator under nitrogen atmosphere wrapped by aluminum foil.

2.4. Instrumentation

The IR and NMR spectra were measured using Jasco FTIR 5300 spectrometer and Bruker AVAnce 400 MHz NMR spectrometer, respectively. Steady-state absorption and fluorescence spectra were recorded on a UV-vis spectrophotometer (Cary100, Varian) and a spectrofluorimeter (FluoroLog-3, Jobin Yvon), respectively. For the measurement of steady-state fluorescence at variable temperatures, FluoroMax-4 (Horiba Jobin Yvon) spectrofluorimeter with an attached Peltier temperature controller (Wavelength electronics) was used. The fluorescence spectra were corrected for the instrumental response. The viscosity of the RTILs and other viscous solvents was measured by a LVDV-III Ultra Brookfield Cone and Plate viscometer (1% accuracy and 0.2% repeatability). For variable temperature viscosity measurement, a Julabo water circulator bath was used.

2.4.1. Picosecond time-correlated single-photon counting setup

Time-resolved fluorescence measurements were carried out using a time-correlated single-photon counting (TCSPC) spectrometer (5000, IBH).[11] Diode lasers were used as excitation sources and a micro-channel plate (MCP) photomultiplier tube was used as the detector. Two diode lasers, namely, the one

having output at 374 nm with FWHM = 65 ps and the other with 439 nm output and 90 ps FWHM were used in the present study. The maximum repetition rate of the diode lasers was 1 MHz. A Hamamatsu R3809U-50 MCP-PMT (160-850 nm range) was used as a detector.

The lamp profile was recorded by placing a scatterer (dilute solution of Ludox in water) in place of the sample. Decay curves were analyzed by nonlinear least-squares iteration procedure using IBH DAS6 (Version 2.2) decay analysis software.

The same setup, with attached polarizers, was used for time-resolved anisotropy measurements and the same software was used to analyze the anisotropy data.

2.4.2. Nanosecond laser flash photolysis setup

The transient absorption measurements were performed by a laser flash photolysis (LFP) setup, which was equipped with a laser system (Q-switched Nd:YAG, pulse width ~8 ns) from Spectra Physics (Quanta-Ray INDI series) and a spectrometer from Applied Photophysics (model LKS.60). The spectrometer consisted of a 150 W pulsed xenon lamp, a programmable f/3.4 grating monochromator, a digitized oscilloscope (Agilent, 600 MHz), and an R-928 photomultiplier tube. The solutions were excited by the third harmonic (355 nm) of the laser. A perpendicular configuration was chosen for the excitation of the sample. Applied Photophysics LKS.60 Kinetic Spectrometer workstation software was used for the collection and analysis of the data. Some of the time-resolved fluorescence measurements were also made using the LFP setup (Chapter 4). For

this purpose, the light from the xenon lamp was blocked and the spectrometer was run in the emission mode.

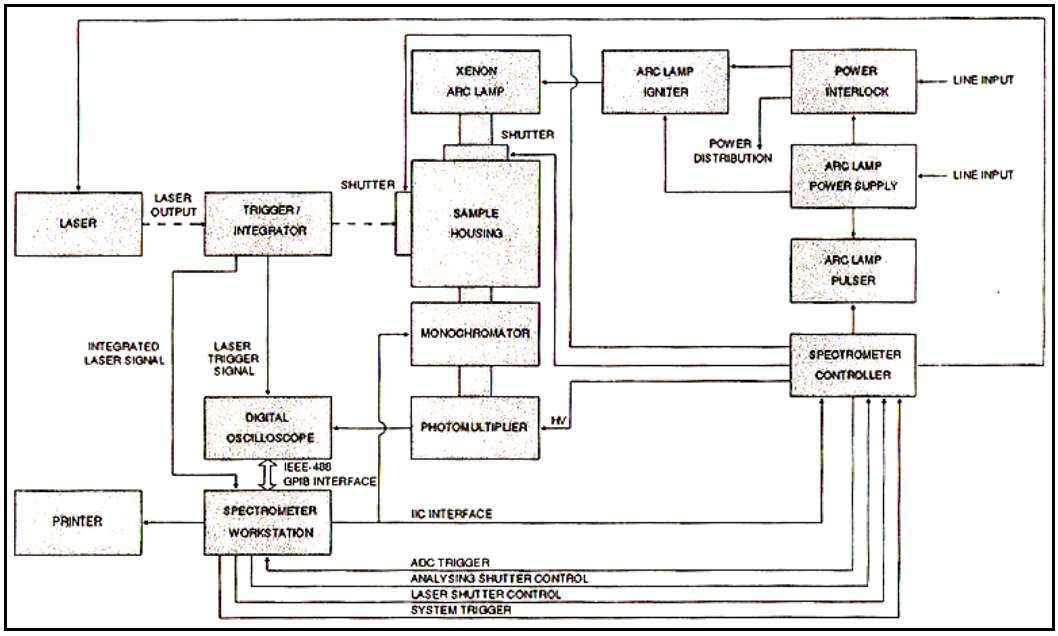

Scheme 2.2. Schematic diagram of the LFP setup (from page 34, LKS.60 hardware section of the user handbook of Applied Photophysics).

2.5. Sample preparation for spectral measurements

For measurements in conventional solvents, the solutions were prepared such that the absorbance of the solution (1 cm pathlength) at the excitation wavelength was around 0.1-0.2. The concentration of the probe molecules corresponding to an absorbance value of 0.2 was found to be in the range of 10^{-6}-10^{-4} M.

In case of experiments in RTILs, the sample preparation was not so straightforward. Prior to the sample preparation, these liquids were dried under high vacuum at 50-60°C for 10-12 hrs in order to ensure the removal of the

trapped moisture, if any, in RTILs. Generally 2.5 ml of RTIL was used to prepare sample solution in 1 cm quartz cuvette. After addition of sample solute, the cuvettes were tightly sealed with septum and parafilm. Since the dissolution of the solid probes in RTILs is slow, the absorption spectra were measured from time to time to ensure the complete dissolution. The concentration of the solute was optimized to have 0.2-0.3 absorbance at the excitation wavelength. For fluorescence probes with long lifetime and oxygen sensitivity, cf. pyrene, the solutions were deoxygenated by purging argon gas.

For laser flash photolysis experiments described in Chapter 4, quartz cuvettes with pathlength of 0.3 cm were used and the probe (pyrene) concentration was such that the absorbance was around 0.1 at the excitation wavelength (355 nm). The solutions were deaerated by purging argon gas into the cuvettes for about 30 minutes prior to the experiments.

2.6. Measurement of the fluorescence quantum yield

For fluorescence quantum yield measurements, optically matched solutions (or solutions with very similar absorbances) of the sample and the standard at a given absorbing wavelength (the excitation wavelength) were prepared. The quantum yield was calculated by measuring the integrated area under the emission curves and by using the following equation,[12]

$$\Phi_{sample} = \frac{A_{sample} \times OD_{std} \times n^2_{sample}}{A_{std} \times OD_{sample} \times n^2_{std}} \times \Phi_{std} \qquad (2.1)$$

where, Φ is the quantum yield, A is the integrated area of emission, OD is the optical density at the excitation wavelength, and n is the refractive index. The

subscripts ‘sample’ and ‘std’ refer to the fluorophore of unknown quantum yield and the reference fluorophore of known quantum yield, respectively.

2.7. Data analysis

The lifetimes of the samples were estimated from the measurements of fluorescence decay curves and the instrumental profiles using a nonlinear least-squares iterative fitting procedure (using decay analysis software IBH DAS6, Version 2.2). This program uses a reconvolution method for the analysis of the experimental data.[13] When the decay time is long compared to the pulse width of the excitation pulse, the excitation may be described as a δ-function. However, when the lifetime is short, distortion of the experimental data occurs by the finite decay time of the lamp pulse and response time of the photomultiplier and associated electronics. Since the measured decay function is convolution of the true fluorescence decay and the instrumental pulse, it is necessary to analyze the data by deconvolution in order to get the actual fluorescence lifetime. The mathematical statement of the problem is given by the following equation:

$$D(t) = \int_0^t P(t')G(t - t')dt' \qquad (2.2)$$

where, D(t) is the fluorescence intensity at any given time t, P(t') is the intensity of the exciting light at time t' and G(t–t') is the response function of the experimental system. The experimental data D(t) and P(t') from the MCA were fed into a personal computer (PC) to determine the lifetime. We used the IBH program to analyze the multi-exponential decays. An excitation pulse profile was recorded and then deconvolution started with mixing of the excitation pulse and a

projected decay to form a new reconvoluted set. The data was compared with the experimental set and the difference between the data points was summed, generating χ^2 function for fitting. The deconvolution proceeded through a series of such iterations until an insignificant change of χ^2 occurred between iterations. The inspection of reduced χ^2, a plot of weighted residuals and autocorrelation function of the residuals allowed assessment of the quality of the fit.

2.8. Construction of time-resolved emission spectra (TRES)

The time-resolved emission spectra (TRES) were constructed by an indirect method described here.[14] A series of time-resolved emission decay profiles were measured at every 5/10 nm interval across the entire steady-state emission spectra. The total number of measurements was 28-30 in each case. Each decay curve was then fitted to a triexponential (or biexponential) decay function with an iterative reconvolution program (IBH), to obtain the best fits with χ^2 around 1.0-1.2. This procedure deconvoluted the measured decay from the instrumental response and increased the effective time resolution of the experiment to ~40 ps. The *impulse response function*, I(λ,t) was then calculated from the best-fitted curve for each wavelength. To make the time-integrated intensity at each wavelength equivalent to the steady-state intensity at that particular wavelength, a normalization factor of the following form

$$H(\lambda) = \frac{I_{ss}(\lambda)}{\sum_i \alpha_i(\lambda)\tau_i(\lambda)} \tag{2.3}$$

was constructed, where, $I_{ss}(\lambda)$ is the steady-state intensity, $\alpha_i(\lambda)$ and $\tau_i(\lambda)$ are the preexponential factor and decay time, respectively, at a particular wavelength

with $\sum\alpha_i(\lambda) = 1$. The time-resolved emission spectra (TRES) were calculated from the appropriately normalized intensity decay (impulse response) function, $I'(\lambda,t)$ for the given set of wavelengths at different times, where $I'(\lambda,t) = H(\lambda) \times I(\lambda,t)$. The peak emission frequencies (in cm^{-1}), $\bar{\nu}(t)$ at various times were obtained by fitting each TRES to the following log-normal function,[15]

$$I = h \exp[-\ln 2\{\ln(1+\alpha)/\gamma\}^2] \qquad for,\ \alpha > -1 \qquad (2.4)$$

$$= 0 \qquad for,\ \alpha \leq -1$$

where, $\alpha = \dfrac{2\gamma(\bar{\nu} - \bar{\nu}_{peak})}{\Delta}$, $\bar{\nu}_{peak}$ = wavenumber corresponding to the peak, h = peak height, Δ = full-width at half-maxima and γ corresponds to the asymmetry of the band-shape. Optimizing these four parameters by nonlinear least-squares iteration technique the best fitted curve was obtained.

2.9. Estimation of polarity in $E_T(30)$ scale

The solvatochromic visible absorption of the betaine dye has been used as a solvent dependent reference probe to define empirically a solvent polarity scale, namely $E_T(30)$ scale.[16] These $E_T(30)$ values are defined as the molar transition energies of the pyridinium-N-phenoxide betaine dye (shown in Chart 1.3), measured in solvents of different polarity at room temperature (25°C) and normal pressure (1 bar). Thus,

$$E_T(30)/\text{kcal mol} = hc\bar{\nu}_{max}N_A = (2.8591 \times 10^{-3})\ \bar{\nu}_{max}\ /cm^{-1}$$

$$= 28591/\lambda_{max}\ (nm) \qquad (2.5)$$

where, $\bar{\nu}_{max}$ is the wavenumber and λ_{max} is the wavelength corresponding to the maximum of the long-wavelength, solvatochromic, intramolecular charge transfer

absorption band of the standard betaine dye; and h, c, and N_A are Planck's constant, speed of light, and Avogadro number, respectively. This is the direct way of solvent polarity measurement.

As mentioned in Chapter 5, the $E_T(30)$ values of the RTILs were also measured using probes other than the standard betaine dye, by an indirect method.[17] Here, the wavenumber corresponding to the fluorescence maximum, $\bar{\nu}_{max}^{fluo}$ of each probe molecule in various conventional solvents was measured at room temperature. A calibration line was drawn by plotting measured $\bar{\nu}_{max}^{fluo}$ values (in cm^{-1}) against the known $E_T(30)$ values of the solvents, from which the $E_T(30)$ value of a RTIL was obtained using the measured $\bar{\nu}_{max}^{fluo}$ value of the probe in the given RTIL.

2.10. Standard error limits

Standard error limits involved in the measurements are:

λ_{max} (abs./fluo.)	± 1 nm
Φ_f	± 10%
τ_f (> 1 ns)	± 5%
τ_f (< 1 ns)	± 5-8% (depending on the excitation source used)
Polarity of RTILs in $E_T(30)$ scale	± 5%
Relaxation time	± 5%
Viscosity	± 2%

References

1. Perrin, D. D.; Armerego, W. L. F.; Perrin, D. R. *Purification of Laboratory Chemicals*; Pergamon Press: New York, 1980.
2. (a) Suarez, P. A. Z.; Dullius, J. E. L.; Einloft, S.; De, Souza, R. F.; Dupont, J. *Polyhedron* **1996**, *15*, 1217. (b) Austin, E.; Gouterman, M. *Bioinorg. Chem.* **1978**, *9*, 281.
3. Hasan, M; Kozhevnikov, I. V.; Siddiqui, M. R. H.; Steiner, A.; Winterton, N. *Inorg. Chem.* **1999**, *38*, 5637.
4. Huddleston, J. G.; Willauer, H. D.; Swatlosky, R. P.; Visser, A. E.; Rogers, R. D. *Chem. Commun.* **1998**, 1765.
5. Bonhote, P.; Dias, A. P.; Papageorgiou, N.; Kalyanasundaram, K.; Gratzel, M. *Inorg. Chem.* **1996**, *35*, 1168.
6. Dzyuba, S. V.; Bartsch, R. A. *Tetrahedron Lett.* **2002**, *43*, 4657.
7. Branco, L. C.; Rosa, J. N.; Ramos, J. J. M.; Afonso, C. A. M. *Chem. Eur. J.* **2002**, *8*, 3671.
8. Fuller, J.; Carlin, R. T; Osteryoung, R. A. *J. Electrochem. Soc.* **1997**, *144*, 3881.
9. Holbray, J. D.; Seddon K. R. *J. Chem. Soc., Dalton Trans.* **1999**, 2133.
10. Seddon, K. R.; Stark, A.; Torres, M. J. In *Clean Solvents: Alternative Media for Chemical Reactions and Processing*; Abraham, M., Moens, L., Eds.; ACS Symposium Series 819; American Chemical Society: Washington, DC, 2002.
11. O. Connor, D. V.; Philips, D. *Time-Correlated Single Photon Counting*; Academic Press: New York, 1984.
12. Austin, E.; Gouterman, M. *Bioinorg. Chem.* **1978**, *9*, 281.
13. Bevington, P. R. *Data Reduction and Analysis for the Physical Sciences*; McGraw-Hill: New York, 1969.
14. Lakowicz, J. R. *Principles of Fluorescence Spectroscopy*; 2nd Ed.; Kluwer Academic/Plenum Press: New York, 1999.
15. (a) Fraser, R. D. B.; Suzuki, E. In *Spectral Analysis*; Blackburn, J. A. Ed.; Marcel Dekker: New York, 1970. (b) Horng, M. L.; Gardecki, J. A.; Papazyan, A.; Maroncelli, M. *J. Phys. Chem.* **1995**, *99*, 17311.
16. Reichardt, C. *Solvents and Solvent Effects in Organic Chemistry*; VCH: Weinheim, Germany, 1988.
17. Mandal, P. K.; Samanta, A. *J. Phys. Chem. B* **2005**, *109*, 15172.

Chapter 3

Optical Properties of the Imidazolium Ionic Liquids

This chapter describes the optical properties of some carefully synthesized and rigorously purified imidazolium ionic liquids, generally believed to be transparent in most of the UV region and fully transparent in the visible region. Contrary to what is known in the literature, we have shown that the imidazolium ionic liquids have significant absorption in the UV region with a long absorption tail in the visible region and give rise to an interesting fluorescence, which shows an unusually large shift of the emission band on changing the excitation wavelength. The observation has been accounted for taking into consideration the existence of energetically different associated species and the inefficiency of the energy transfer process between them.

3.1. Introduction

Room temperature ionic liquids (RTILs), particularly those based on substituted imidazolium cations, are currently being extensively studied for a variety of applications. The most commonly used salts are the ones involving unsymmetrically substituted imidazolium cations and bulky inorganic anions such as PF_6^-, BF_4^-, $(CF_3SO_2)_2N^-$ (commonly known as Tf_2N^-) etc. The property of the RTIL that is most attractive from the point of view of its environmentally benign nature is its negligible vapor pressure. Wide liquidus, thermal stability, miscibility with other solvents, high ionic conductivity and wide electrochemical window etc are some of the other properties that make these liquids suitable as solvents for various applications.[1-8] These ionic liquids are considered as “designer solvents”

as RTIL with a desired property can be designed using an appropriate combination of the cationic and anionic constituents. A brief account of the physicochemical properties, structural features and applications of RTILs has already been given in Chapter 1.

Among the versatile application of RTILs, its utility as novel media for studying various photophysical processes is also noteworthy. The optical behavior of several dissolved solutes has been examined in RTILs. The UV-vis absorption and luminescence spectral studies involving several dye molecules have been carried out to measure the polarity or solvent strength of these ionic liquids.[9-18] Empirical polarity parameters of various RTILs, which have been determined using a number of dye molecules,[9] suggest that most of the imidazolium RTILs are more polar than acetonitrile but less polar than methanol. Other photophysical studies like solvent relaxation dynamics,[10-13] electron and energy transfer kinetics,[14] photoisomerization[15] etc have also been carried out in RTILs. Unconventional fluorescence of dipolar molecules showing an excitation wavelength dependent behavior has also been observed in these media.[16] Several optical studies on dissolved solutes in RTILs based mixed solvents and microheterogeneous systems have also been performed.[17,18]

Even though the optical properties of a large number of systems, most of which are fluorescent, have been studied in detail in various RTILs, there was hardly any focused study on the optical properties of these liquids. Most of the remarks on the optical properties of the RTILs have been made while examining some other properties. Most of these studies give an impression that RTILs are optically transparent for most of the UV region and completely in the visible

region.[19-23] While some groups have indicated that the RTILs are transparent from 300 nm onward,[19-21] some others have suggested that one of the imidazolium ionic liquids is transparent above 240 nm.[22] The most comprehensive exploration of the optical properties of an ionic liquid has been made by Billard et al.[23] during a study of the spectral behavior of Eu(II) in [bmim][PF_6] (Chart 3.1). These authors examined the effect of repeated purification of [bmim][PF_6] on the absorption behavior and showed that the absorption band of [bmim][PF_6] in the 250-300 nm range was suppressed on purification. However, since the spectra have been shown on a high OD scale, it is not clear whether pure [bmim][PF_6] is fully transparent in the 250-300 nm range, and, if not, whether the residual absorption in this region is due to some impurity present in RTIL. Secondly, an emission is reported for the purified [bmim][PF_6]. However, it is not clear whether or not the emission is due to some impurity that cannot be separated from the given RTIL.[23] In recent years some more efforts have been directed towards the *decolorization* of imidazolium RTILs for their use in spectroscopic studies.[24-26] These authors have described many decolorization procedures, most of which are rather conventional, such as the use of charcoal as decolorizing material or passing through an alumina column etc at various steps of synthesis. But, none has shown that the absorption spectrum of any imidazolium RTIL is optically transparent in the aforementioned UV-visible range.[24-26] In order to obtain definite information on the optical behavior of RTILs, we have undertaken the present work of exploring the absorption and emission properties of the RTILs based on imidazolium salts in detail. The RTILs studied here are depicted in Chart 3.1. With the help of the control experiments on the 1-methylimidazolium ion,

generated from 1-methylimidazole, we unambiguously establish that the weak absorption at 300 nm and beyond is indeed due to ionic liquids and that all the liquids exhibit a highly interesting fluorescence that stretches well into the visible region.

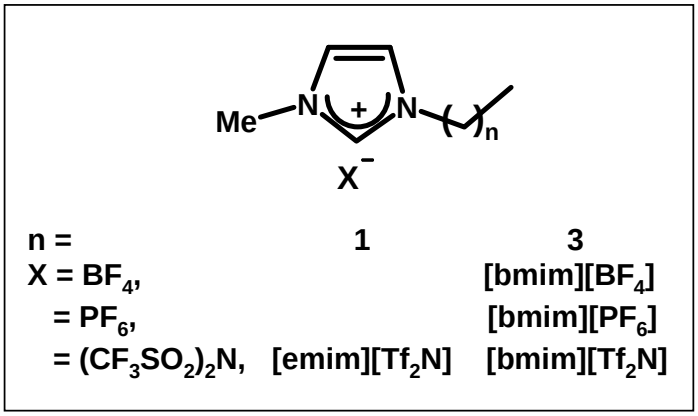

Chart 3.1. Structure and abbreviation of the RTILs described in this work. emim ≡ 1-ethyl-3-methylimidazolium, bmim ≡ 1-butyl-3-methylimidazolium, Tf_2N ≡ bis(trifluoromethanesulfonyl)imide.

The methods of preparation and purification of the RTILs described in this chapter have been discussed in detail in Chapter 2. More importantly, the RTILs were rigorously purified to ensure complete removal of the precursors and dried for several hours (10-12 hours) under high vacuum (10^{-2} mbar) to minimize the water content. The purified ionic liquids were characterized by both IR and NMR spectroscopy and stored in a desiccator under dry nitrogen wrapped by aluminum foils. However, only freshly prepared RTILs were used for the optical studies to avoid its contamination from any probable decomposition products.

3.2. Investigation on optical properties

3.2.1. Absorption

Fig. 3.1 depicts the absorption spectra of some most commonly used imidazolium RTILs as measured with a 1 cm pathlength cuvette. The spectral shape and nature of the absorption spectra of [bmim][PF_6] are consistent with those reported by Billard et al.[23] From Fig. 3.1 it is obvious that the absorption of RTILs is far from negligible and a long tail of the absorption extends even beyond 350 nm, though no clear maximum is observable above 250 nm. However, the molar extinction coefficient of this absorption of RTILs is quite low, e.g., the value estimated in acetonitrile solutions of [bmim][PF_6] is nearly 0.2 M^{-1} cm^{-1} at 275 nm, but it contributes to an OD of 0.8 at this wavelength in neat RTIL (Fig. 3.1(a)). In all cases, the absorbance is significant (around 0.07-0.14) even at 350 nm, suggesting that more than 15-25% of the incident light is absorbed by the RTIL at this wavelength.

Apart from the neat ionic liquids, we have also examined the absorption characteristics of [bmim]Cl. Since [bmim]Cl is a solid at room temperature, we have examined its spectral behavior in acetonitrile (Fig. 3.2). Again, the long tail is clearly visible in this case as well.

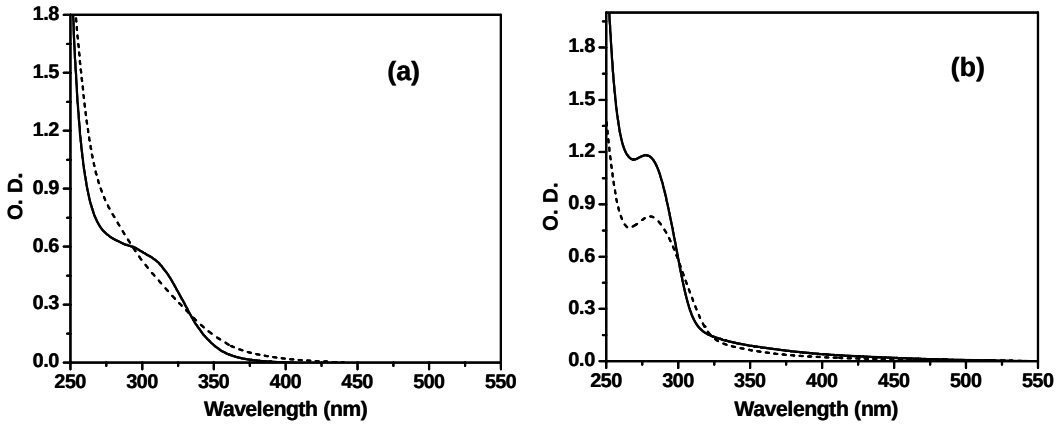

Fig. 3.1. Absorption spectra of neat RTILs as obtained using a 1 cm pathlength cuvette: (a) [bmim][BF_4] (—), [bmim][PF_6] (---) and (b) [bmim][Tf_2N] (—) and [emim][Tf_2N] (---).

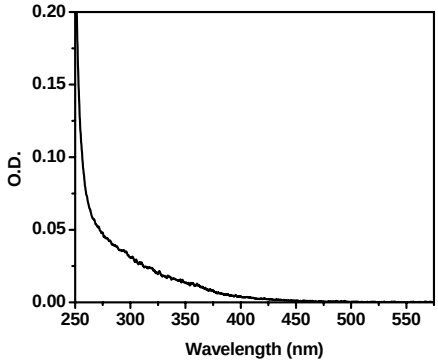

Fig. 3.2. Absorption spectra of [bmim]Cl (0.35 M) in acetonitrile as obtained using a 1 cm pathlength cuvette.

3.2.2. Emission

The fluorescence behavior of the RTILs employed in this study, namely [bmim][PF_6], [bmim][BF_4], [bmim][Tf_2N] and [emim][Tf_2N] is illustrated in Fig. 3.3. Interestingly, the most common feature of the fluorescence spectra of *all*

RTILs is that the spectral behavior is strongly dependent on excitation wavelength. Moreover, in each case, the emission for a single excitation wavelength is characterized by two components. For example, when [bmim][PF_6] is excited around 280-290 nm, the peaks corresponding to the two components appear at 337 and 410 nm (Fig. 3.3(a)). As the excitation wavelength (λ_{exc}) is increased, the 337 nm band becomes less intense and eventually disappears and the long wavelength band becomes prominent. Similarly, when [bmim][BF_4] is excited at wavelengths below 340 nm, it exhibits an emission band centered around 365 nm with a shoulder around 425 nm and the band profile extending beyond 500 nm. This two-component emission characteristic is also apparent in other two RTILs, [bmim][Tf_2N] and [emim][Tf_2N].

As mentioned earlier, the most interesting part of the observation is the excitation wavelength (λ_{exc}) dependence of the emission spectra of these RTILs. In case of [bmim][PF_6], as the λ_{exc} is increased beyond 320 nm, the long-wavelength emission peak starts to shift towards the longer wavelength. As can be seen (inset to Fig. 3.3(a)), the extent of the shift of the peak is unusually large (>100 nm). It is also important to note that the fluorescence is observable even when λ_{exc} > 400 nm, where the absorption due to the RTIL is almost negligible (Fig. 3.1(a)). Similar is the case with other RTILs, except for the fact that (i) the relative intensities of the two components, (ii) the value of λ_{exc} from which λ_{exc} dependent red shift of emission starts and (iii) the magnitude of red shift are different for different RTILs.

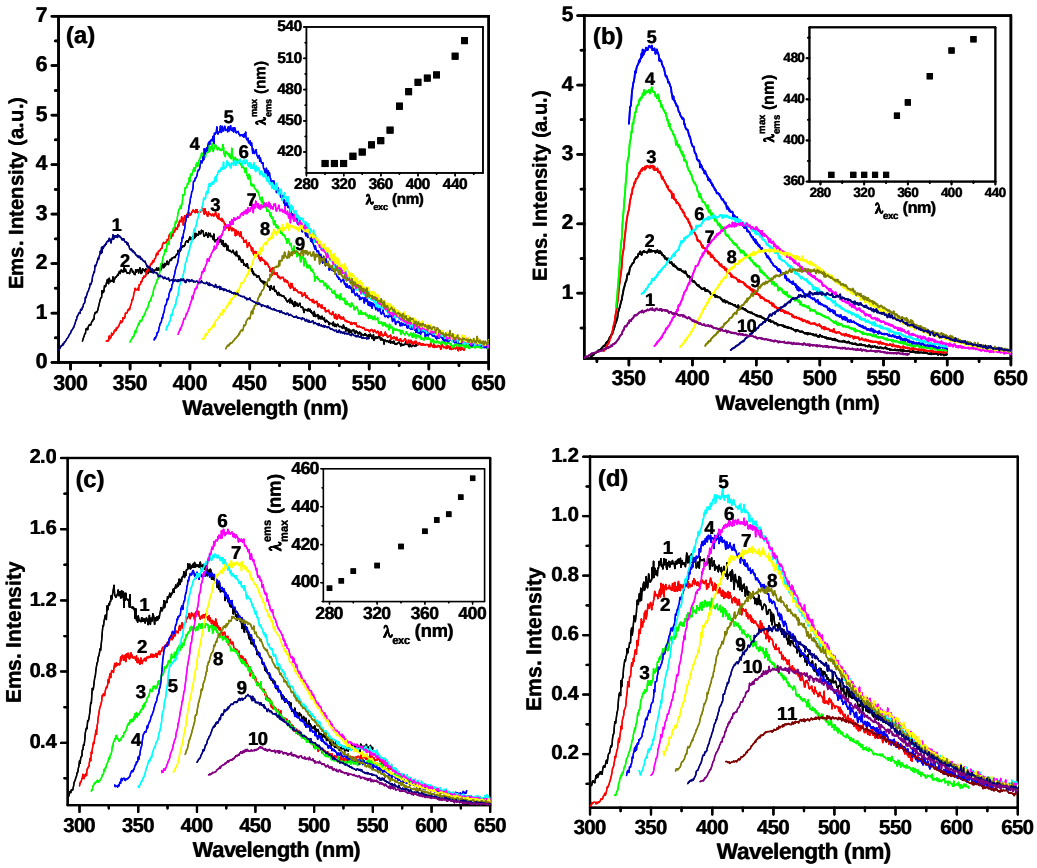

Fig. 3.3. Excitation wavelength-dependent emission behavior of neat RTILs: (a) [bmim][PF_6], λ_{exc} (nm) = 280 (1), 300 (2), 320 (3), 340 (4), 360 (5), 370 (6), 380 (7), 400 (8), 420 (9). (b) [bmim][BF_4]. λ_{exc} (nm) = 290 (1), 310 (2), 320 (3), 330 (4), 340 (5), 350 (6), 360 (7), 380 (8), 400 (9), 420 (10). (c) [bmim][Tf_2N], λ_{exc} (nm) = 280 (1), 290 (2), 300 (3), 320 (4), 340 (5), 360 (6), 370 (7), 380 (8), 390 (9), 400 (10). (d) [emim][Tf_2N], λ_{exc} (nm) = 280 (1), 290 (2), 310 (3), 320 (4), 330 (5), 340 (6), 350 (7), 360 (8), 370 (9) 380 (10), 400 (11). The inset shows the variation of the fluorescence peak position with the excitation wavelength for respective RTILs.

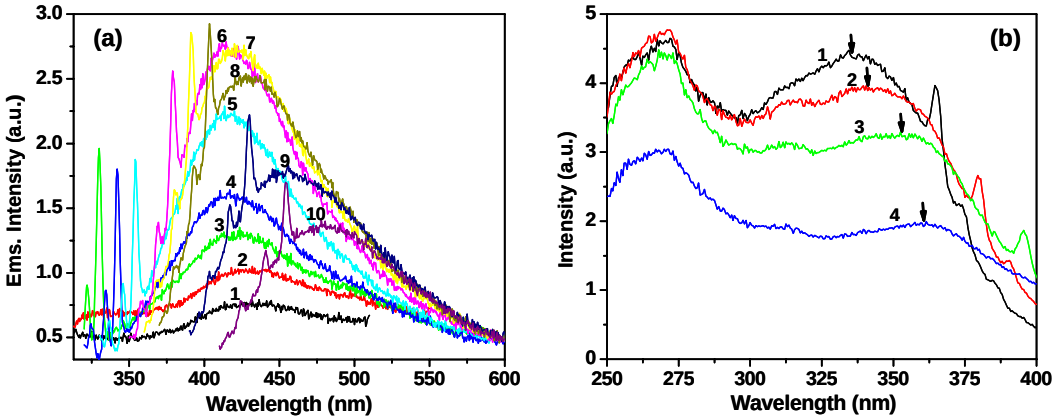

Fig. 3.4. (a) Emission spectra of [bmim]Cl in acetonitrile solution (0.35 M). λ_{exc} (nm) = 260 (1), 280 (2), 300 (3) 310 (4), 320 (5), 340 (6), 350 (7), 360 (8), 380 (9), 400 (10). The sharp peaks are Raman lines. (b) Fluorescence excitation spectra of [bmim]Cl in acetonitrile (0.35 M). λ_{ems} (nm) = 410 (1), 430 (2), 450 (3), 475 (4). The sharp peaks are Raman lines.

The fluorescence emission as well as excitation spectra of the acetonitrile solution of [bmim]Cl is shown in Fig. 3.4. Here also the two-component feature of the fluorescence is quite distinct: on excitation at around 270-280 nm, a short-wavelength band around 335 nm and a long-wavelength band around 415 nm is observed (Fig. 3.4(a)). With increase in the excitation wavelength, the long-wavelength emission gains intensity with no shift of the maximum up to an excitation wavelength of 340 nm. With further increase in the excitation wavelength, a shift of the fluorescence maximum similar to that observed in neat RTILs can be noticed (Fig. 3.4(a)). Figure 3.4(b) depicts the fluorescence excitation spectra of [bmim]Cl in acetonitrile for various monitoring wavelengths. As can be seen, the short wavelength band appears at the same place (270 nm),

whereas the long-wavelength emission band shifts progressively towards red. This shift is observable as long as it is possible to record an excitation spectrum.

In this context we note some of the recent investigations on the optical properties of imidazolium and other RTILs. Earle et al.[24] have tried for decolorization of RTILs, mostly using activated charcoal column to obtain a transparent liquid. However, though these RTILs are transparent in naked eye like our samples, they posses non-negligible absorption in the UV-visible region.[24] A similar attempt has been made by other groups using different methods, but a significant absorption in the aforementioned range has eventually been remained.[25,26] Burrell et al.[25] have tried to 'purify' imidazolium RTILs free from fluorescent impurities. However, using the same method of decolorization by activated charcoal, they have reported a fluorescence-free pyrrolidinium RTIL,[25] which is expected to be so because of lack of polarizable π-cloud. On the other hand, Gutkowski et al. have repoted the fluorescence spectra of [bmim][BF_4], which is very much similar to what we have observed for the same.[27] In summary, it can be said that the imidazolium RTILs possess non-negligible absorption and fluorescence in the UV-visible regime of the spectra.

3.2.3. Quantum yield and lifetime

The fluorescence efficiency and lifetime of the neat RTILs have also been measured. The fluorescence quantum yield measurements were performed using 4-aminophthalimide as the reference compound ($\Phi_f = 0.1$ in methanol).[28] Because of the λ_{exc} dependence of the two-component emission and its shifting nature, the fluorescence quantum yield (Φ_f) of the RTILs is dependent on λ_{exc}. Therefore, the fluorescence quantum yield has been estimated for a given excitation wavelength.

Thus, in case of neat [bmim][PF_6], for λ_{exc} = 360 nm, the Φ_f value is estimated to be 5 × 10^{-3}. A more or less similar value of Φ_f is obtained in case of neat [bmim][BF_4] for the same excitation wavelength. For the two Tf_2N-salts, the yield is also in the same range (4-7 × 10^{-3}).

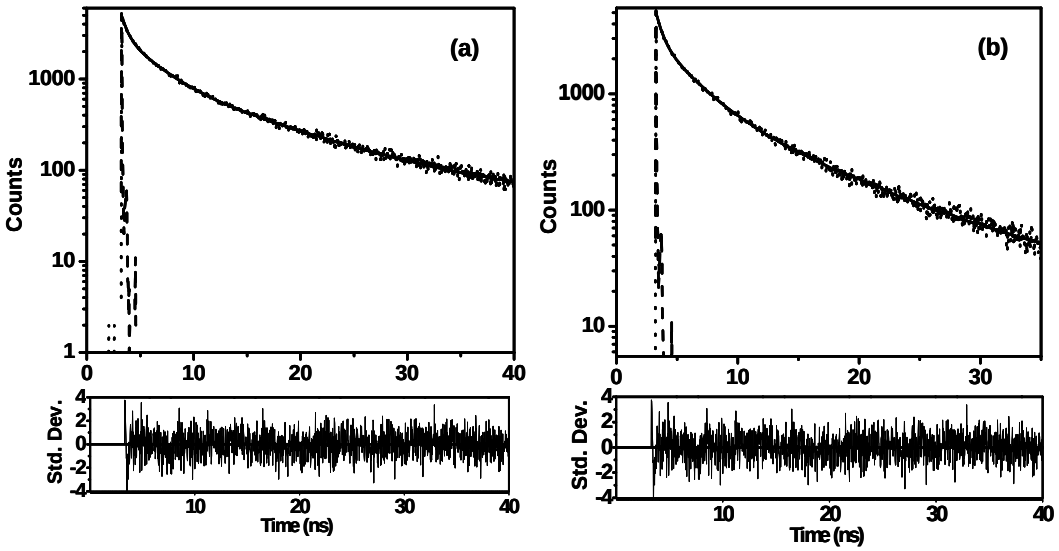

Fig. 3.5. Fluorescence decay profile of (a) [bmim][PF_6] and (b) [bmim][BF_4] as monitored at 550 nm. The experimental decay curve is shown as a dotted line and the instrument profile as a dashed line. The solid line is the triexponential fit to the decay curve. The residuals are indicated below. The χ^2 value corresponding to both plots is 1.1.

The fluorescence decay behavior of the RTILs has been studied by exciting the samples at 375, 390 and 420 nm and monitoring the fluorescence at various wavelengths between 400 and 600 nm. The variation of the decay parameters with the change in the monitoring wavelength and with the excitation wavelength is minimal for a given ionic liquid, and it did not show any particular trend. Further,

the lifetime components for the different ionic liquids are also very similar. The major component (~90%) of the decay consisted of a lifetime varying between 470 and 590 ps. Two other minor components with lifetimes of 2.4-2.9 ns (7%) and 8.5-11 ns (3%) are also observed. The typical fluorescence decay profiles for [bmim][PF_6] and [bmim][BF_4], as measured at around 550 nm, are shown in Fig. 3.5.

3.3. Discussion

The present results clearly suggest that imidazolium ionic liquids possess very similar absorption characteristics. All of them have non-negligible absorption at 300 nm and at longer wavelengths. A concentrated solution of [bmim]Cl also displays a similar absorption behavior. In order to prove that the absorption is not due to any impurity, we have adopted a strategy that is different from the one of comparing the absorption spectra of repeatedly purified samples of RTILs. That the absorption is actually due to the imidazolium moiety is proved by starting with pure 1-methylimidazole (MIM), generating the corresponding imidazolium cation by protonation and then examining whether the latter has negligible absorption in the region of interest.

Fig. 3.6 shows the absorption spectrum of a concentrated acetonitrile solution of MIM and the effect of addition of acid. Addition of HCl or CF_3COOH to a concentrated solution of MIM produces a new species, which absorbs relatively strongly in the longer wavelength region compared to MIM. The observation of an isosbestic point rules out the possibility of the formation of any third species. That the new species is the imidazolium ion is evident from the fact that the pK_a for the protonation equilibrium of MIM is reported to be 7.2.[29] In the presence of

excess acid, when MIM is expected to be fully protonated, the ~275 nm band and ~330 nm shoulder persisted implying that the imidazolium cation does absorb above 300 nm. Hence, we unambiguously establish that it is impossible to prepare imidazolium ionic liquids with no absorption above 300 nm.

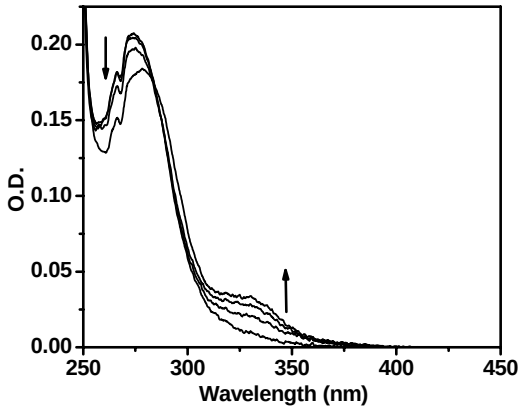

Fig. 3.6. Effect of addition of HCl on the absorption spectrum of acetonitrile solution of N-methylimidazole (1.7 M). The concentrations (in 10^{-2} M) of the acid (in increasing absorbance at 325 nm) are 0, 1.25, 2.5 and 4.8.

As far as the emission behavior is concerned, all imidazolium ionic liquids display rather similar emission characteristics. The higher energy band, centering around 330-360 nm (exact position depending upon the specific RTIL), remains stationary with respect to the increasing excitation wavelength, whereas the long wavelength (i.e., lower energy) band, continually shifts with increasing λ_{exc} value.

We now attempt to find out what gives rise to the long wavelength emission band and why the emission maximum corresponding to this band shifts continuously. It is evident from Fig. 3.3 that the long-wavelength emission band is observed when the excitation is made at the tail of the absorption band. We

have tentatively assumed that the long tail in the absorption band might be due to the presence of various associated species that are energetically different. At this point, let us take into consideration the necessary information relating to the structure of the imidazolium salts in their liquid state and examine whether the existence of energetically different associated structures has been indicated by recent studies. Several experimental and computer simulation studies have been carried out with a view to obtaining insight into the structures of the imidazolium salts in their liquid state.[30-36] Among the experimental studies, the results of the neutron scattering, NMR, X-ray scattering, and Raman spectroscopic measurements are particularly important.[32,33] Recent X-ray diffraction[34], XAFS,[35] optical Kerr effect[36] etc studies have shown the evidence of nanoscale ordering and local structure in RTILs. Even though the liquid state structure of the RTILs is still not fully understood, these studies clearly indicate several structures with both short and long-range spatial correlations of the cation-anion and cation-cation pairs, which we term as associated species. Again, though the large anions are located mostly above and below the plane of the imidazolium ring,[30] the existence of the multiple structures, and the large region of probability of finding an anion in the vicinity of a cation and vice versa, is expected to broaden the energy states of the absorbing species, and this can lead to a long tail.

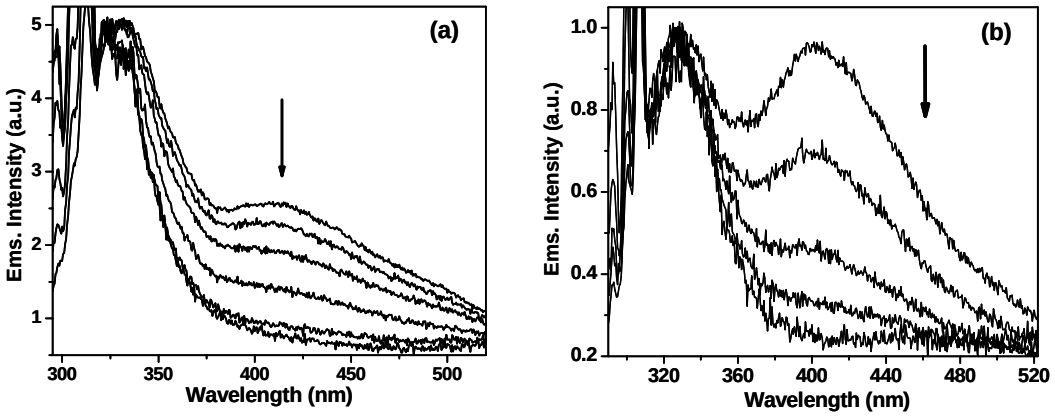

Fig. 3.7. Effect of dilution (using acetonitrile) on the fluorescence profile of (a) [bmim][PF_6], where λ_{exc} = 285 nm and (b) [bmim][Tf_2N] where λ_{exc} = 280 nm. The spectra are normalized at the lower wavelength emission maximum. The concentrations of [bmim][PF_6] in decreasing order of the fluorescence intensity at 425 nm are 0.35, 0.15, 0.07, 0.03, 0.007 and 0.0015 M, whereas that for [bmim][Tf_2N] are 0.4, 0.2, 0.1, 0.04 and 0.004 M.

That the long-wavelength emission band indeed arises from the excitation of the different associated structures, which comprise the long absorption tail of the RTILs, is evident from the effect of dilution on the fluorescence spectra. Fig. 3.7 shows that sufficient dilution of the ionic liquid results in complete disappearance of the long-wavelength emission band indicating the breaking of different kinds of associated structures of the ionic liquid.

The excitation wavelength dependence of the long-wavelength emission band can then be accounted for taking into consideration the existence of energetically different associated species. As the excitation wavelength is changed, a slightly different associated species is excited and an emission characteristic of this species is observed. This is clearly evident from the shift of the peak of the fluorescence excitation spectra with the monitoring wavelength (Fig. 3.4(b)).

These individual overlapping bands in the excitation spectra contribute to the tail of the absorption spectra of the ionic liquids. Thus, the excitation wavelength-dependent shift of the emission maximum arises from the heterogeneity (or multiplicity) of the structure of the ionic liquids.

Finally, the kind of fluorescence behavior observed for the RTILs, though not very common, is not unprecedented. Dipolar probes in viscous media, in organized assemblies such as membranes and proteins and even in the RTILs, exhibit this kind of excitation wavelength-dependent fluorescence behavior when excited at the red edge of the absorption band.[37-40] The phenomenon is commonly known as red-edge effect (REE) and is particularly useful in applications such as the measurement of the depth of a fluorophore in a membrane.[40] The literature suggests that REE can be observed when there exists a ground-state heterogeneity and when the excited-state relaxation (which can be an energy transfer or solvation process) is slow.[37] We believe that the heterogeneity of the structure of RTIL, which allows photoselection of energetically different associated species, and the high viscosity and short fluorescence lifetime, which make the relaxation of the photoexcited species inefficient, contribute to REE-like behavior in ionic liquids.

3.4. Conclusion

The electronic absorption and fluorescence spectra of several commonly utilized imidazolium salts have been examined. The results suggest that none of the imidazolium ionic liquids is transparent in the entire UV region. These liquids display a very interesting excitation wavelength-dependent fluorescence covering a significant portion of the visible region. Though the absorbance above 300 nm is

rather small and as such this may not constitute any serious problem to optical studies of the dissolved solutes, the fact that these liquids are fluorescent implies that one needs to be extremely careful in fluorescence studies, especially involving weakly fluorescent samples. Ionic liquids based on pyrrolidinium cation, which contain a saturated ring system, may be better suited for optical studies.

References

1. (a) Welton, T. *Chem. Rev.* **1999**, *99*, 2071. (b) Dupont, J.; de Suza, R. F.; Suarez, P. A. Z. *Chem. Rev.* **2002**, *102*, 3667. (c) *Ionic Liquids in Synthesis*; Welton, T., Wasserscheid, P., Eds.; VCH-Wiley: Weinheim, Germany, 2002.
2. (a) Seddon, K. R.; Stark, A.; Torres, M. J. In *Clean Solvents: Alternative Media for Chemical Reactions and Processing*; Abraham, M., Moens, L., Eds.; ACS Symposium Series 819; American Chemical Society: Washington, DC, 2002. (b) *Ionic Liquids, Industrial Applications for Green Chemistry*; Rodgers, R., Seddon, K. R., Eds.; ACS Symposium Series 818; American Chemical Society: Washington, DC, 2002.
3. (a) Wasserscheid, P.; Keim, W. *Angew. Chem., Int. Ed.* **2000**, *39*, 3772. (b) Sheldon, R. *Chem. Commun.* **2001**, 2399.
4. (a) Buzzeo, M. C.; Evans, R. G.; Compton, R. G. *Chem. Phys. Chem.* **2004**, *5*, 1106. (b) Abedin, S. Z. E.; Endres, F. *Acc. Chem. Res.* **2007**, *40*, 1106. (c) MacFarlane, D. R.; Forsyth, M.; Howlett, P. C.; Pringle, J. M.; Sun, J.; Annat, G.; Neil, W.; Izgorodina, E. I. *Acc. Chem. Res.* **2007**, *40*, 1165.
5. (a) Huddleston, J. G.; Willauer, H. D.; Swatlowski, R. P.; Visser, A. E.; Rodgers, R. D. *Chem. Commun.* **1998**, 1765. (b) Dai, S.; Ju, Y. H.; Barnes, C. E. *J. Chem. Soc., Dalton Trans.* **1999**, 63.
6. (a) Itoh, H.; Naka, K.; Chujo, Y. J. Am. Chem. Soc. 2004, 126, 3026. (b) Wei, G.-T.; Yang, Z.; Lee, C.-Y.; Yang, H.-Y.; Wang, C. R. C. *J. Am. Chem. Soc.* **2004**, *126*, 5036. (c) Tatumi, R.; Fujihara, H. *Chem. Commun.* **2005**, 83.
7. Borra, E. F.; Seddiki1, O.; Angel, R.; Eisenstein, D.; Hickson, P.; Seddon, K. R.; Worden, S. P. *Nature* **2007**, *447*, 979.
8. (a) Davis, J. H. *Chem. Lett.* **2004**, *33*, 1072. (b) Lee, S. *Chem. Commun.* **2006**, 1049.
9. (a) Aki, S. N. V. K.; Brennecke, J. F.; Samanta, A. *Chem. Commun.* **2001**, 413. (b) Crowhurst, L.; Mawdsley, P. R.; Perez-Arlandis, J. M.; Salter, P. A.; Welton, T. *Phys. Chem. Chem. Phys.* **2003**, *5*, 2790. (c) Muldoon, M. J.; Gordon, C. M.; Dunkin, I. R. *J. Chem. Soc., Perkin Trans. 2* **2001**, 433. (d) Carmichael, A. J.; Seddon, K. R. *J. Phys. Org. Chem.* **2000**, *13*, 591.
10. (a) Karmakar, R.; Samanta, A. *J. Phys. Chem. A* 2002, *106*, 4447. (b) Karmakar, R.; Samanta, A. *J. Phys. Chem. A* 2002, *106*, 6670. (c) Karmakar, R.; Samanta, A. *J. Phys. Chem. A* 2003, *107*, 7340.
11. (a) Mandal, P. K.; Saha, S.; Karmakar, R.; Samanta, A. *Curr. Sci.* 2006, *90*, 301. (b) Samanta, A. *J. Phys. Chem. B* 2006, *110,* 13704.
12. Jin, H.; Baker, G. A.; Arzhantsev, S.; Dong, J.; Maroncelli, M. *J. Phys. Chem. B* 2007, *111*, 7291.

13. (a) Ingram, J. A.; Moog, R. S.; Ito, N.; Biswas, R.; Maroncelli, M. *J. Phys. Chem. B* 2003, *107*, 5926.(b) Arzhantsev, S.; Ito, N.; Heitz, M.; Maroncelli, M. *Chem. Phys. Lett.* 2003, *381*, 278. (c) Ito, N.; Arzhantsev, S.; Heitz, M.; Maroncelli, M. *J. Phys. Chem. B* 2004, *108*, 5771.
14. (a) Gordon, C. M.; McLean A. J. *Chem. Commun.* **2000**, 1395. (b) Alvaro, M.; Ferrer, B.; Garcia, H.; Narayana, M. *Chem. Phys. Lett.* **2002**, *362*, 435. (c) Marquis, S.; Ferrer, B.; Alvaro, M.; Garcia, H.; Roth, H. D. *J. Phys. Chem. B* **2006**, *110*, 14956. (d) Skrzypczak, A.; Neta, P. *J. Phys. Chem. A* **2003**, *107*, 7800. (e) McLean, A. J.; Muldoon, M. J.; Gordon, C. M.; Dunkin, I. R. *Chem. Commun.* **2002**, 1880.
15. (a) Ozawa, R.; Hamaguchi, H. *Chem. Lett.* **2001**, *30*, 736. (b) Chakrabarty, D.; Chakraborty, A.; Hazra, P.; Seth, D.; Sarkar, N. *Chem. Phys. Lett.* **2004**, *397*, 216.
16. Mandal, P. K.; Sarkar, M.; Samanta, A. *J. Phys. Chem. A* **2004**, *108*, 9048.
17. (a) Chakrabarty, D.; Chakraborty, A.; Seth, D.; Hazra, P.; Sarkar, N. *Chem. Phys. Lett.* **2004**, 397, 469. (32) Fletcher, K. A.; Baker, S. N.; Baker, G. A.; Pandey, S. *New. J. Chem*. **2003**, *27*, 1706. (33) Baker, S. N.; Baker, G. A.; Kane, M. A.; Bright, F. V. *J. Phys. Chem. B* **2001**, *105*, 9663.
18. (a) Chakrabarty, D.; Seth, D.; Chakraborty, A.; Sarkar, N. *J. Phys. Chem. B* **2005**, *109*, 5753. (b) Seth, D.; Chakraborty, A.; Setua, P.; Sarkar, N. *J. Phys. Chem. B* **2007**, 111, 4781.
19. Muldoon, M. J.; McLean, A. J.; Gordon, C. M.; Dunkin, I. R. *Chem. Commun.* **2001**, 2364.
20. Bonhote, P.; Dias, A. P.; Papageorgiou, N.; Kalyanasundaram, K.; Gratzel, M. *Inorg. Chem.* **1996**, *35*, 1168.
21. Huddleston, J. G.; Willauer, H. D.; Swatlowski, R. P.; Visser, A. E.; Rodgers, R. D. *Chem. Commun.* **1998**, 1765.
22. Lancaster, N. L.; Salter, P. A.; Welton, T.; Young, G. B. *J. Org. Chem.* **2002**, *67*, 8855
23. Billard, I.; Moutiers, G.; Labet, A.; El Azzi, A.; Gaillard, C.; Mariet, C.; Lutzenkirchen, K. *Inorg. Chem.* **2003**, *42*, 1726.
24. Earle, M. J.; Gordon, C. M.; Plechkova, N. V.; Seddon, K. R.; Welton, T. *Anal. Chem.* **2007**, *79*, 758.
25. Burrell, A. K.; Sesto, R. E. D.; Baker, S. N.; McCleskey, T. M.; Baker, G. A. *Green Chem.* **2007**, *9*, 449.
26. Nockemann, P.; Binnemans, K.; Driesen, K. *Chem. Phys. Lett.* **2005**, *415*, 131.
27. Gutkowski, K. I.; Japas, M. L.; Aramendia, P. F. *Chem. Phys. Lett.* **2006**, *426*, 329.
28. Soujanya, T.; Krishna, T. S. R.; Samanta, A. *J. Phys. Chem.* **1992**, *96*, 8544.
29. Paiva, A. C. M.; Juliano, L.; Boschov, P. *J. Am. Chem. Soc.* **1976**, *98*, 7645.

30. (a) Urahata, S. M.; Ribeiro, M. C. C. *J. Chem. Phys.* **2004**, *120*, 1855. (b) Del Popolo, M. G.; Voth, G. A. *J. Phys. Chem. B* **2004**, *108*, 1744. (c) Margulis, C. J.; Stern, H. A.; Berne B. J. *J. Phys. Chem. B* **2002**, *106*, 12017.
31. (a) Hu, Z.; Margulis, C. J. *Proc. Natl. Acad. Sci.* **2006**, *103*, 831. (b) Hu, Z.; Margulis, C. J. *J. Phys. Chem. B* **2006**, *110*, 11025. (c) Hu, Z.; Margulis, C. J. *Acc. Chem. Res.* **2007**, *40*, 1097. (d) Popolo, M.; Kohanoff, J.; Lynden-Bell, R. M.; Pinilla, C. *Acc. Chem. Res.* **2007**, *40*, 1156. (e) Jiang, W.; Wang, Y.; Voth, G. *J. Phys. Chem. B* **2007**, *111*, 4812.
32. (a) Mele, A.; Tran, C. D.; Lacerda, S. H. D. P. *Angew. Chem., Int. Ed.* **2003**, *42*, 4364. (b) Headley, A. D.; Jackson, M. N. *J. Phys. Org. Chem.* **2002**, *15*, 52. (c) Hardacre, C.; Holbrey, J. D.; McMath, S. E. J.; Bowron, D. T.; Soper, A. K. *J. Chem. Phys.* **2003**, *118*, 273. (d) Hardacre, C.; McMath, S. E. J.; Nieuwenhuyzen, M.; Bowron, D. T.; Soper, A. K. *J. Phys.: Condens. Matter* **2003**, *15*, S159.
33. (a) Katayanagi, H.; Hayashi, S.; Hamaguchi, H.; Nishikawa, K. *Chem. Phys. Lett.* **2004**, *392*, 460. (b) Iwata, K.; Okazima, H.; Saha, S.; Hamaguchi, H. *Acc. Chem. Res.* **2007**, *40*, 1174.
34. (a) Triolo, A.; Russina, O.; Bleif, H.-J.; Di Cola, E. *J. Phys. Chem. B* **2007**, *111*, 4641. (b) Moutiers, B. G.; Labet, A.; Azzi A. E.; Gaillard, C.; Mariet, C.; Lutzenkirchen, K. *Inorg. Chem.* **2003**, *42*, 1726.
35. Carmichael, A. J.; Hardacre, C.; Holbrey, J. D.; Nieuwenhuyzen, M.; Seddon, K. R. *Anal. Chem.* **1999**, *71*, 4572.
36. (a) Xiao, D.; Rajian, J. R.; Li, S. F.; Bartsch, R. A.; Quitevis, E. L. *J. Phys. Chem. B* **2006**, *110*, 16174. (b) Xiao, D.; Rajian, J.; Cady, A.; Li, S.; Bartsch, R.; Quitevis, E. *J. Phys. Chem. B* **2007**, *111*, 4669.
37. Demchenko, A. P. *Luminescence* **2002**, *17*, 19.
38. (a) Demchenko, A. P. In *Topics in Fluorescence Spectroscopy*; Lakowicz, J. R., Ed.; Plenum Press: New York, 1991; Vol. 3. (b) Lakowicz, J. R. *Principles of Fluorescence Spectrosopy*, 2nd ed.; Plenum Press: New York, 1999.
39. (a) Valeur, B.; Weber, G. *Chem. Phys. Lett.* **1977**, *45*, 140. (b) Weber, G.; Shinitzky, M. *Proc. Natl. Acad. Sci. U.S.A.* **1970**, *65*, 823.
40. (a) Chattopadhyay, A.; Mukherjee, S. *Biochemistry* **1993**, *32*, 3804. (b) Chattopadhyay, A.; Mukherjee, S. *J. Phys. Chem. B* **1999**, *103*, 8180.

Chapter 4

Photoinduced Electron Transfer Reaction in RTILs

This chapter delineates the photoinduced electron transfer (PET) reaction between pyrene and N,N-dimethylaniline in four RTILs, monitored by using steady-state and time-resolved fluorescence and laser flash photolysis techniques. No exciplex emission could be observed for this well-known pair. The rate constants of fluorescence quenching due to electron transfer process, although found to be much lower compared to normal solvents, are 2-4 times higher than the diffusion-controlled rates in RTILs. The yield of PET products, i.e. solvent-separated radical ions, was also found to be very low, and in highly viscous RTILs the absorption due to radical ions could not be observed. This observation has been attributed to slower escape rate of the ions compared to fast back electron transfer in the geminate ion pair.

4.1. Introduction

Though RTILs are emerging as media of diverse application, the number of photophysical studies carried out in this novel solvent system is still comparatively less. As such, only a few PET processes have been studied so far in RTILs.[1-4] These studies have largely been confined to determining the effect of viscosity and/or polarity on the rate constant of such processes. It has been shown that the rate of diffusion-controlled PET is considerably slower in RTILs compared to conventional solvents, and, higher the viscosity slower is the rate of the PET process.[1-4] While Gordon et al. explained this observation considering a higher activation energy for PET because of high viscosity,[1] others interpreted it

in terms of "screening of an ionic liquid" toward primary photoprocesses.[2] In a recent work, Garcia and co-workers have pointed out some similarity in various aspects of a PET reaction in RTILs and zeolite.[3] Recently, Vieira and Falvey have demonstrated the Rehm-Weller relationship for a series of PET reactions in RTILs with an emphasis on solvent reorganization energy of these media.[4] In many PET processes studied in RTILs the rate constant is found to be higher than that expected for a fully diffusion-controlled process,[1,4] which is calculated using Smoluchowski equation:

$$k_{diff} = \frac{8RT}{3\eta} \qquad (4.1)$$

where, η is the viscosity (in cP) of media at temperature T (in K). The same has been found in case of pulse radiolysis studies of ground state electron transfer or electron capture process.[5,6] Thus, it is of interest to see whether or to what extent this behavior is general.

Again, how the *course* of a PET reaction is influenced by the viscosity, polarity, and ionic constituents of the RTILs is still an open question. Gordon et al. determined the efficiency of cage escape of the geminate ion pair to form solvated ions, and found that this was not drastically lower than that in acetonitrile.[1] This observation was somewhat unexpected because of huge viscosity difference between the two solvents. These authors thus hypothesized that the back electron transfer rate in the geminate ion pair is slower in RTIL than in acetonitrile, because of the competition between the diffusional separation of the geminate ions with the molecular reorganization prior to back electron transfer.[1] Because of very limited number of studies on the PET processes in

RTILs, there is hardly any information on how the mechanism, dynamics and yield of these reactions can be influenced by the bulk properties such as the viscosity, polarity and ionic nature of the constituents of the RTILs.

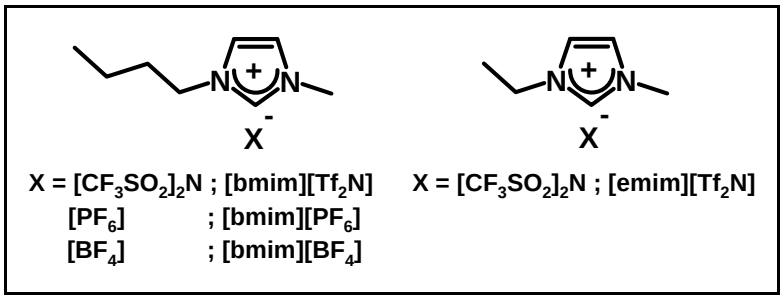

Chart 4.1. Structure and abbreviation of the RTILs used in the present work; [bmim] ≡ 1-butyl-3-methylimidazolium, [emim] ≡1-ethyl-3-methylimidazolium, [Tf_2N] ≡ bis(trifluoromethanesulfonyl)imide.

In order to study these aspects, we have chosen a simple but extensively studied PET reaction between pyrene and N,N-dimethylaniline (DMA), in which pyrene fluorescence is quenched by DMA through a diffusion-controlled process in conventional solvents.[7-15] This is evident from the fact that the quenching constant (k_q) for the present system (~10^{10} M^{-1} s^{-1}) is very similar to the k_{diff} values, 10^9-10^{10} M^{-1} s^{-1} (depending on solvent viscosity).[8] Apart from the fact that PET between pyrene and DMA is diffusion-controlled, the second reason for selecting this pair is that PET gives rise to the formation of a fluorescent exciplex in a nonpolar medium.[9] Well-characterized absorption data of the transient species of this PET reaction offers additional advantages.[9-15] This chapter thus describe the study of PET reaction between pyrene and DMA in four different

RTILs (Chart 4.1), which cover a wide range of viscosity, using steady-state and time-resolved fluorescence and laser flash photolysis techniques.

4.2. Fluorescence quenching experiment

Steady-state absorption as well as fluorescence spectra of pyrene in RTILs are similar to what observed in conventional solvents. With the addition of DMA to the solution of pyrene in an RTIL the pyrene fluorescence is quenched, as shown in Fig. 4.1. However, no additional fluorescence band due to the exciplex could be observed in the long wavelength region in any RTIL. As can be seen from Fig. 4.1, even when the DMA concentration is as high as 0.5 M, no trace of exciplex emission can be detected. Fig. 4.2 depicts the variation of fluorescence lifetime of pyrene as a function of DMA concentration. The Stern-Volmer plot of τ_0/τ versus [DMA] is also shown as an inset to Fig. 4.2. The calculated quenching constants (k_q) in different RTILs, which range between 0.7×10^8 and 3.7×10^8 M^{-1} s^{-1}, are collected in Table 4.1. As can be seen, these values are nearly 2 orders of magnitude lower than those measured in conventional solvents.

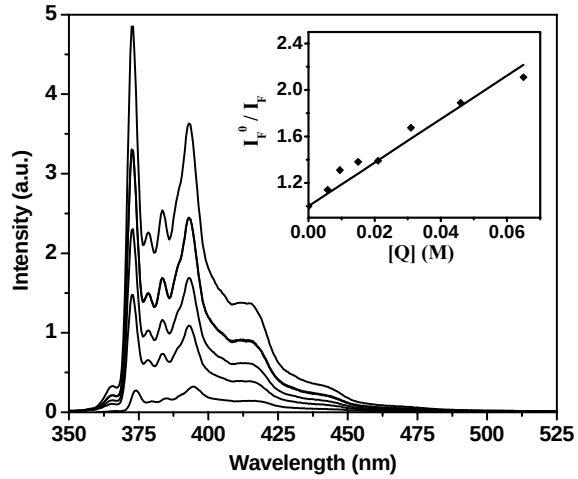

Fig. 4.1. Steady-state fluorescence spectra of pyrene in [bmim][PF_6] for various concentrations of DMA (λ_{exc} = 340 nm). DMA concentrations, from top to bottom, are 0.0, 0.015, 0.065, 0.13 and 0.5 M. The inset shows the Stern-Volmer plot for the quenching experiment ($k_q = 6.3 \times 10^7$ $M^{-1}s^{-1}$).

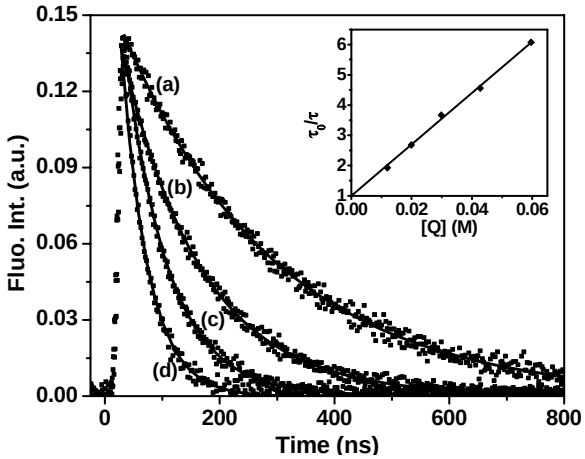

Fig. 4.2. Decay profiles of pyrene fluorescence in [emim][Tf_2N], monitored at 370 nm, for various concentrations of DMA. DMA concentrations are (a) 0.0 M, (b) 0.012 M, (c) 0.02 M and (d) 0.06 M. Inset: Stern-Volmer plot for the corresponding data.

Table 4.1. Quenching constant values obtained from the fluorescence decay measurements (at 20°C).

RTILs	Viscosity (cP)[a]	k_q (M^{-1} s^{-1})[b]	k_{diff} (M^{-1} s^{-1})[c]	k_q/k_{diff}
[bmim][PF_6]	330	6.9×10^7	2.0×10^7	3.45
[bmim][BF_4]	154	1.8×10^8	4.3×10^7	4.18
[bmim][Tf_2N]	52	2.7×10^8	1.25×10^8	2.16
[emim][Tf_2N]	34	3.7×10^8	1.95×10^8	1.9

[a]Viscosity values are obtained from literature (refs 1, 16 and 17), [b]quenching constants (k_q) values were obtained from the Stern-Volmer plots of τ_0/τ vs. [quencher] with the lifetime values obtained by monitoring the fluorescence decay profiles in the LFP setup, [c]diffusional rate constant (k_{diff}) values are obtained from viscosities of RTILs using the eqn. 4.1.

It is to be noted here that the quenching constants (k_q) estimated from the Stern-Volmer plots of τ_0/τ vs [DMA] were found to be very similar to those obtained from the plots of I_0/I vs [DMA] using the steady-state intensities (see inset to Fig. 4.1). For example, in [bmim][PF_6], the estimated k_q value from steady-state data is 6.3×10^7 M^{-1} s^{-1}, which is very close to that obtained (6.9×10^7 M^{-1} s^{-1}) from time-resolved study.

4.3. Transient absorption measurement

Laser flash photolysis (λ_{exc} = 355 nm) of pyrene in RTILs gives rise to transient absorption bands having a sharp peak at around 360 nm and a relatively broader absorption in the 450-550 region (Fig. 4.3). The time profiles of both of the absorption bands are found to be very similar (inset to Fig. 4.3), indicating that both of the absorption bands arise from the same transient. In view of the similarity of the lifetimes associated with these absorption bands and that due to

the fluorescence, these transients can be attributed to S_1-S_n transitions of pyrene. This assignment is consistent with the literature.[18]

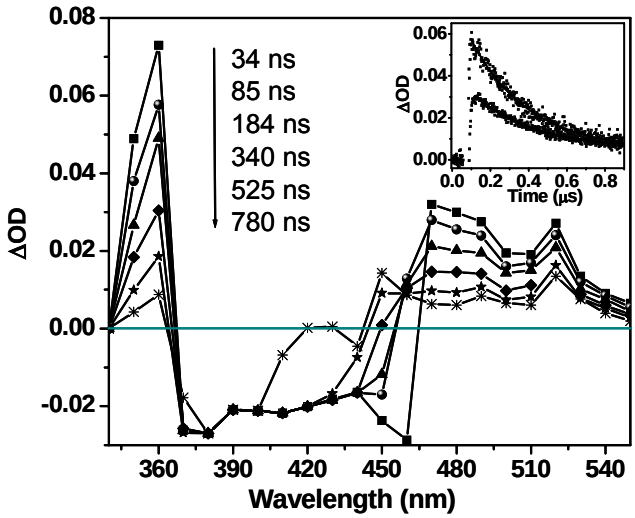

Fig. 4.3. Transient absorption spectra of pyrene in [bmim][PF_6] in the short time-scale. The negative absorption in the 370-460 nm region is due to the emission of pyrene. The inset shows the decay traces of the transient absorption at 360 nm (top) and 470 nm (bottom). The exponential fits to these decay curves yielded decay times of 303 ns and 310 ns, respectively, which are quite similar to the fluorescence lifetime of pyrene in that solvent (295 ns).

While the absorptions due to the S_1-S_n transitions decay completely in ≤ 1 μs, another absorption centering around 410-415 nm could be observed in the longer time-scale (nearly millisecond range), as depicted in Fig. 4.4. The long lifetime associated with this absorption suggests that this absorption is due to T_1-T_n transitions of pyrene.[8,10]

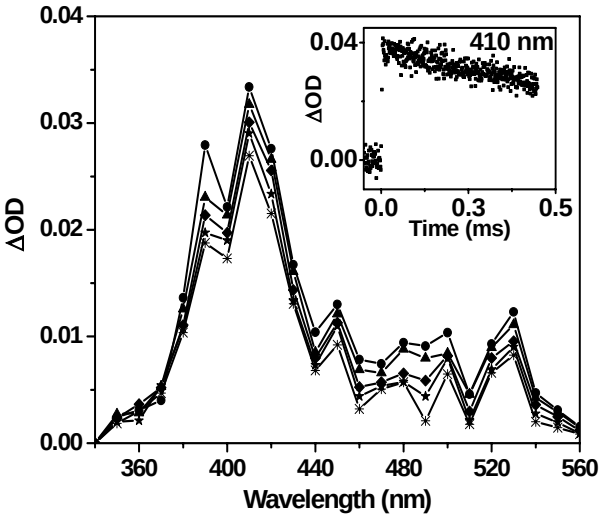

Fig. 4.4. Transient absorption spectra of pyrene in [bmim][PF_6] in the long time-scale. The peak of the absorption at around 410 nm characterizes the pyrene triplet. Delay times (top to bottom) are 2 μs, 9.2 μs, 45 μs, 110 μs and 172 μs. The inset shows the decay trace of the transient absorption at 410 nm.

The evidence of dynamic electron transfer quenching of the S_1 state of pyrene in RTILs is evident from the quenching of the S_1-S_n absorption in the presence of DMA. A Stern-Volmer plot of the transient absorption data in [bmim][PF_6], obtained by monitoring the absorptions at 360 and 470 nm, gives k_q values of 6.6 $\times$ 10^7 and 6.0 $\times$ 10^7 M^{-1} s^{-1}, respectively at 20°C, which are very similar to those obtained from the fluorescence studies (see Table 4.1). In this context, we note that the lifetime of the long-lived absorption due to the T_1-T_n transition remained unaffected in the presence of DMA. This observation is consistent with the fact that the PET process between pyrene and DMA proceeds only through the S_1 state.[8]

In relatively less viscous RTILs such as [emim][Tf_2N] and [bmim][Tf_2N], additional absorption bands, which can be assigned to the products of the PET reaction, namely, pyrene radical anion (intense peak at ~493 nm) and DMA radical cation (relatively less intense peak around 455-460 nm), can also be observed in the presence of DMA in the large time-scale (e.g., 100-200 μs range).[8,10] The transient absorption spectra of the pyrene-DMA system in [emim][Tf_2N] and [bmim][Tf_2N] are shown in Fig. 4.5. Interestingly, in more viscous RTILs, [bmim][PF_6] and [bmim][BF_4], the absorption bands due to the transient radical ions were not observed.

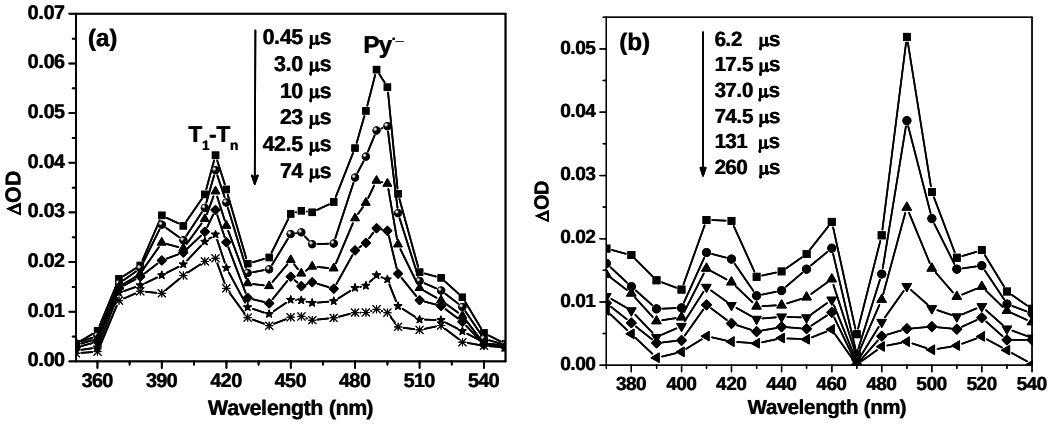

Fig. 4.5. Transient absorption spectra of pyrene in presence of DMA (0.1 M) in (a) [emim][Tf_2N] and (b) [bmim][Tf_2N]. The absorption near 420 nm and the peak around 495 nm correspond to the triplet pyrene and pyrene radical anion, respectively. However, the shoulder around 455-460 nm is due to DMA radical cation.

4.4. Discussion

4.4.1. Fluorescence quenching and thermodynamic parameters

One of the important findings of the present work is the absence of the exciplex emission in the steady-state measurement as well as in the laser flash photolysis studies. In general, for the donor-acceptor systems comprising of amines and aromatic hydrocarbons, the PET processes can lead to the formation of an exciplex, which is often an intermediate for PET reactions occurring in conventional nonpolar solvents.[7,19] In polar media, the exciplexes are generally not observed because of rapid dissociation of the primary photoproducts to, most commonly, the solvated radical cations and anions.[19] As described earlier, pyrene-DMA is regarded as a typical exciplex forming system, for which the exciplex emission is most pronounced in nonpolar solvents.[9,19] Since weak exciplex emission for the present system can even be observed in polar solvents such as acetone and acetonitrile,[10,11] where the formation of the solvated ions competes with the exciplex emission, lack of this emission in RTILs suggests that these media are more polar than acetonitrile. While this inference is consistent with the findings of various absorption and fluorescence studies, which suggested the polarity of the RTILs to be higher than that of acetonitrile,[20,21] recently measured static dielectric constants of some RTILs (ε = 11.4-12.3, at 25°C),[22] however, indicate that these media are much less polar than acetonitrile (ε = 35.9 at 25°C).[23] It is therefore evident from the present results that it is the microscopic polarity parameter, such as the $E_T(30)$ value of the RTIL, which determines whether or not exciplex emission can be observed in a given RTIL.

Another noticeable feature of the present study is that the measured k_q values are 2-4 times higher than the k_{diff} values for the respective RTILs, calculated using eqn. 4.1 employing the literature values of viscosity of RTILs (see Table 4.1). In conventional solvents, the k_q values are comparable to the k_{diff} values. In fact, in acetonitrile, the k_q value (1.3×10^{10} M^{-1} s^{-1} at 25°C)[8] is slightly lower than the k_{diff} value (~1.9×10^{10} M^{-1} s^{-1} using $\eta = 0.341$ cP for acetonitrile, at 25°C).

Before probing the difference in the k_q and k_{diff} values, let us focus on the thermodynamic parameters of PET to have an understanding of these physical quantities for PET reaction in RTILs. According to Rehm and Weller, the thermodynamic driving force (ΔG_{ET}) of the overall PET process, i.e., the formation of solvent-separated species from the photoexcited species is given by,[24,25]

$$\Delta G = E_D^{ox} - E_A^{red} - E_{0,0} - e^2/\varepsilon r_q \qquad (4.2)$$

where, E_D^{ox} and E_A^{red} are the oxidation and reduction potentials of the donor and the acceptor, respectively. $E_{0,0}$ is the energy corresponding to the 0-0 transition of the photoexcited molecule (donor or acceptor) and $e^2/\varepsilon r_q$ is the coulomb energy of interaction of the ion pair at the effective encounter distance of the donor and acceptor (i.e., $r_q = r_d + r_a$). The coulomb energy term depends on solvent polarity (i.e., dielectric constant) and becomes negligible when the solvent is highly polar, cf. acetonitrile. It is also shown by Rehm and Weller that k_q increases sharply with a decrease of ΔG_{ET} and it attains the diffusion-controlled limited value (~2×10^{10} M^{-1} s^{-1} in acetonitrile) when $\Delta G_{ET} \leq -10$ kcal (~ –0.43 eV).[25] For the pyrene-DMA system, the ΔG_{ET} value in acetonitrile is estimated to be –0.47 eV at

25°C,[10,12] which is close to the critical value of ΔG_{ET} required for an electron transfer process to be diffusion-controlled.[25]

Now, since the redox potentials of pyrene and DMA in the present RTILs are not known, we assume that the $[E_D^{ox} - E_A^{red}]$ value for the present system in [emim][Tf_2N] is the same as that in pyridine (3.08 eV),[12] as the two solvents are isopolar in terms of dielectric constant (the ε values are 12.25 and 12.3 for [emim][Tf_2N] and pyridine, respectively, at 25°C).[22] Subsequent calculation using eqn. 4.2 with an r_q value of 7 Å for the pyrene-DMA system[12,13] and $E_{0,0}$(A*) = 3.34 eV leads to slightly lower ΔG_{ET} values (–0.4 to –0.42 eV) in the four RTILs compared to that in acetonitrile. (For RTILs other than [emim][Tf_2N], the $[E_D^{ox} - E_A^{red}]$ value was assumed to be ~3.0 eV, as their dielectric constants are marginally lower than that of [emim][Tf_2N]).

Since for the pyrene-DMA system the ΔG_{ET} value in acetonitrile is close to its critical value required for diffusion-controlled electron transfer, a drop in the ΔG_{ET} value is expected to result in a reduction of the k_q value, making it less than the k_{diff} value.[18] However, in the present case, the k_q values in RTILs are, in fact, 2-4 fold higher than the k_{diff} values (Table 4.1), despite the lower ΔG_{ET} values in these media. This observation was unexpected but not "unprecedented", as a similar observation, i.e. $k_q > k_{diff}$ has been noted by Neta coworkers in the pulse radiolysis study of ground state electron transfer or capture reactions[5,6] and in some recent PET studies.[1,4] The present result, perhaps, is a reflection of the fact that the microviscosity surrounding the electron donor-acceptor moieties is different from the bulk viscosity of the RTILs, as suggested by Skrzypczak and Neta.[5]

4.4.2. Transient absorption spectra and yield of ions

Mataga et al. have shown that the yield of the solvent-separated ions (Φ_{ion}) of the present system decreases with a decrease in the ε value of the solvents.[10,13-15] For example, Φ_{ion} in acetonitrile is 0.5, whereas, in less polar solvent pyridine, this value is only 0.08.[13] A rough estimate of the yield of the solvent-separated radical ions (Φ_{ion}) can be made from the transient absorption data, using the following equation: $\Phi_{ion} = N_{ion}/N_p$, where N_{ion} and N_p denote the total number of ions produced per pulse and total number of exciting photons per pulse, respectively.[26] The former is obtained from the concentration of the ions produced (c_{ion}) for each laser excitation using $c_{ion} = \Delta OD/\varepsilon_\lambda \cdot l$ where ΔOD is the differential absorption due to the radical ion at a given wavelength, ε_λ is the molar extinction coefficient of the same species at this wavelength, and *l* is the optical path length. Again, the number of exciting photons per pulse (N_p) is obtained for each excitation from the laser energy monitor ($N_p = 1.2 \times 10^{17}$ per unit volume per pulse).[10,13,26] Under the condition when pyrene fluorescence is highly quenched (~90%), the maximum ΔOD value due to the pyrene radical anion allows estimation of c_{ion} assuming that the ε_λ value (4.8×10^4 M^{-1} cm^{-1} at 493 nm in acetonitrile)[10] is solvent independent. It is to be noted here that the absorption due to the pyrene radical anion at 493 nm was obtained after subtracting the absorption due to the triplet at this wavelength from the total ΔOD value. The contribution due to the triplet was estimated by performing a control experiment without DMA. Thus, the estimated Φ_{ion} value is 0.015±0.005 in [emim][Tf_2N] and slightly less in [bmim][Tf_2N]. Such low yield of the solvent-separated ions is in agreement with the high viscosity and low dielectric constant of the RTILs.[13-15,27]

Here Φ_{ion} was estimated from the yield of the pyrene radical anion because of the prominence of the transient absorption due to the pyrene radical anion than that of the DMA radical cation (see Fig. 4.5). The yield of the radical cation is, however, the same as that of the radical anion, according to Scheme 4.1 depicted below. Since the absorption due to the pyrene radical anion or DMA radical cation could not be observed in more viscous RTILs, [bmim][PF_6] and [bmim][BF_4], the Φ_{ion} values in these solvents could not be calculated from the transient absorption studies. However, one can obtain an estimate of this quantity when taking into consideration the fact that Φ_{ion} is closely related to the yield of dissociation of the geminate ion pair (GIP), Φ_{diss}, with $\Phi_{ion} \leq \Phi_{diss}$. It should be noted that, $\Phi_{ion} = \Phi_{diss}$, when no process other than those depicted in Scheme 4.1 is involved. In reality, the exciplex formation in competition with the formation of the GIP, annihilation of the GIP resulting in the formation of triplet species, and so forth, often leads to a difference in these two quantities.

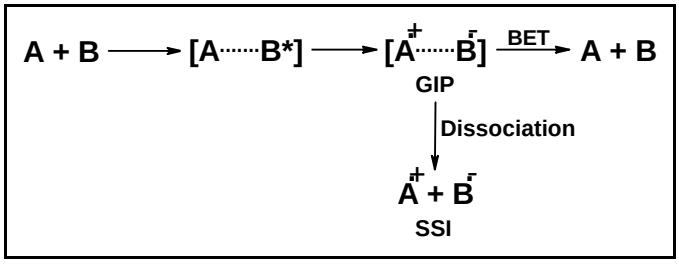

Scheme 4.1. Mechanism of the PET reaction in RTILs. GIP, BET and SSI stand for geminate ion pair, back electron transfer and solvent-separated ions, respectively.

According to Scheme 4.1, the dissipation of GIP occurs only through dissociation to solvent-separated free ions (SSI) and geminate recombination by the back electron transfer (BET) process. Hence, Φ_{diss} can be written as

$$\Phi_{diss} = \frac{k_{diss}}{k_{diss} + k_{BET}} \tag{4.3}$$

where k_{diss} is the rate constant for dissociation of the GIP yielding free ions and k_{BET} is the rate constant for back electron transfer leading to geminate recombination in the GIP. The estimated value of Φ_{diss} for the pyrene-DMA system is almost unity in acetonitrile and ~0.7 in acetone.[12,14] However, in pyridine and other weakly polar solvents, this value is much lower.[28] Herein, we have attempted to calculate an approximate value of Φ_{diss} for the pyrene-DMA system in RTILs using the Tachiya method,[29] which is based on the Onsager diffusion-controlled ion-recombination model.[30] According to this method, the rate of dissociation of the ion pair (k_{diss}) in the initial separation distance (r_{IP}) is given by

$$k_{diss} = \frac{Dr_c}{r_{IP}^3[\exp(r_c/r_{IP}) - 1]} \tag{4.4}$$

where D is the sum of the diffusion constants of the donor and acceptor, that is, $D = D_a + D_d$ and r_c is the Onsager distance, which is given by the expression $r_c = e^2/k_bT$ (k_b = Boltzmann constant) and is constant for a given solvent at a constant temperature (T).[29] The equation suggests that k_{diss} is strongly dependent on r_{IP}, and therefore, an accurate choice of r_{IP} value is necessary for the estimation of k_{diss} using the above equation.

Since the RTILs are viscous solvents, the diffusion coefficient (D) of the small solutes in these media is expected to be significantly lower than that in conventional solvents. According to Stokes-Einstein law, the diffusion coefficient for a small molecule is given by, $D_{small} = k_BT/6\pi\eta r$, where r is the radius of the molecule (hydrodynamic radius), assumed to be spherical, and η is the viscosity of the solvent at temperature T. It is a common practice to use an average D (= D_a + D_d) value of 3.5×10^{-5} cm^2 s^{-1} at 25°C in acetonitrile, as estimated by Weller,[9] for a large number of common organic donor-acceptor systems.[31] To estimate the diffusion constant in RTILs, we have assumed that the hydrodynamic radius of the molecules (r) remains the same as in acetonitrile, and thus according to the Stokes-Einstein law, we have $D_{IL}/D_{AN} = \eta_{AN}/\eta_{IL}$ where the subscripts '$_{IL}$' and '$_{AN}$' stands for RTIL and acetonitrile, respectively. Now, using known values of D_{AN} and η_{AN} we can calculate D_{IL} values in respective RTILs, which are, for instance, 3.45×10^{-7} and 3.55×10^{-8} cm^2 s^{-1} in [emim][Tf_2N] and [bmim][PF_6], respectively, at 20°C. Now, to calculate k_{diss} values in RTILs we need to know the r_{IP} values. If it is assumed that the distance between radical ions in the GIP is not much different from that during the quenching, then we have $r_{IP} \approx r_q \approx 7$ Å. To arrive at this assumption, we have speculated that since RTILs are highly viscous, the diffusional separation of the radical ions of the GIP is significantly slower than that in conventional solvents. Therefore, the radical ions of the GIP cannot move far before being dissipated by either of the two processes described in the Scheme 4.1, thereby leading to a situation where $r_{IP} \approx r_q$. Then, subsequent calculation based on eqn. 4.4 leads to a k_{diss} value of 6.1×10^5 and 4.1×10^4 s^{-1} in [emim][Tf_2N] and [bmim][PF_6], respectively. The measured k_{diss} value for the

present system in acetonitrile (5×10^8 s^{-1})[15,28,32] is 10^3-10^4 fold higher than that in RTILs.

The estimation of Φ_{diss} also requires the understanding of k_{BET} values in RTILs. In acetonitrile and acetone the k_{BET} values are reported to be $<5 \times 10^7$ and $\sim 3 \times 10^7$ s^{-1}, respectively.[28,32] Since k_{BET} shows weak solvent polarity dependence and is especially independent of viscosity,[14] one can assume a similar k_{BET} value in RTILs as well. Using a k_{BET} value of 3×10^7 s^{-1}, the Φ_{diss} values for the pyrene-DMA system in [emim][Tf_2N] and [bmim][PF_6] are estimated to be 0.02 and ~0.001, respectively, according to eqn. 4.3. An extremely low dissociation yield ($\Phi_{diss} \approx 10^{-3}$) in highly viscous [bmim][PF_6] explains why the radical ions could not be observed in this RTIL. Near identical values of experimentally determined Φ_{ion} and calculated Φ_{diss} in [emim][Tf_2N] are also noteworthy. The observation not only confirms that the reaction course depicted in Scheme 4.1 is true but also implies that an efficient BET is the primary deactivation channel responsible for the poor yield of the products of the electron transfer reactions in RTILs. In this context, it should be noted that, in an earlier work on PET between a ruthenium complex and methyl viologen, an unexpectedly higher yield of the solvent-separated PET products was observed despite a slower escape rate in highly viscous [bmim][PF_6].[1] The observation was interpreted by speculating that the rates of both BET and dissociation are lowered in RTIL. Our findings, wherein a lower yield of the PET products has been obtained in several RTILs of varied viscosity, appears to be more realistic in view of the high viscosity of the RTILs.

The low escape efficiency of the radical ions from the GIP can also be understood in terms of the cage effect, which in high-viscosity RTILs such as

[bmim][PF_6] and [bmim][BF_4] cannot be neglected. The dynamics of the solvent reorganization in these RTILs is so slow that the geminate ion pair is virtually confined to a solvent cage in which the residency period of the radical ions in close proximity will be so long that scarcely any radical ion can escape from the cage before being annihilated by the geminate recombination. Such a situation arises in water-in-oil type of microemulsions where the GIP is effectively trapped in the water pool and subsequently dissipated through BET; the net result is little or no yield of ions.[27] Consideration of the cage effect in highly viscous RTILs leads to a Φ_{diss} value lower than that calculated from the diffusion theory, making the yield of the free ions (Φ_{ion}) a negligible quantity.

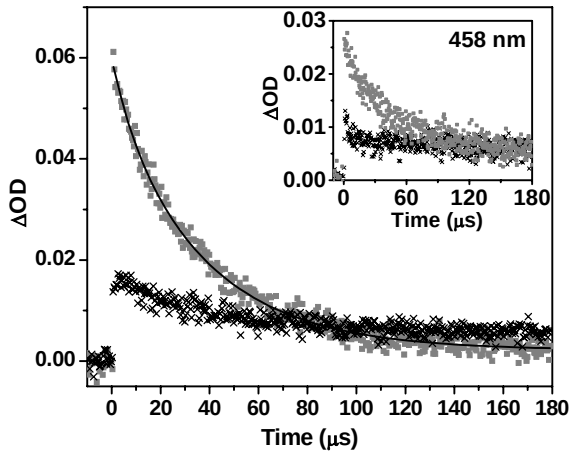

Fig. 4.6. Decay profiles at 493 nm (where $Py^{\cdot -}$ absorption is maximum) for pyrene in [emim][Tf_2N] in the absence (×××) and in presence (0.1 M) of DMA (▪▪▪). The inset shows the decay at 458 nm ($DMA^{\cdot +}$ absorption). The lifetime of the $Py^{\cdot -}$ is estimated to be 35 μs.

The effect of slow diffusion and probable confinement of the solvated species is also reflected in the lifetime of the radical ions. Once the free solvent-separated

radical ions are formed in less viscous RTILs, they are found to be quite long-lived. This is evident from the fact that the lifetime of the pyrene anion radical in [emim][Tf_2N] is 35 μs (Fig. 4.6), whereas the same in methanol is only 8.7 μs (which is obtained from the reported half-life of 6 μs[27]).

4.5. Conclusion

This comprehensive study of the PET reaction between the well-known donor-acceptor pair reveals several interesting aspects concerning the mechanism of the PET, the time-scale of the various rate processes involved, and the overall yield of the primary photoproducts in RTILs. First, the system chosen for the present study is one in which PET is diffusion-controlled and well-known for its exciplex emission. On one hand, the lack of exciplex emission for this system appears to be consistent with the microscopic polarity parameters (such as the $E_T(30)$ value) of the RTILs, which indicated these media to be more polar than acetonitrile. On the other hand, since the measured dielectric constants indicate a much lower polarity of the RTILs, lack of exciplex emission is completely unexpected. Therefore, it appears from the present results that the $E_T(30)$ value of the medium better describes the behavior of donor-acceptor couples than the dielectric constant. A relatively lower rate constant for the PET induced fluorescence quenching process in RTILs compared to conventional solvents is consistent with a slower rate of diffusion in these media. However, the observation of a rate constant that is 2-4 fold higher than the diffusion-controlled value possibly suggests that the microviscosity around the donor-acceptor pair is different from the bulk viscosity of the RTILs.

Transient absorption studies, wherein the solvent-separated radical ions could be observed in low-viscosity RTILs, [emim][Tf_2N] and [bmim][Tf_2N], indicate a low yield of the PET products. This observation along with the fact that the products could not be observed in high-viscosity analogues implies that the escape rate of the radical ions from the geminate ion pair is viscosity dependent. A significantly lower escape rate compared to the rate of geminate recombination is shown to be responsible for the low overall efficiency of the solvent-separated PET products. The cage effect in highly viscous RTILs may also contribute to the high efficiency of the back electron transfer process and consequent decrease in the yield of the solvent-separated ions. It is also shown that slow diffusion and probable confinement contribute to the long lifetime of the small fraction of the PET products that escape geminate recombination.

References

1. Gordon, C. M.; McLean A. J. *Chem. Commun.* **2000**, 1395.
2. Alvaro, M.; Ferrer, B.; Garcia, H.; Narayana, M. *Chem. Phys. Lett.* **2002**, *362*, 435.
3. Marquis, S.; Ferrer, B.; Alvaro, M.; Garcia, H.; Roth, H. D. *J. Phys. Chem. B* **2006**, *110*, 14956.
4. Vieira, R. C.; Falvey, D. E. *J. Phys. Chem. B* **2007**, *111*, 5023.
5. Skrzypczak, A.; Neta, P. *J. Phys. Chem. A* **2003**, *107*, 7800.
6. Wishart, J. F.; Neta, P. *J. Phys. Chem. A* **2007**, *107*, 7800.
7. For a review, see: Kavarnos, G. J.; Turro, N. J. *Chem. Rev.* **1986**, *86*, 401.
8. Okada, T.; Oohari, H.; Mataga, N. *Bull. Chem. Soc. Jpn.* **1970**, *43*, 2750.
9. (a) Leonhardt, H.; Weller, A. *Ber. Bunsen-Ges. Phys. Chem.* **1963**, *67*, 791. (b) Leonhardt, H.; Weller, A. *Z. Phys. Chem.* **1961**, *29*, 277. (c) Knibbe, H.; Rehm, D.; Weller, A. *Ber. Bunsen-Ges. Phys. Chem.* **1968**, *72*, 257.
10. Hinto, T.; Akazawa, H.; Mashuhara, H.; Mataga, N. *J. Phys. Chem.* **1976**, *80*, 33.
11. Hirata, Y.; Kanada, Y.; Mataga, N. *J. Phys. Chem.* **1983**, *87*, 1659.
12. Taniguchi, Y.; Nishina, Y.; Mataga, N. *Bull. Chem. Soc. Jpn.* **1972**, *45*, 764.
13. Mashuhara, H.; Hinto, T.; Mataga, N. *J. Phys. Chem.* **1975**, *79*, 994.
14. Mashuhara, H.; Mataga, N. *Acc. Chem. Res.* **1981**, *14*, 312.
15. Mataga, N. *Pure Appl. Chem.* **1984**, *56*, 1255.
16. seddon, K. R.; Stark, A.; Torres, M. J. In *Clean Solvents: Alternative Media for Chemical Reactions and Processing*; Abraham, M., Moens, L., Eds.; ACS Symposium Series 819; American ChemicalSociety: Washington, DC, 2002.
17. Bonhote, P.; Dias, A. P.; Papageorgiou, N.; Kalyanasundaram, K.; Gratzel, M. *Inorg. Chem.* **1996**, *35*, 1168.
18. Nakato, Y.; Yamato, N.; Tsubomura, H. *Chem. Phys. Lett.* **1968**, *2*, 57.
19. *The Exciplex*; Gordon, M., Ware, W. R. Eds.; Academic Press: New York, 1974.
20. (a) Aki, S. N. V. K.; Brennecke, J. F.; Samanta, A. *Chem. Commun.* **2001**, 413. (b) Carmichael, A. J.; Seddon, K. R. *J. Phys. Org. Chem.* **2000**, *13*, 591. (c) Reichardt, C. *Green Chem.* **2005**, *7*, 339.
21. (a) Muldoon, M. J.; Gordon, C. M.; Dunkin, I. R. *J. Chem. Soc., Perkin Trans.* **2001**, *2*, 433. (b) Fletcher, K. A.; Baker, S. N.; Baker, G. A.; Pandey, S. *New J. Chem.* **2003**, *27*, 1706.
22. (a) Daguenet, C.; Dyson, P. J.; Krossing, I.; Oleinikova, A.; Slattery, J.; Wakai, C.; Weingartner, H. *J. Phys. Chem. B* **2006**, *110*, 12682. (b) Wakai, C.; Oleinikova, A.; Ott, M.; Weingartner, H. *J. Phys. Chem. B* **2005**, *109*, 17028.
23. Reichardt, C. *Solvents and Solvent Effects in Organic Chemistry*; VCH: Weinheim, Germany, 1988.
24. Rehm, D.; Weller, A. *Ber. Bunsen-Ges. Phys. Chem.* **1969**, *73*, 834.
25. Rehm, D.; Weller, A. *Isr. J. Chem.* **1970**, *8*, 259.

26. (a) Mashuhara, H.; Shimada, M.; Tsujino, N.; Mataga, N. *Bull. Chem. Soc. Jpn.* **1971**, *44*, 3310. (b) Shimada, M.; Mashuhara, H.; Mataga, N. *Bull. Chem. Soc. Jpn.* **1973**, *46*, 1903.
27. (a) Katusin-Razem, B.; Wong, M.; Thomas, J. K. *J. Am. Chem. Soc.* **1978**, *100*, 1679. (b) Atik, S. S.; Thomas, J. K. *J. Am. Chem. Soc.* **1981**, *103*, 3550.
28. Mataga, N.; Okada, T.; Kanda, Y.; Shioyama, H. *Tetrahedron* **1986**, *42*, 6143.
29. Sano, H.; Tachiya, M. *J. Chem. Phys.* **1979**, *71*, 1276.
30. Mazumdar, A. In *Advances in Radiation Chemistry*, Vol. 1; Burton, M., Magee, J. L., Eds.; Willey Interscience: New York, 1969; p 83.
31. (a) Niwa, T.; Kikuchi, K.; Matsusita, N.; Hayashi, M.; Katagiri, T.; Takahasi, Y.; Miyashi, T. *J. Phys. Chem.* **1993**, *97*, 11960. (b) Inada, T.; Kikuchi, K.; Takahashi, Y.; Ikeda, H.; Miyashi, T. *J. Phys. Chem. A* **2002**, *106*, 4345.
32. Mataga, N.; Asahi, T.; Kanada, Y.; Okada, T. *Chem. Phys.* **1988**, *127*, 249.

Chapter 5

Solvation Dynamics in an Alcohol-Functionalized Ionic Liquid

Steady-state and time-resolved fluorescence behavior of some dipolar solutes, C153, AP and prodan, have been studied in an alcohol-functionalized room temperature ionic liquid, 1-(hydroxyethyl)-3-methylimidazolium bis(trifluoromethanesulfonyl)imide. The steady-state fluorescence parameters have been exploited for the estimation of the polarity of this ionic liquid and to obtain information on the hydrogen bonding interaction between the ionic liquid and the probe molecules. The time-resolved measurements have been focused on the dynamics of solvation by studying the dynamic Stokes shift in the ps-ns time scale and solute rotation by measuring the time dependence of the fluorescence anisotropy. The influence of hydrogen bonding interaction between the probe molecules and the ionic liquids on the solute rotation and various components of the solvation dynamics is carefully analyzed in an attempt to obtain further insight into the mechanism of solvation in these novel media.

5.1. Introduction

Among the various photophysical studies carried out in RTILs, the most explored one is the study of solvation dynamics by probing the dynamic Stokes shift of fluorescence spectrum of dipolar molecules.[1-18] These studies have revealed that the dynamics in RTILs is rather slow and is of biphasic or nonexponential nature.[1-10] A substantial portion of the dynamics has also been

found to be too fast to be detectable in the usual experimental setups of finite time-resolution (typically around 25 ps). The exact time scale and physical nature of this missing or ultrafast dynamics has still remained a matter of considerable speculation and debate.[5-13] It has also been found that the solvation dynamics in RTILs is highly probe dependent.[5,7] A number of solvation dynamics studies have been carried out in ionic liquid based microemulsion and in the mixture of RTILs with conventional solvents.[16-18] A more detailed description on this topic covering its crucial aspects has been given in Chapter 1.

Taking into consideration the fact that a clear understanding of the solvation process in RTILs is possible only when the dynamical data is available in a large variety of the RTILs, we have studied solvation dynamics in an alcohol-functionalized imidazolium ionic liquid, namely, 1-(hydroxyethyl)-3-methylimidazoilum bis(trifluoromethanesulfonyl)imide, abbreviated as [OH-emim][Tf_2N] in this discussion (Chart 5.1).[19] In addition to the solvation process, we have studied the rotational dynamics of the probe molecules in this medium by measuring the time-dependent rotational anisotropy. The factors that motivated us toward the selection of this protic RTIL are as follows. First, the presence of the OH group in the imidazolium cation makes it a better hydrogen bond donor. This is expected to enhance the hydrogen bonding interaction of the cation with the probe molecules, particularly those that are hydrogen bond acceptors. At the same time, the interactions between the cationic and anionic components of the RTIL *may* also be enhanced due to additional hydrogen bonding interaction. Clearly, the present RTIL provides an opportunity to study the influence of the local effect, which is expected to be dominated by the hydrogen bonding interaction between

the [OH-emim] cation and the photoexcited fluoroprobe, and its consequence on the overall dynamics. Second, [OH-emim][Tf_2N] is reported to be much more polar compared to most of the other imidazolium ionic liquids,[19] presumably due to the presence of the alcohol-functionalized side chain in the imidazolium moiety (Chart 5.1). Because the high polarity of [OH-emim][Tf_2N] implies greater stabilization of the fluorescent state of the dipolar probe molecules, the time-dependent shift of any given probe molecule in this RTIL is expected to be larger than that observed in other RTILs. This should allow one to monitor the dynamics over a larger frequency domain. Furthermore, because the RTILs comprising the Tf_2N^- anion are commonly less viscous compared to other RTILs, [OH-emim][Tf_2N] is expected to be one of those low-viscosity ionic liquids.

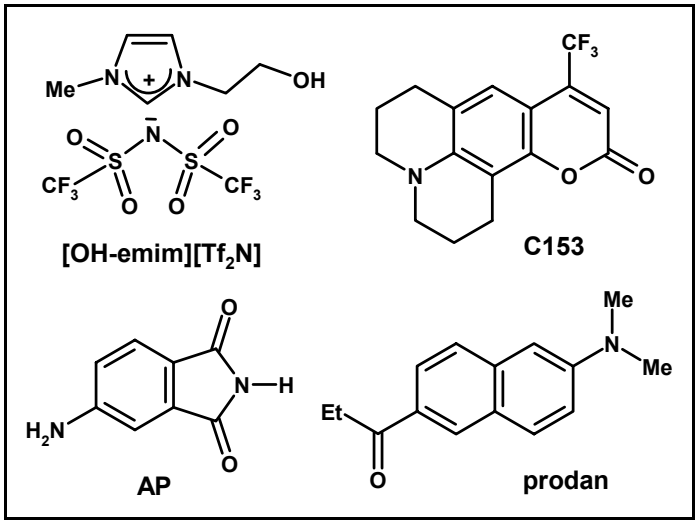

Chart 5.1. Structure and abbreviation of the ionic liquid and probe molecules employed in the present study.

Three well-known fluoroprobes of solvation dynamics study, namely, C153, AP and prodan (Chart 5.1), have been employed in the present study. Our choice has been guided by the fact that, among these systems, AP, in particular, is well-known for its strong hydrogen bonding interaction with the hydroxylic solvents.[20,21] Therefore, any difference in the rotational and solvation dynamics of these probes may provide useful information on the influence of hydrogen bonding interactions and the proximity of the cationic component on these processes.

5.2. Steady-state behavior

The steady-state absorption and fluorescence spectra of C153, AP and prodan in [OH-emim][Tf_2N] are shown in Fig. 5.1. The spectral data of the two systems in this RTIL along with the same in a few other imidazolium RTILs are summarized in Table 5.1 for comparison. It can be seen that the emission maxima for all of the probes appear at higher wavelengths relative to their respective maxima in other RTILs. In the case of AP, which is highly prone to hydrogen bonding interaction with the hydroxylic solvents,[20] this difference is much more pronounced (Table 5.1). This observation is clearly a reflection of higher polarity of [OH-emim][Tf_2N] compared to other imidazolium RTILs, which lack the hydroxyl group, and also specific hydrogen bonding interaction of the present ionic liquid with the probe molecules, in particular, with AP.

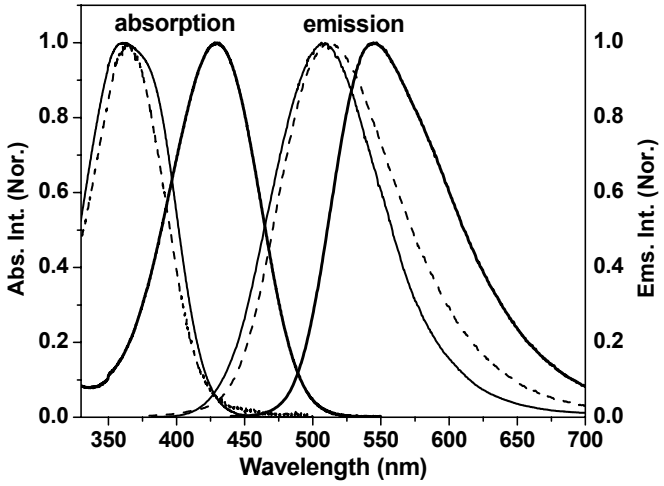

Fig. 5.1. Steady-state absorption and emission spectra of C153 (—), AP (----) and prodan (—) in [OH-emim][Tf_2N]: excitation wavelength for emission (λ_{exc}) = 374 nm. All spectra are normalized at the corresponding peak maximum.

Table 5.1. Absorption and fluorescence properties of the fluoroprobes in RTILs of different viscosities.

RTILs	Viscosity at 20°C (cP)	C153[d]		AP[d]		prodan[d]	
		λ_{abs}^{max} nm	λ_{fluo}^{max} nm	λ_{abs}^{max} nm	λ_{fluo}^{max} nm	λ_{abs}^{max} nm	λ_{fluo}^{max} nm
[bmim][BF_4]	154[a]	435	536	371	483	378	475
[emim][Tf_2N]	34[a]	424	530	361	476	350	472
[OH-emim][Tf_2N]	71[b] (58)[c]	428[b]	546[b]	364[b]	511[b]	365[b]	508[b]

[a]From ref. 22, [b]this study, [c]this study (at 25°C), [d]obtained from the values measured in previous experiments done in our lab.

An earlier measurement involving the betaine dye has indicated a polarity of 60.8 for this RTIL in the $E_T(30)$ scale.[19] However, the $E_T(30)$ values estimated for

[OH-emim][Tf_2N] from the observed fluorescence maxima ($\bar{\nu}_{max}^{fluo}$) of the two flouroprobes in this RTIL and in a series of normal solvents of known $E_T(30)$ values[23] are 50.5 and 54.0 with C153 and AP, respectively (Table 5.2).[5] Even though these values are lower than the literature value,[19] the present data confirms that [OH-emim][Tf_2N] is significantly more polar than other imidazolium ionic liquids that lack the hydroxyl moiety (Table 5.2). Another point of interest is relatively large difference in the estimated $E_T(30)$ values with these probe molecules. This departure is quite significant in case of AP as compared to other two (C153 and prodan) probes. Interestingly, in other RTILs, where the hydrogen bonding interaction with the probe molecule is not significant, the estimated $E_T(30)$ values are fairly similar for these molecules (Table 5.2).

Table 5.2. Wavenumber corresponding to the fluorescence maxima of the systems and the estimated $E_T(30)$ values.

Probe	$\bar{\nu}_{max}^{fluo}$ [a] (cm^{-1})	$E_T(30)$ (indicated by the $\bar{\nu}_{max}^{fluo}$)			
		[OH-emim][Tf_2N][a]	[bmim][PF_6][b]	[bmim][BF_4][b]	[emim][Tf_2N][b]
C153	18315	50.5	47.9	49.1	47.7
AP	19555	54.0	47.2	50.1	48.5
prodan	19675	49.8	46.1	47.1	46.5
betaine dye	—	60.8[c]	52.3[d]	52.7[d]	52.6[d]

[a]this study, [b]obtained from the values measured in previous experiments done in our lab, [c]from ref. 19, [d]from ref. 24.

5.3. Time-resolved measurements

5.3.1. Rotational dynamics

Time-resolved fluorescence anisotropy, r(t), is calculated using the following equation:

$$r(t) = \frac{I_{\parallel}(t) - GI_{\perp}(t)}{I_{\parallel}(t) + 2GI_{\perp}(t)} \tag{5.1}$$

where G is the correction factor for the detector sensitivity to the polarization direction of the emission and $I_{\parallel}(t)$ and $I_{\perp}(t)$ are the fluorescence decays polarized parallel and perpendicular to the polarization of the excitation light, respectively.

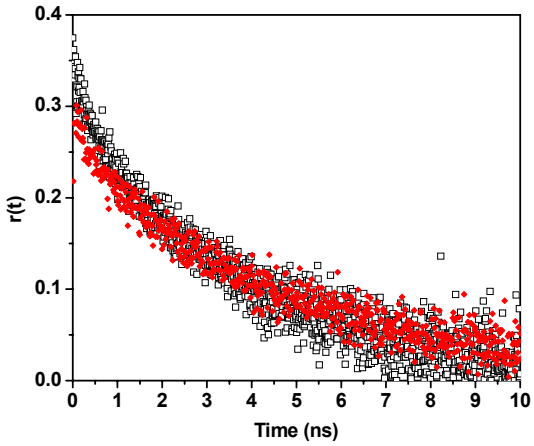

Fig. 5.2. Decay the fluorescence anisotropy, r(t), of C153 (□) and AP (◆) in [OH-emim][Tf_2N].

The anisotropy results are collected in Table 5.3 and the anisotropy decay curves are shown in Fig. 5.2 for the two probes, C153 and AP. The anisotropy decay profiles were fitted to both bi- and single-exponential functions of time. Although the biexponential fits were found to be marginally better than the single-

exponential fits, the average rotational correlation times, $\langle\tau_{rot}\rangle$, obtained from the biexponential fits were found to be very similar to those obtained from the single-exponential fits (τ_{rot}). The anisptropy decay with associated single-exponential fit has been shown in Fig. 5.3 for prodan in the given protic RTIL. The τ_{rot} values obtained for C153, AP and prodan are 3.7, 4.3 and 5.1 ns, respectively.

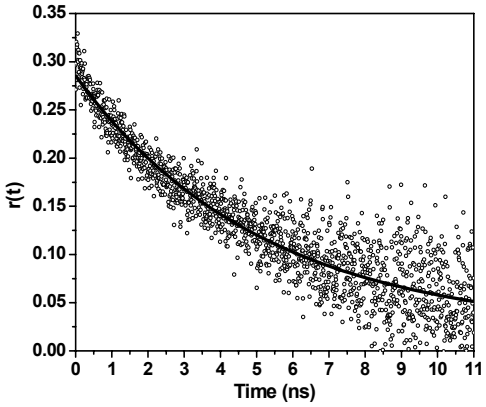

Fig. 5.3. Decay the fluorescence anisotropy, r(t), of prodan in [OH-emim][Tf_2N]. The solid line depicts the single-exponential fit to the data.

Table 5.3. Rotational relaxation parameters of the three probes in [OH-emim][Tf_2N].

Probe	r_0	τ_{rot} (ns)	V (Å^3)[a]	f_{stk}[a]	C_{rot}	C'_{rot}[b]
C153	0.32	3.7±0.07	243	1.5	0.7	0.1-0.7 (many solvents)[c]
AP	0.27	4.3±0.07	134	1.6	1.4	2.7±0.2 (alcohols)[d]
						1.0±0.1 (many aprotic)[d]
prodan	0.28	5.1±0.2	227	2.4	0.66	——

[a]From ref. 7, [b]C'_{rot} are the literature values of rotational coupling constants of the probe molecules in conventional solvents, [c]from ref. 25. [d]from ref. 6.

In the absence of any specific interaction, the solute rotation is primarily governed by the volume of the solute and viscosity of the medium. That the

average rotational time for C153 is higher than that for AP (12 ns and 8.7 ns in [bmim][PF_6], respectively, at 25°C)[6,7] is consistent with a larger size of the former molecule. Interestingly, in the present case, AP has a higher τ_{rot} value than C153 (Table 5.3). This certainly owes to significant hydrogen bonding interaction between the ionic liquid and AP,[20,21] which hinders the rotational motion.

The significant hydrogen bonding interaction between AP and [OH-emim][Tf_2N] is also evident from the following consideration. According to the stick hydrodynamic prediction, the rotational time constant (τ_{stk}) of a nonspherical solute of volume V, rotating along the longest axis of the ellipsoid in a medium of viscosity η at temperature T is given by,

$$\tau_{stk} = \frac{V f_{stk} \eta}{k_B T} \tag{5.2}$$

where f_{stk} is a factor accounting for the nonspherical shape of the solute and k_B is the Boltzman constant. Using the literature value of V and f_{stk},[7] we have calculated the τ_{stk} values for two probes for the present ionic liquid at 25°C. From the calculated τ_{stk} values, the rotational coupling constants, C_{rot}, defined as $C_{rot} = \tau_{rot}/\tau_{stk}$, which are a measure of the extent of departure from normal hydrodynamic behavior of a solute due to specific interaction, are estimated (Table 5.3). The estimated C_{rot} values for AP (C_{rot} = 1.4) differ by a factor of ~2 from that of the other two probes (0.7 for C153 and 0.66 for prodan) in [OH-emim][Tf_2N]. On the other hand, the corresponding values for C153 and AP in other ionic liquid, e.g., in [bmim][PF_6], are 0.5 and 0.7, respectively.[6,7] It can also be seen from Table 5.3, although the C_{rot} values for C153 are very similar in conventional solvents (both protic and aprotic), these values for AP are higher in protic solvents. The

C_{rot} value for AP in [OH-emim][Tf_2N], though lower than that observed in alcohols (Table 5.3), is considerably larger than those in aprotic media. As for prodan, the literature C_{rot} values in conventional solvents are not available. However, from the similarity of the C_{rot} values in case of prodan and C153 (0.66 and 0.7, respectively) we can assume a fairly similar situation in both cases. Therefore, we can conclude that a significant hydrogen bonding interaction between AP and the protic ionic liquid is evident from the hydrodynamic behavior of AP, whereas, no significant interaction is indicative in case of C153 and prodan.

Thus, the steady-state fluorescence and rotational anisotropy data unambiguously establish that AP is strongly hydrogen bonded to the ionic liquid. That this hydrogen bonding is mediated by the interaction of the >C=O group of AP and the –OH moiety of the imidazolium cation is evident from the literature.[20]

5.3.2. Solvation dynamics

To study the dynamic Stokes shift and associated solvation dynamics, the fluorescence decay profiles of the systems have been measured at 28-30 different wavelengths covering the entire emission spectra. Wavelength-dependent decay profiles, which are a typical signature of slow solvation dynamics, have been observed for all of the three systems. The representative wavelength-dependent decay behavior is illustrated for two probes, namely AP and prodan, in Fig. 5.4. When monitored at the shorter wavelength region, only monotonous decay is observed, and at the longer wavelengths, the time profiles consist of a slow rise followed by the decay.

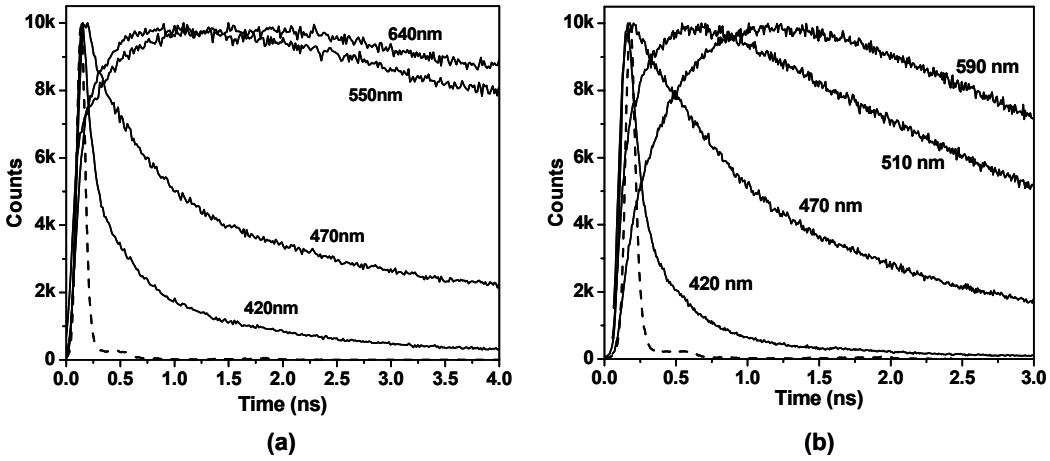

Fig. 5.4. Wavelength-dependent decay profiles of (a) AP and (b) prodan in [OH-emim][Tf_2N]. The monitoring wavelengths are indicated in the respective graphs; the lamp profile in each case is shown as dotted line.

Time-resolved emission spectra (TRES) have been constructed by fitting the individual decay curves to a multiexponential function followed by normalization of the decay traces by steady-state spectra, a process described in Chapter 2 in detail. The TRES for the two probes at five different time intervals are shown in Fig. 5.5. In each case, a time-dependent shift of the emission spectra toward the lower energy, indicating solvent-mediated relaxation of the excited state of the fluorophore, is observable. The total shift of time-dependent emission ($\Delta\bar{\nu}$), has been calculated from the difference between the peak frequencies (in cm^{-1}) of the measured spectra at zero time ($\bar{\nu}(0)$) and infinite time ($\bar{\nu}(\infty)$). The $\Delta\bar{\nu}$ values are 1352, 1834 and 2896 cm^{-1} for C153, AP and prodan, respectively (Table 5.4).

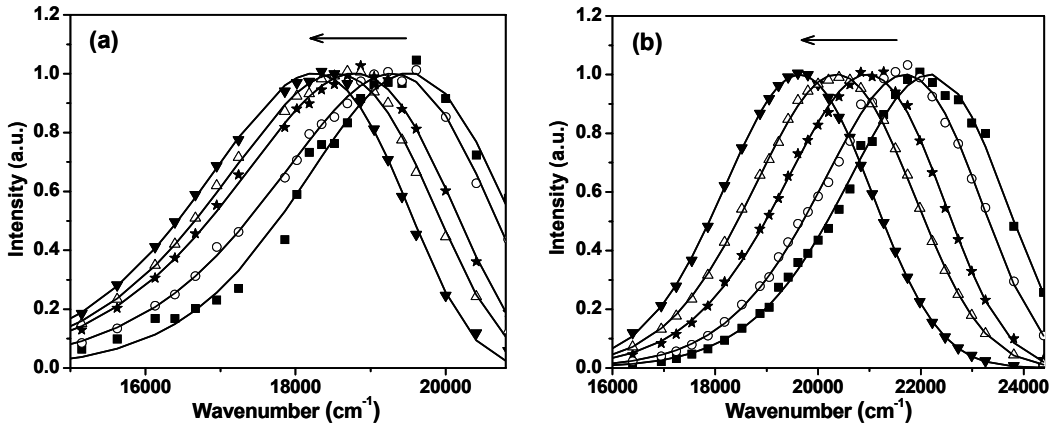

Fig. 5.5. Time-resolved emission spectra (TRES) of (a) C153 in [OH-emim][Tf_2N]: (■) 0 ps, (○) 50 ps, (⋆) 250 ps, (△) 500 ps and (▼) 2.0 ns, and (b) prodan in [OH-emim][Tf_2N]: (■) 0 ps, (○) 50 ps, (⋆) 200 ps, (△) 500 ps and (▼) 2.0 ns. All spectra are normalized at the corresponding peak maximum. λ_{exc} = 374 nm

Table 5.4. Relaxation parameters of solvation and observed shift for the three probes in [OH-emim][Tf_2N].

Probe	From biexponential fit[a]					Stretched exponential fit[c]		Observed shift	f_{miss}[e]
	τ_1 (ps)	τ_2 (ns)	a_1	a_2	$\langle\tau\rangle$[b] (ps)	β	$\langle\tau_{solv}\rangle$[d] (ps)	$[\bar{\nu}(0)-\bar{\nu}(\infty)]$ (cm^{-1})	
C153	180	1.14	0.63	0.37	535	0.67	520	1352	25%
AP	435	1.77	0.63	0.37	930	0.77	850	1834	45%
prodan	180	1.16	0.51	0.49	660	—	—	2896	20%

[a]Using eqn. 5.4, [b]average solvation time $\langle\tau\rangle = a_1\tau_1 + a_2\tau_2$, where $a_1 + a_2 = 1$, experimental error is ±5%, [c]using eqn. 5.5, [d]by eqn. 5.6, [e]missing component.

The time constant for the observable part of the solvation dynamics is calculated from the peak frequencies at various times obtained by the log-normal fit to the TRES. Generally, a correlation function, C(t), of the following form is constructed.

$$C(t) = \frac{\bar{\nu}(t) - \bar{\nu}(\infty)}{\bar{\nu}(0) - \bar{\nu}(\infty)} \tag{5.3}$$

These C(t) values are then plotted against time and fitted to a biexponential function of the following form:

$$C(t) = a_1 \exp(-t/\tau_1) + a_2 \exp(-t/\tau_2) \tag{5.4}$$

where τ_1 and τ_2 are the solvent relaxation time constants. The representative plots for the three probes, C153, AP and prodan with the biexponential fit to the data are depicted in Fig. 5.6.

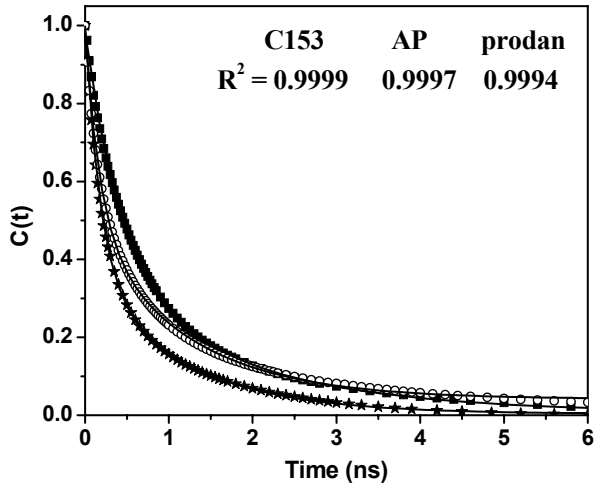

Fig. 5.6. Decay of the spectral shift correlation function, C(t), of C153 (★), AP (■) and prodan (○) in [OH-emim][Tf_2N]. In each case the solid line denotes the biexponentioal fit to the data, where R^2 denotes correlation coefficient.

As can be seen (Fig. 5.6), the observable part of the solvation dynamics is biphasic and similar to those observed in our earlier studies.[3] The average solvation times, $\langle\tau\rangle$, estimated with C153, AP and prodan are 535 ps, 930 ps and 660 ps, respectively (Table 5.4). In this context, we note that Maroncelli and

coworkers treated the observable dynamics as nonexponential and fitted their data to a stretched exponential equation: [6-9]

$$\bar{\nu}(t) = \bar{\nu}(\infty) + \Delta\bar{\nu}\exp(-(t/\tau_0)^{\beta}) \tag{5.5}$$

where, $0 < \beta \leq 1$, and the average time of solvation is obtained by

$$\langle \tau_{solv} \rangle = \frac{1}{\Delta\bar{\nu}} \int_0^{\infty} [\bar{\nu}(t) - \bar{\nu}(\infty)]\,dt = \frac{\tau_0}{\beta}\Gamma(\beta^{-1}) \tag{5.6}$$

where, Γ is the gamma function. A representative stretched exponential fit to our data according to eqn. 5.5 is shown in Fig. 5.7 and the corresponding average solvation time $\langle \tau_{solv} \rangle$ (obtained from eqn. 5.6) and β-values are given in Table 5.4. As can be seen (Fig. 5.7), the fit to the stretched exponential function is inferior to our biphasic fit to the C(t) data (Fig. 5.6). However, the average solvation time obtained by these two methods is quite similar to each other (Table 5.4).

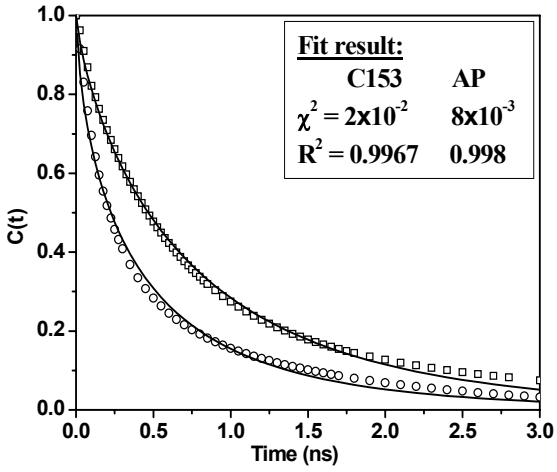

Fig. 5.7. Decay of the spectral shift correlation function, C(t), of C153 (○) and AP (□) in [OH-emim][Tf_2N]. The solid line represents the stretched exponential fit to the data, where, χ^2 is standard deviation and R^2 denotes correlation coefficient.

The solvation dynamics in RTILs is fundamentally different from that in ordinary polar solvents. In molecular solvents, reorientation of the solvent diploes around the probe molecule mainly contributes to solvation. However, the diffusional motion of the constituent ions is expected to contribute significantly to the relaxation process in RTILs. This could be the motion of the individual ions and/or the collective motion of the cation and anion. At the same time, small amplitude motion of the ions in the immediate vicinity of the probe molecule is likely to play an important role, especially in the early part of the solvation dynamics. Also, for polarizable ionic constituents, electronic redistribution in these ions influenced by the change in the dipole moment of the photoexcited probe, may significantly contribute to the early time domain of the dynamics. Clearly, understanding the mechanism of solvation dynamics in RTILs is a complex problem, and at this stage, it is impossible to pinpoint the various motions that contribute to the different components of the dynamics. Despite the complex nature of the dynamics in ionic liquids, recent literature suggests that the dielectric continuum model may work for ionic liquids,[11] and also, orientation dynamics of ionic liquids can be similar to that in van der Waals liquids.[15]

At first, let us focus on the time-resolvable slow component(s) of the dynamics. Because the biphasic nature of the solvation dynamics in imidazolium ionic liquids was found to be similar to that observed in molten salts by Huppert and co-workers,[26] the short component of the observable dynamics was attributed to the translational motion of the anion by Samanta and coworkers, taking into consideration the amplitudes associated with the two observable components.[3-5] The relatively long component was assigned to the collective cation-anion

diffusional motion without speculating what contributes to the missing or ultrafast component of the dynamics.[3-5] Maroncelli and co-workers, on the other hand, treated the dynamics as nonexponential, and their interpretation was focused on the average solvation time, which was assigned to the large-scale diffusion of the constituent ions.[6-9] However, the average solvation time, whether obtained from a biexponential or a stretched exponential fit, does correlate with the viscosity of the medium, at least for the RTILs that are not too viscous.[5] In the present case, judging by the quality of the fits to the spectral shift data (Fig. 5.6 and 5.7), the biphasic description clearly appears to be more suitable than the nonexponential one, even though the nature of the motions responsible for these components may not be very clear.

Let us attempt to see whether the probe dependence of the two resolvable components signifies something. As far as the shorter component of the observable dynamics is concerned, the dynamics is slower in the case of AP by a factor of ~2.5 compared to the other two probes (Table 5.4). Although probe dependence of the solvation dynamics in RTILs is a common observation, such a large difference of the magnitude of this component in the present case is most likely to be the direct consequence of a strong hydrogen bonding interaction of AP with the cation and, hence, could be due to local effects in the proximity of the probe molecule. We are however unable to comment on anything more at this point. Interestingly, because the longer component is not so different for the three probes (1.14, 1.77 and 1.16 ns, from Table 5.4), this component is presumably due to the long-range collective cation-anion motion. It is also important to take

note of the fact that the average solvation time obtained with AP does not correlate with the usual trend of the viscosity dependence (Fig. 5.8).

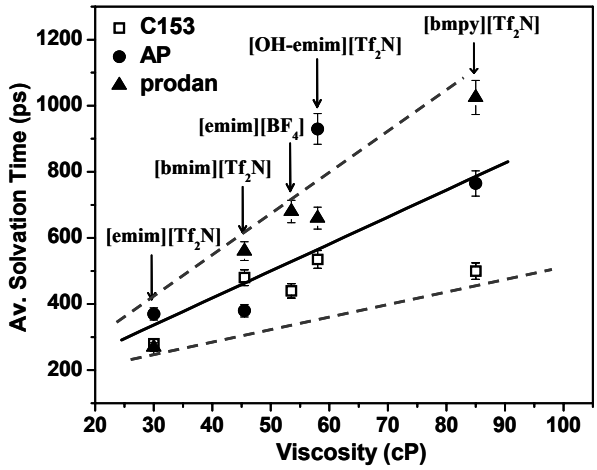

Fig. 5.8. Viscosity dependence of the average solvation time of C153, AP and prodan in low viscosity ionic liquids (η < 100 cP). The data points shown in the plot are collected from the previous studies done in our lab (ref. 3, 5) and the present one. The solid line represents average trend of variation, from which AP in [OH-emim][Tf_2N] clearly stands out. The dashed lines indicate the maximum deviation from the trend line for all other data points. bmpy ≡ N-butyl-N-methylpyrrolidinium.

Because one important aspect of solvent relaxation dynamics in RTILs is the extent of the spectral shift missed due to the ultrafast nature of this component of relaxation, we now concentrate on the component missed in this study. In this context, let us have a look at the literature information on the time scale and origin of this ultrafast component. Maroncelli and coworkers suggested a time scale of 5 ps or <1 ps,[7-9] whereas Petrich et al. have indicated a value of 7 ps for this component on the basis of an upconversion setup with a time-resolution of 1 ps.[10] The latter have also indicated that 50% of the initial dynamics occurs with a

time constant of 40-70 ps. However, because this conclusion regarding the early part of the dynamics is based upon a single-wavelength solvent response function, we are not sure whether one should attach too much importance to this findings. More recent data on this aspect have come from two recent works.[12,13] Maroncelli and co-workers observed the full solvation response of 4-dimethylamino-4′-cyanostilbene in three imidazolium ionic liquids using the Kerr-gated emission spectroscopy (450 fs resolution) and single-photon counting fluorescence technique.[12] The results of this work suggest that the ultrafast component of the dynamics is of the order of 300-700 fs at room temperature. A recent work is based on a femtosecond upconversion technique (230 fs resolution) involving C153 where the authors have shown that only 10-20% of the total dynamics is ultrafast and occurs within 10 ps.[13] The authors have pointed out that, due to factors such as conformational changes of the fluorophore in polar and nonpolar solvents, superimposition of the internal relaxation of the probe with the early part of solvent relaxation, etc, precise construction of the 'zero-time' spectrum may not be possible by following the method suggested by Fee and Maroncelli[27] from the steady-state data.

While Maroncelli and coworkers attributed the ultrafast component in imidazoilum ionic liquid to small amplitude motion of imdazolium cations in close contact with the probe, facilitated by the coplanar arrangement of the probe and imidazolium moiety,[8,9] others have speculated that the ultrafast dynamics could be due to the polarizability of the cation.[10,11] Recent simulations[28] have indicated collective cation-anion motion on the subpicosecond time scales that argues against a purely anionic subpicosecond solvation response.[29] Though the

role of the cation in the ultrafast component of dynamics was reinforced by the absence of this component in alkylammonium or alkylphophonium ionic liquids,[8,9] later studies on a pyrrolidinium ionic liquid,[5] which is a cyclic analogue of tetraalkylammonium ionic liquid, where substantial ultrafast component was indicated, implies that the planarity and polarizability of the cation are not the only factors responsible for the ultrafast component of the dynamics.

In most of the earlier studies in imidazolium ionic liquids, nearly 40-50% of the total expected shift was missed in TCSPC setups having a time-resolution ~25 ps. For example, in [bmim][BF_4] and [emim][Tf_2N], the observed shift is 900 and 1010 cm^{-1}, respectively. Hence, the extent of missing component, which is obtained by assuming the total expected shift in these RTILs to be comparable to that reported for the isopolar solvents[30] (namely, 1-pentanol and 1-decanol, respectively),[22] is nearly 50% for the former and 45% for the latter. The missing component has been estimated to be ~35-40% in the case [bmim][PF_6].[6,14] In the present study, the missing component for C153 is estimated assuming that the 'expected' total shift in [OH-emim][Tf_2N] is the same as in an isopolar solvent. Considering that the $E_T(30)$ value of this ionic liquid (50.5, using C153 as probe) is close to that of 1-propanol ($E_T(30)$ = 50.7),[23] the total shift expected in [OH-emim][Tf_2N], calculated from the 'zero-time' spectra for C153 in 1-propanol,[30] is 1820 cm^{-1}. Hence, the calculated missing component for C153 is ~25%, which is substantially less than those reported in other imidazolium ionic liquids. In the case of AP and prodan, however, the missing component was calculated according to the conventional procedure described by Fee and Maroncelli.[27] The values are 45% and 20%, respectively, which are again substantially less than

those observed in alkylimidazolium RTILs (e.g., the missing component in [bmim][PF_6] is reported to be ~63%).[6] Since the effective time-resolution of the present setup (~40 ps) is less than that of the usual laser-based TCSPC setup (~25 ps), these numbers are quite significant.

To rationalize why the extent of missing component is less in the present case, we note that in a recent study of solvation dynamics in [bmim][BF_4]-based microemulsion (ionic liquid-in-oil type) the missing component (15-25%) for C153 was substantially less than that in neat ionic liquid.[16] The authors suggested that restricted motion of ions in microemulsion pool slows down the dynamics thereby retarding the ultrafast component by a sizable proportion. In our case, such local effects must play an important role. We have shown that the cations in the first solvation shell are hydrogen bonded to the probe molecules and that this hydrogen bonding interaction is particularly significant in the case of AP. This hydrogen bonding interaction can restrict the motion of the cations, and slow down the dynamics of the ultrafast component. Again, at the same time, significant hydrogen bonding interaction between the cations and anions in the first solvation shell can also contribute to the retardation of the individual motion of the ionic constitutents as well as the collective cation-anion motion. At any rate, the net result will be a substantial retardation of the ultrafast dynamics leading to a net decrease of the 'expected' missing component.

5.4. Conclusion

In summary, we have studied for the first time the steady-state and time-resolved fluorescence behaviors of dipolar molecules, namely C153, AP and prodan, in an alcohol-functionalized ionic liquid based on the imidazolum moiety

in order to investigate the influence of specific hydrogen bonding interactions on the solvation and rotational dynamics in RTILs. Hydrogen bonding interactions between the probe molecules and the hydroxylated cations have been demonstrated by the steady-state and time-resolved anisotropy studies. The present ionic liquid is found to be more polar than other imidazolium ionic liquids that lack the hydroxyl functionality. However, the estimated polarity of the ionic liquid using these probe molecules is found to be significantly lower than that estimated using the betaine dye. Hydrogen bonding interactions are shown to have a significant influence on the dynamics of the solute rotation. The solvation dynamics is shown to be biphasic with the relatively shorter component strongly dependent on the hydrogen bonding interaction and, hence, is highly dependent on the identity of the probe molecule. It is also found that in this ionic liquid the ultrafast component of the dynamics, which is commonly missed in most studies because of limited time-resolution, is substantially less than that in other ionic liquids. This observation has been primarily attributed to the local effect due to hydrogen bonding interactions between the probe and the cationic moiety. However, the hydrogen bond mediated cation-anion association in the first solvation shell can also contribute to the reduction of the ultrafast component.

Reference

1. (a) Mandal, P. K.; Saha, S.; Karmakar, R.; Samanta, A. *Curr. Sci.* **2006**, *90*, 301. (b) Samanta, A. *J. Phys. Chem. B* **2006,** *110,* 13704.
2. Jin, H.; Baker, G. A.; Arzhantsev, S.; Dong, J.; Maroncelli, M. *J. Phys. Chem. B* **2007**, *111*, 7291.
3. (a) Karmakar, R.; Samanta, A. *J. Phys. Chem. A* **2002**, *106*, 4447. (b) Karmakar, R.; Samanta, A. *J. Phys. Chem. A* **2002**, *106*, 6670. (c) Karmakar, R.; Samanta, A. *J. Phys. Chem. A* **2003**, *107*, 7340.
4. (a) Saha, S.; Mandal, P. K.; Samanta, A. *Phys. Chem. Chem. Phys.* **2004**, *6*, 3106. (b) Mandal, P. K.; Paul, A.; Samanta, A. *Res. Chem. Intermed.* **2005**, *31*, 575.
5. Mandal, P. K.; Samanta, A. *J. Phys. Chem. B* **2005**, *109*, 15172.
6. Ingram, J. A.; Moog, R. S.; Ito, N.; Biswas, R.; Maroncelli, M. *J. Phys. Chem. B* **2003**, *107*, 5926.
7. Ito, N.; Arzhantsev, S.; Maroncelli, M. *Chem. Phys. Lett.* **2004**, *396*, 83.
8. Arzhantsev, S.; Ito, N.; Heitz, M.; Maroncelli, M. *Chem. Phys. Lett.* **2003**, *381*, 278.
9. Ito, N.; Arzhantsev, S.; Heitz, M.; Maroncelli, M. *J. Phys. Chem. B* **2004**, *108*, 5771.
10. Chowdhury, P. K.; Halder, M.; Sanders, L.; Calhoun, T.; Anderson, J. L.; Armstrong, D. W.; Song, X.; Petrich, J. W. *J. Phys. Chem. B* **2004**, *108*, 10245.
11. Halder, M.; Headley, L. S.; Mukherjee, P.; Song, X.; Petrich, J. W. *J. Phys. Chem. A* **2006**, *110*, 8623.
12. Arzhantsev, S.; Jin, H.; Ito, N.; Maroncelli, M. *Chem. Phys. Lett.* **2006**, *417*, 524.
13. Lang, B.; Angulo, G.; Vauthey E. *J. Phys. Chem. A* **2006**, *110*, 7028.
14. Chakrabarty, D.; Hazra, P.; Chakraborty, A.; Seth, D.; Sarkar, N. *Chem. Phys. Lett.* **2003**, *381*, 697.
15. Cang, H.; Li, J.; Fayer, M. D. *J. Chem. Phys.* **2003**, *119*, 13017.
16. Chakrabarty, D.; Seth, D.; Chakraborty, A.; Sarkar, N. *J. Phys. Chem. B* **2005**, *109*, 5753.
17. (a) Seth, D.; Chakraborty, A.; Setua, P.; Sarkar, N. *J. Phys. Chem. B* **2007**, *111*, 4781. (b) Adhikari, A.; Sahu, K.; Dey, S.; Ghosh, S.; Mandal, U.; Bhattacharyya, K. *J. Phys. Chem. B.* **2007**, *111*, 12809.
18. (a) Chakrabarty, D.; Chakraborty, A.; Seth, D.; Sarkar, N. *J. Phys. Chem. A* **2005**, *109*, 1764. (b) Chakrabarty, D.; Chakraborty, A.; Seth, D.; Hazra, P.; Sarkar, N. *Chem. Phys. Lett.* **2004**, *397*, 469. (c) Baker, S. N.; Baker, G. A.; Munson, C. A.; Chen, F.; Bukowski, E. J.; Cartwright, A. N.; Bright, F. V. *Ind. Eng. Chem. Res.* **2003**, *42*, 6457.
19. Dzyuba, S. V.; Bartsch, R. A. *Tetrahedron Lett.* **2002**, *43*, 4657.
20. Soujanya, T.; Krishna, T. S. R.; Samanta, A. *J. Phys. Chem.* **1992**, *96*, 8544.

21. Soujanya, T.; Krishna, T. S. R.; Samanta, A. *J. Photochem. Photobiol.* **1992**, *66*, 185.
22. (a) Seddon, K. R.; Stark, A.; Torres, M. J. In *Clean Solvents: Alternative Media for Chemical Reactions and Processing*; Abraham, M., Moens, L., Eds.; ACS Symposium Series 819; American Chemical Society: Washington, DC, 2002; p 34. (b) Bonhote, P.; Dias, A. P.; Papageorgiou, N.; Kalyanasundaram, K.; Gratzel, M. *Inorg. Chem.* **1996**, *35*, 1168.
23. Reichardt, C. *Solvents and Solvent Effects in Organic Chemistry*; VCH: Weinheim, Germany, 1988.
24. Reichardt, C. *Green Chem.* **2005**, *7*, 339.
25. Horng, M.-L.; Gardecki, J.; Maroncelli, M. *J. Phys. Chem.* **1997**, *101*, 1030.
26. (a) Bart, E.; Meltsin, A.; Huppert, D. *J. Phys. Chem.* **1994**, *98*, 3295. (b) Bart, E.; Meltsin, A.; Huppert, D. *J. Phys. Chem.* **1994**, *98*, 10819. (c) Bart, E.; Meltsin, A.; Huppert, D. *J. Phys. Chem.* **1995**, *99*, 9253.
27. Fee, R. S.; Maroncelli, M. *Chem. Phys.* **1994**, *183*, 235.
28. Kobrak, M. N.; Znamenskiy, V. *Chem. Phys. Lett*. **2004**, *395*, 127.
29. Shim, Y.; Duan, J. S.; Choi, M. Y.; Kim, H. J. *J. Chem. Phys*. **2003**, *119*, 6411.
30. Horng, M. L.; Gardecki, J. A.; Papazyan, A.; Maroncelli, M. *J. Phys. Chem.* **1995**, *99*, 17311.

Chapter 6

Solvation Dynamics in the Mixtures of an RTIL with Nonpolar Solvents

Recognizing the potential of the mixed solvent systems comprising ionic liquid as one of the constituents in real applications, the steady-state and time-resolved fluorescence behavior of C153 has been studied in neat 1-butyl-3-methylimidazolium hexafluorophosphate and its mixtures with nonpolar solvents, namely, toluene and 1,4-dioxane. Though no significant effect of the nonpolar solvent was observed in the steady-state behavior of the probe, time-resolved anisotropy study shows a decrease of rotational correlation time. On gradual addition of nonpolar solvents, a continuous blue shift of the time-zero spectrum was observed, resulting in larger Stokes shift of the time-dependent spectra. The average solvation time also gradually decreases during the same course. A comparison of the time-dependent spectral data of the RTIL-toluene and RTIL-dioxane systems shows that, while a small amount of toluene can significantly affect the dynamics, comparatively, a larger amount of dioxane is required to bring about the same effect.

6.1. Introduction

As mentioned earlier, there is a growing number of recent studies focusing on the physicochemical properties of mixtures of RTIL and conventional molecular solvent, because of the potential utility of such mixed systems.[1-7] It is found that the addition of a cosolvent significantly changes a number of physical properties of the RTILs such as the viscosity,[1] polarity,[2-4] solvation[3,4] and electrochemical[5-7]

behavior. From solvatochromic probe behavior in the RTIL-molecular solvent mixtures it is known that the probe is preferentially solvated in the RTIL core, unless the cosolvent is highly polar and protic one.[3,4] For, in the latter case, cybotactic region of the probe is also enriched with the cosolvent. The electrical conductivity measurements in the mixed solvent systems revealed that ionic association is promoted by addition of molecular solvents to RTILs, with the exception of highly polar solvents which may promote dissociation.[6]

There have been a few studies on solvation dynamics in RTIL-based microheterogeneous systems like microemulsions, micelles and so forth[8] and in mixtures of RTIL and *polar* conventional solvents.[9] However, dynamical study in mixed solvents containing RTIL and nonpolar solvents has not yet been carried out. It will be of interest to study the effect of nonpolar solvents on the solvation dynamics of a probe molecule in an RTIL, for, in one hand, enhanced ionic association promoted by nonpolar solvents, as has been found experimentally,[4,6] is likely to slow down the dynamics because of restricted ionic mobility. On the other hand, the dynamics is expected to be faster in RTIL-nonpolar solvent mixture due to the reduced viscosity of the solution. Therefore, it will be quite interesting to see how the dynamic solvation of a probe in an RTIL is perturbed by addition of a nonpolar solvent and whether or how this effect can be connected to the ion association or aggregation in the RTILs.

In the present study, we have chosen toluene as the primary nonpolar cosolvent to study its effect on solvation dynamics in an RTIL, namely, 1-butyl-3-methylimidazolium hexafluorophosphate, [bmim][PF_6] (Chart 6.1). The choice was guided by the fact that toluene is one of the most nonpolar solvents having an

appreciable solubility in [bmim][PF_6]. The solvation dynamics has been studied in neat RTIL and in a number of RTIL-toluene mixtures of varying toluene content. RTIL-1,4-dioxane mixtures have also been studied for a comparison. In all experiments, one of the most widely used solvation probes C153 was employed (Chart 6.1). The polarity parameters of these media are depicted in the Table 6.1.

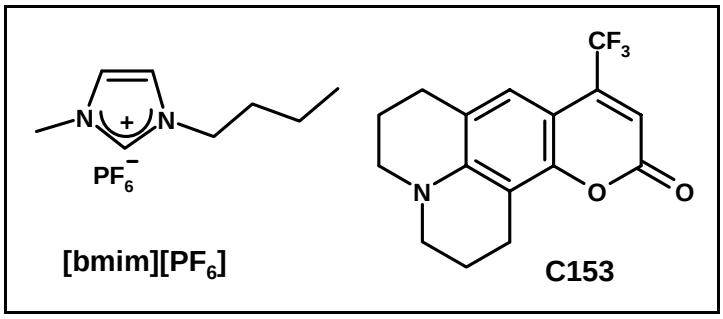

Chart 6.1. Structure and abbreviation of the RTIL and probe molecule employed in this study.

Table 6.1. Polarity parameters of the RTIL and conventional solvents used in this study.

System	$E_T(30)$	Dielectric constant
[bmim][PF_6]	52.0[a]	11.4[c]
Toluene	33.9[b]	2.38[b]
Dioxane	36.0[b]	2.21[b]

[a]From ref. 10, [b]from ref. 11, [c]from ref. 12.

6.2. Steady-state behavior

The UV-visible absorption and fluorescence behavior of C153 in [bmim][PF_6] is found to be similar to that reported previously.[13,14] With successive addition of toluene to a solution of C153 in the RTIL, the intensities of the absorption and fluorescence spectra are decreased as a result of dilution, but the wavelengths

corresponding the absorption and fluorescence maximum suffer negligible shift. This feature is depicted in Fig. 6.1. A similar observation is made in the RTIL-dioxane mixture. This steady-state behavior of C153 suggests that the solvation shell of the probe is unaffected by the addition of toluene or dioxane.

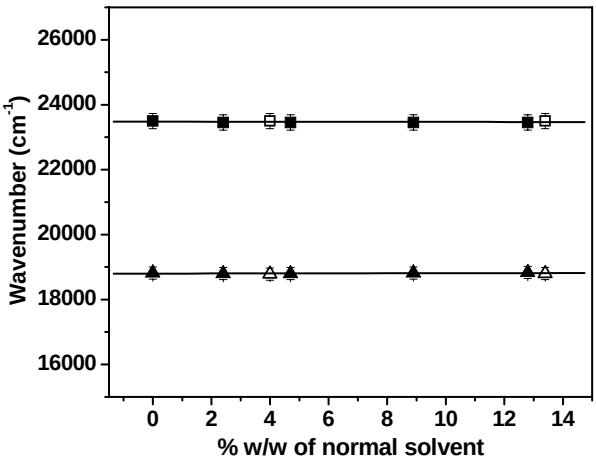

Fig. 6.1. Absorption (■ or □) and emission (▲or △) maxima (in wavenumber) of C153 in neat RTIL and in RTIL-toluene (filled) and RTIL-dioxane (hollow) mixtures of different wt percentage. The trend lines indicate that both $\bar{\nu}_{max}^{abs}$ and $\bar{\nu}_{max}^{ems}$ are invariant to the added solvent in the given concentration range.

6.3. Time-resolved measurements

6.3.1. Rotational dynamics

Time-resolved fluorescence anisotropy, r(t), is calculated using the following equation:

$$r(t) = \frac{I_{||}(t) - GI_{\perp}(t)}{I_{||}(t) + 2GI_{\perp}(t)} \qquad (6.1)$$

where, G is the correction factor for the detector sensitivity to the polarization direction of the emission and $I_{||}(t)$ and $I_{\perp}(t)$ are the fluorescence decays polarized

parallel and perpendicular to the polarization of the excitation light, respectively. The anisotropy results in neat RTIL and two RTIL-toluene mixtures of different toluene content are collected in Table 6.2 and the associated anisotropy decay curves are shown in Fig. 6.2. The initial anisotropy r_0 of the probe C153 in neat [bmim][PF_6] is found to be 0.28 and it does not changes much with increasing toluene content. The anisotropy decay profiles were fitted to both biexponential and single-exponential functions of time. While the biexponential fits were found somewhat better than the single-exponential fits, the average rotational correlation times, $\langle\tau_{rot}\rangle$, obtained from the biexponential fits were found very similar to those (τ_{rot}) obtained from the single-exponential fits. The τ_{rot} value for C153 in neat RTIL is measured to be 6.6 ns and this value decreases with increasing toluene content in the mixtures, i.e., with decreasing viscosity of the medium (Table 6.2). In this context, we note that the τ_{rot} value of C153 in neat [bmim][PF_6] has been measured previously by different groups. While Chakrabarty et. al.[13] reported a value of 3.58 ns with $r_0 = 0.3$, Ito et. al.[14] have reported a value of 12 ns by fitting the anisotropy data to a stretched exponential fit using a fixed r_0 value of 0.37.

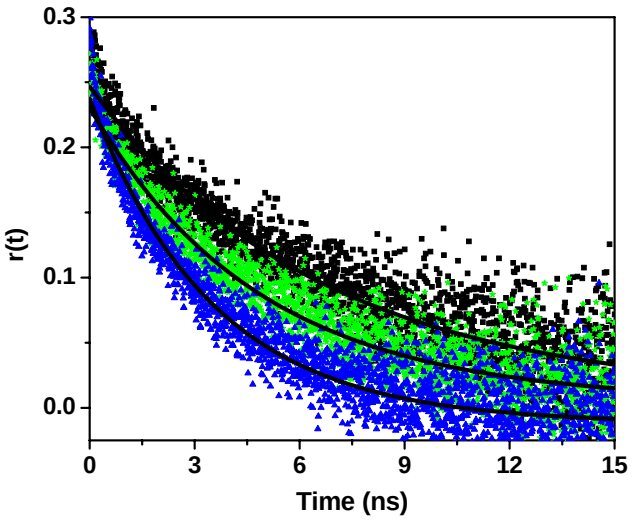

Fig. 6.2. Decay the fluorescence anisotropy, r(t), of C153 in neat RTIL (■) and in RTIL-toluene mixtures having 2.3% w/w of toluene (★) and 6.6% w/w of toluene (▲). In each case the solid line denotes the appropriate fit to the anisotropy data.

In the absence of any specific interaction, the solute rotation is primarily governed by the volume of the solute and the viscosity of the medium. According to the stick hydrodynamic prediction, the rotational time-constant (τ_{stk}) of a nonspherical solute of volume V, rotating along the longest axis of the ellipsoid in a medium of viscosity η at temperature T is given by

$$\tau_{stk} = \frac{V f_{stk} \eta}{k_B T} \tag{6.2}$$

where f_{stk} is a factor accounting for the non-spherical shape of the solute, and k_B is the Boltzmann constant. Using the literature value of V and f_{stk},[14] the τ_{stk} values for the probe are calculated for neat RTIL and different RTIL-toluene mixtures at 25°C. From the calculated τ_{stk} values, the rotational coupling constants, C_{rot}, defined as $C_{rot} = \tau_{rot}/\tau_{stk}$, which are a measure of the extent of departure from

normal hydrodynamic behavior of a solute due to specific interaction, are estimated (Table 6.2). The estimated C_{rot} values for the probe in different solutions are essentially similar to what is observed in neat RTIL (0.35), and these C_{rot} values lie within the normal range, i.e., those obtained in conventional solvents (typically 0.1-0.7).[15]

Table 6.2. Rotational relaxation parameters for C153 in neat [bmim][PF_6] and in different binary mixtures.

Systems	Viscosity (cP)	r_0	τ_{rot} (ns)[a]	V (Å^3)[b]	f_{stk}[b]	C_{rot}	C'_{rot}[c]
Neat RTIL	210	0.28	6.6 ± 0.15	243	1.5	0.35	0.1-0.7 (many solvents)[d]
RTIL+ 2.3% w/w of toluene	158	0.27	4.8 ± 0.10			0.34	
RTIL + 6.6% w/w of toluene	110	0.28	3.5 ± 0.06			0.35	
RTIL + 6.6% w/w of dioxane	130	0.28	4.1 ± 0.07			0.35	

[a]These τ_{rot} values are obtained from the single-exponential fit to the anisotropy data. [b]From ref. 14, [c]C'_{rot} are the literature values of rotational coupling constants of the probe molecules in conventional solvents, [d]from ref. 15.

A similar result is obtained with the RTIL-dioxane mixtures (Table 6.2). Therefore, as far as the rotational dynamics is concerned, the behavior of the RTIL is similar to that of the molecular solvents, and the addition of nonpolar solvents does not change the situation.

6.3.2. Solvation dynamics

Representative TRES for C153 in a given RTIL-toluene mixture at five different time-intervals are shown in Fig. 6.3. In all cases, a time-dependent shift of the emission spectrum toward the lower energy, indicating solvent-mediated relaxation of the excited state of the fluorophore, is observable. The total time-dependent Stokes shift ($\Delta\bar{\nu}$) due to solvation, measured from the wavenumbers corresponding to the fluorescence maxima at zero time (given by $\bar{\nu}(0)$) and infinite time (given by $\bar{\nu}(\infty)$), is found to be 965 cm^{-1} for C153 in [bmim][PF_6] (Table 6.3). The $\Delta\bar{\nu}$ values reported by Chakrabarty et al.[13] is 900 cm^{-1}, whereas Ito et al.[14] observed a time-dependent shift of 1370 cm^{-1} in neat [bmim][PF_6].

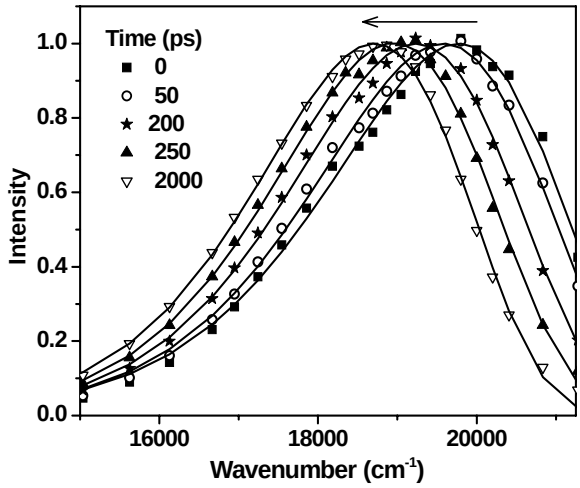

Fig. 6.3. Time-resolved emission spectra (TRES) of C153 in [bmim][PF_6] + toluene (4.7% w/w) mixture. The time-intervals are indicated for the symbols in the graph. All spectra are normalized at the corresponding peak maximum. λ_{exc} = 374 nm

Table 6.3. Observed shift, $\bar{\nu}(0)$ values and the extent of missing component for C153 in neat [bmim][PF_6] and in [bmim][PF_6]-toluene mixtures.

Sets	Wt % of toluene	Viscosity (cP)	$\bar{\nu}(0)$ (cm^{-1})	Observed shift ($\Delta\bar{\nu}$) (cm^{-1})	Missing Component
I	0	210	19520	965	52%
II	2.4	156	19670	1050	48%
III	4.7	125	19780	1130	44%
IV	8.9	98	19800	1155	42%
V	12.8	79	19850	1160	42%

6.3.2.1. Time-zero spectra

One very interesting feature of the TRES in neat RTIL and RTIL-toluene mixtures is the observation of a steady blue shift of the measured time-zero spectrum with increasing toluene content (Table 6.3). The blue shift, as observed from the difference in the $\bar{\nu}(0)$ values measured in neat RTIL (set I) and in the last set of the mixture (set V, having 12.8% w/w of toluene), is nearly 330 cm^{-1}. The corresponding shift of the $\bar{\nu}(\infty)$ value (indicative of the completion of dynamic solvation) is much less, i.e., ~130 cm^{-1}. This differential shift of the $\bar{\nu}(0)$ and $\bar{\nu}(\infty)$ values results in a larger time-dependent Stokes shift ($\Delta\bar{\nu}$) upon increasing the toluene content in the mixture. It can be seen from Table 6.3 that the observed Stokes shift ($\Delta\bar{\nu}$) for set V (12.8% w/w of toluene) is ~200 cm^{-1} larger than that for set I (neat RTIL). The blue shift of the $\bar{\nu}(0)$ values with increasing toluene content is an indication of the involvement of nonpolar cosolvent in the early part of the dynamics. It is clearly evident that toluene is interspersed into the RTIL-rich cybotactic region of the probe. In other words, the

blue shift of the time-zero spectrum in the presence of toluene implies a definite proximity and involvement of the nonpolar cosolvent in the solvation of the probe prior to the photoexcitation. Interestingly, the steady-state data, which indicates only an average behavior, cannot provide information of this nature.

6.3.2.2. Observed shift and missing component

As mentioned earlier, the observed Stokes shift ($\Delta\bar{\nu}$) due to solvent relaxation is around 965 cm^{-1} in neat [bmim][PF_6], and this value is higher in the RTIL-toluene mixtures (Table 6.3), because of the blue shift of $\bar{\nu}(0)$ with increasing toluene content and a larger blue shift of $\bar{\nu}(0)$ compared to $\bar{\nu}(\infty)$. This observation indicates that, in presence of the nonpolar solvent, the microenvironment of the probe is comparatively nonpolar at the initial stage of dynamics, whereas the probe environment is relatively more polar at the final stage, i.e., upon the completion of dynamics. Thus, there occurs a *polarity shift* during the course of the dynamic solvation in the mixed solvent systems. Since the excited state of a dipolar probe such as C153 is more polar than the ground state, the photoexcited probe is stabilized in a more polar environment, which is created by the displacement of some nonpolar toluene molecules from the cybotactic region of the probe by the constituent ions of the RTIL during the course of dynamics.

Since the total Stokes shift expected as a result of solvation, as calculated by Maroncelli and co-workers,[14] is ~2000 cm^{-1} for [bmim][PF_6], our data suggests that more than 50% of the dynamics is missed (Table 6.3) because of limited time-resolution of our TCSPC setup. However, since $\Delta\bar{\nu}$ increases with

increasing toluene content of the mixture, the missing component appears to be significantly lower: only 42% in the solution having highest toluene content (set V, Table 6.3). However, this may be misleading, as the larger $\Delta\bar{\nu}$ value for the mixed solutions is simply due to the blue shift of $\bar{\nu}(0)$. The situation arises because the total expected Stokes shift, calculated from steady-state spectra,[16] do not reflect the influence of toluene on solvation. Clearly, the procedure of calculation of the missing component using the steady-state spectra cannot be applied in the present case. Since it is difficult to pinpoint the *actual* time-zero spectra (the starting point of the solvation) in this case, the extent of the missing component cannot be precisely determined for the mixed systems.

6.3.2.3. Observable dynamics

The time constants of the observable dynamics have been obtained from the plot of the spectral shift correlation function, C(t), defined as

$$C(t) = \frac{\bar{\nu}(t) - \bar{\nu}(\infty)}{\bar{\nu}(0) - \bar{\nu}(\infty)} \tag{6.3}$$

versus time. A biexponential function of the form

$$C(t) = a_1\exp(-t/\tau_1) + a_2\exp(-t/\tau_2) \tag{6.4}$$

where τ_1 and τ_2 are the solvent relaxation time-constants, and a_1 and a_2 are normalized preexponential factors, was found to describe the time dependence of C(t). The C(t) versus time plots for neat RTIL and the RTIL-toluene mixtures are shown in Fig. 6.4 along with the biexponential fits. The various time-constants (τ_i) and a_i values are collected in Table 6.4.

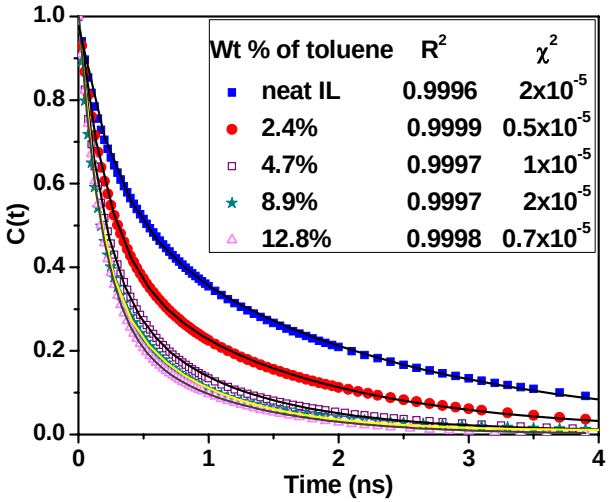

Fig. 6.4. Decay of the spectral shift correlation function, C(t), of C153 in [bmim][PF_6] and different RTIL-toluene mixtures. In each case the solid line denotes the biexponentioal fit to the data (eqn. 6.4), where, χ^2 is standard deviation and R^2 is correlation coefficient.

Table 6.4. Relaxation parameters of solvation for C153 in neat RTIL and in RTIL-toluene mixtures.

Sets	Wt % of toluene	Viscosity (cP)	From biexponential fit[a]					Stretched exponential fit[c]	
			τ_1 (ns)	τ_2 (ns)	a_1	a_2	τ_{av} [b] (ns)	β	τ_{av}^{str} [d] (ns)
I	0	210	0.28	1.99	0.43	0.57	1.25	0.645	1.34
II	2.4	156	0.22	1.43	0.56	0.44	0.75	0.65	0.75
III	4.7	125	0.19	0.92	0.62	0.38	0.47	0.7	0.46
IV	8.9	98	0.15	0.74	0.6	0.4	0.38	0.69	0.38
V	12.8	79	0.17	0.87	0.71	0.29	0.37	0.75	0.34

[a]Using eqn. 6.4, [b]average solvation time $\tau_{av} = a_1\tau_1 + a_2\tau_2$, where $a_1 + a_2 = 1$, experimental error is ±5%, [c]using eqn. 6.5, [d]by eqn. 6.6.

This biphasic solvation dynamics is similar to what has been observed in the previous studies from our laboratory.[17,18] The estimated average solvation time ($\tau_{av} = a_1\tau_1 + a_2\tau_2$) in neat [bmim][$PF_6$] is found to be somewhat higher (1.25 ns) than the previously reported value (1.0 ns),[14] even though our sample (210 cP) is slightly less viscous than the previously used (260 cP) [bmim][PF_6]. The results presented in Table 6.4 show that τ_{av} monotonically decreases with increasing toluene content in the mixture, obviously because of a steady decease of the viscosity of the solution. The decrease of τ_{av} is less pronounced for higher weight percentage of toluene.

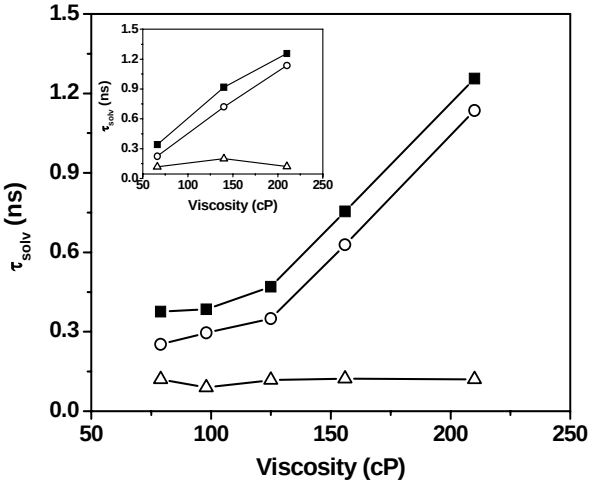

Fig. 6.5. Variation of average and weighted solvation times with respect to the viscosity of different RTIL-toluene mixtures. The respective plots are: average solvation time, τ_{av} (■), weighted short time-component, $a_1\tau_1$ (△) and weighted long time-component, $a_2\tau_2$ (○). The same for RTIL-dioxane mixtures has been shown in the inset.

This feature is more clearly evident from Fig. 6.5, wherein the average solvation time is plotted against the viscosity of the RTIL-toluene mixture. Interestingly, while the individual τ_i values decrease continually with increasing toluene content (or decreasing viscosity) in the mixture (Table 6.4), we find that the dependence of the two weighted solvation times ($a_i\tau_i$) on the viscosity of the medium is quite different. Fig. 6.5 indicates that, while the weighted short component ($a_1\tau_1$) is more or less *insensitive* to the viscosity change (i.e., dilution effect), the longer counterpart ($a_2\tau_2$) follows a trend similar to that of τ_{av}.

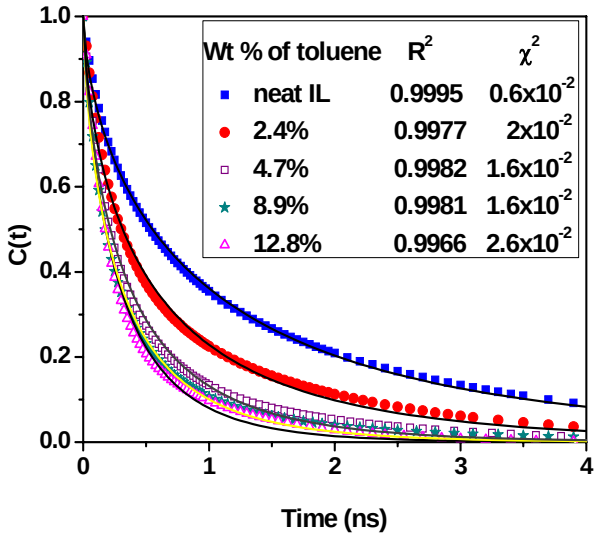

Fig. 6.6. Decay of the spectral shift correlation function, C(t), of C153 in [bmim][PF_6] and different RTIL-toluene mixtures. The solid line represents the stretched exponential fit to the data according to eqn. 6.5, where, χ^2 is standard deviation and R^2 denotes correlation coefficient.

In this context, we note that, while a biphasic description of the solvation dynamics is preferred by many groups,[8,9,13,17,18] others have considered the

dynamics as nonexponential with a distribution of solvation times estimated from a stretched exponential fit to the $C(t)$ data according to:[14,19]

$$C(t) = \exp(-t/\tau_{solv})^{\beta} \tag{6.5}$$

where $0 < \beta \leq 1$, and the average solvation time is obtained by

$$\tau_{av}^{str} = \frac{1}{\Delta\bar{\nu}}\int_0^{\infty}[\bar{\nu}(t) - \bar{\nu}(\infty)]dt = \frac{\tau_{solv}}{\beta}\Gamma(\beta^{-1}) \tag{6.6}$$

where Γ is the gamma function. The stretched exponential fit to our data according to eqn. 6.5 is shown in Fig. 6.6, and the corresponding average solvation time (τ_{av}^{str}) and β values are given in Table 6.4. Although both biphasic and nonexponential treatment to the observable dynamics yield similar average solvation times (Table 6.4), judging by the quality of the fit to our present data (comparing Fig. 6.4 and 6.6) one can readily see that the biphasic description is more appropriate than the stretched exponential one (especially in the case of RTIL-toluene mixtures), even though the significance of the individual component is not clear.

The correlation highlighted in Fig. 6.5 perhaps points to the importance of the weighted components ($a_i\tau_i$ values) over the individual τ_i values. As can be seen from Fig. 6.7, the weighted long component ($a_2\tau_2$) correlates with the average value (τ_{av}), whereas the short component ($a_1\tau_1$) remains almost constant. A plot based on the data obtained for a few other RTILs (with C153 as the probe) also indicates a similar trend (inset to Fig. 6.7). We must admit in this context that the physical significance of this correlation is not so obvious. One can perhaps presume that the average solvation time is composed of two distinct time-components (represented by $a_i\tau_i$'s), the shorter one having much less contribution

from the overall diffusional motion of the ions as compared to that of the longer component. Recalling the insensitivity of the early (ultrafast) dynamics to the viscosity of the medium,[13,14,18-20] such a situation may not be altogether impossible.

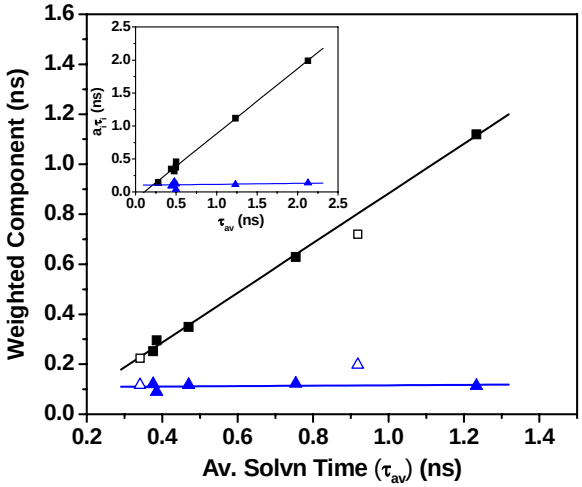

Fig. 6.7. Variation of the weighted solvation time-components, namely, weighted short component, $a_1\tau_1$ (▲ or △) and weighted long component, $a_2\tau_2$ (■ or □) with the average solvation time (τ_{av}) for RTIL-toluene (filled) and RTIL-dioxane (hollow) mixtures of varying wt percentage. Inset shows the similar variation in a few other RTILs reported in the literature, namely, [emim][Tf_2N],[17c] [bmim][Tf_2N],[17c] [emim][BF_4],[17b] [OH-emim][Tf_2N],[21] [BuPy][Tf_2N],[18] [bmim][BF_4][17b] and [bmim][PF_6] (this work). (BuPy≡ 1-butyl-1-methylpyrrolidinium, OH-emim ≡ 1-hydroxyethyl-3-methylimidazolium).

6.3.2.4. RTIL-toluene versus RTIL-dioxane mixture

We have also studied two sets of RTIL-dioxane mixtures, primarily to corroborate the findings with the RTIL-toluene mixtures. The choice of dioxane is governed by the fact that it is only slightly more polar than toluene in terms of $E_T(30)$, but is much less polar than the RTIL, both in terms of $E_T(30)$ and

dielectric constant values (Table 6.1). The relevant dynamical data for RTIL-dioxane systems are collected in Table 6.5.

Table 6.5. Relaxation parameters of solvation and observed shift for C153 in different RTIL-dioxane mixtures.

Sets	Wt % of dioxane	Viscosity (cP)	From biexponential fit[a]					$\bar{\nu}(0)$ (cm^{-1})	Observed shift ($\Delta\bar{\nu}$) (cm^{-1})	Missing Comp.
			τ_1 (ns)	τ_2 (ns)	a_1	a_2	τ_{av}[b] (ns)			
X	4.0	140	0.31	2.0	0.64	0.36	0.92	19530	940	53%
Y	13.4	66	0.15	1.02	0.78	0.22	0.34	19705	1040	48%

[a]Using eqn. 6.4, [b]average solvation time $\tau_{av} = a_1\tau_1 + a_2\tau_2$, where $a_1 + a_2 = 1$, experimental error is ±5%.

In the case of an RTIL-dioxane mixture, the general features of the dynamic solvation are similar to those observed in RTIL-toluene systems. There are, however, some differences as well. The extent of the blue shift of the time-zero spectrum for the RTIL-dioxane system is not as pronounced as that in the RTIL-toluene system. For example, upon going from neat RTIL to the solution having ~13% w/w of dioxane (set Y, Table 6.5), the observed blue shift (~180 cm^{-1}) is nearly half of that observed (~330 cm^{-1}) for the same concentration (~13% w/w) of toluene (set V, Table 6.3). More significantly, this total blue shift for the given RTIL-dioxane mixture (~13% w/w of dioxane) is even *less* than that observed for a mixture containing a rather small amount of toluene (~260 cm^{-1} shift is found for solution containing only 4.7% w/w of toluene, v*ide* set III, Table 6.3). For a comparable weight percentage of dioxane (4.2% w/w) virtually *no shift* (only 30 cm^{-1}) was observed (set X, Table 6.5). As opposed to the $\bar{\nu}(0)$ shift, the blue shift

of time-infinity spectrum is found to be more or less the same for both systems (130 cm^{-1} in RTIL-toluene vs. ~100 cm^{-1} in RTIL-dioxane) having the same concentration (~13% w/w) of the cosolvents. These features indicate that dioxane exerts a comparatively less nonpolar effect than toluene at the early stage of dynamics, while, in the final state, the effect of both is essentially the same. In other words, the polarity shift during the course of the dynamics is less pronounced in case of the RTIL-dioxane system.

As far as the observable dynamics is concerned, the average solvation time (τ_{av}), as expected, decreases with increasing dioxane content in the solution, because of lowering of the viscosity of the solution (Table 6.5). Interestingly, at a lower weight percentage of dioxane (typically, 4.2% w/w), the τ_{av} value (0.92 ns) is significantly higher than that observed for a similar toluene weight percentage (set III, Table 6.4), although, at higher concentrations (say, ~13% w/w), both systems behave similarly (v*ide* set V, Table 6.4, and set Y, Table 6.5). In other words, the viscosity variation of τ_{av} for the two systems does not follow the same trend. The τ_{av} for the mixture with low dioxane content is substantially greater than that for a similar solution with toluene. However, the characteristic variation of the $a_i\tau_i$ values with respect to the dioxane content or viscosity is found to be very similar; $a_1\tau_1$ varies little with the viscosity of the solution, while $a_2\tau_2$ varies in accordance with τ_{av} (Fig. 6.7).

A comparison of the dynamic solvation in RTIL-toluene and RTIL-dioxane mixtures obviously suggests that, while a small concentration of toluene is sufficient to influence the dynamics, a larger amount of dioxane is required to produce similar effects. The fact that both cosolvents are almost equally nonpolar

with respect to the given RTIL, the differential behavior of the two solvents cannot be explained in terms of the polarity parameters. Considering the structural and dynamical complexity of the RTILs, even though it may not be possible to pinpoint the origin of this difference, one can speculate that, since toluene has a planar ring system with a polarizable π-electron system, it is possible for the toluene molecules to penetrate into the interstitial region of the imidazolium ring system of RTIL cations by virtue of the π-π interactions and polarizability effect. This is why, even with a relatively smaller concentration, toluene molecules can be effectively *solubilized* in the cybotactic region of the probe where dioxane cannot effectively penetrate because of its nonplanarity and lack of favorable interactions owing to the absence of the polarizable π-cloud. However, when the number of molecules is increased at higher concentrations, the probability of finding the dioxane molecules near the probe is also increased. In a simulation study aimed at explaining the higher solubility of aromatic compounds in imidazolium RTILs as compared to the aliphatic counterparts, Hanke et al. have indeed observed favorable electrostatic interactions between aromatic solute and imidazolium ring systems, by virtue of a polarizable π-cloud.[22]

6.4. Conclusion

We have studied the steady-state and time-resolved fluorescence behavior of C153 in mixed solvents comprising [bmim][PF_6] and toluene or dioxane to investigate the influence of RTIL-cosolvent interaction on the solvation and rotational dynamics. While the steady-state spectral behavior of C153 is hardly affected by the nonpolar cosolvent, direct or indirect involvement of toluene/dioxane in the solvation and rotational processes is clearly evident from

the dynamical studies. The rotational dynamics of the probe becomes faster in the presence of the cosolvents owing to lowering of the viscosity of the medium. A shift of the time-zero spectrum toward the higher energy is observed upon increasing the content of the nonpolar cosolvent, indicating a slightly nonpolar surrounding of C153 in the mixed solvents at the moment of excitation. The time-resolved study also reveals that blue shift of the time-zero maximum of the fluorescence spectrum is more than the shift of the time-infinity maximum. This observation is attributed to a shift of the polarity around the photoexcited probe molecule on displacement of some toluene/dioxane molecules, which were present at the start or early part of the dynamics, by more polar constituents of the RTIL during the course of the solvation process. A biphasic description of the observable dynamics appears to be more appropriate than the stretched exponential one, and when one focuses on the weighted components ($a_i\tau_i$) instead of the individual time-components and associated amplitudes, an interesting correlation between the weighted long component and average solvation time is observed. The difference of the dynamic solvation data in RTIL-toluene and RTIL-dioxane suggests that, while a small amount of toluene can effectively penetrate into the cybotactic region, a larger amount of dioxane is required to observe a similar effect. The data seems to suggest that the planar π-cloud of toluene makes it possible to get interspersed with the imidazolium ring system with favorable quadrupolar or multipolar electrostatic interactions.

References

1. (a) Seddon, K. R.; Stark, A.; Torres, M. J. *Pure Appl. Chem.* **2000**, *72*, 2275. (b) Wang, J. J.; Tian, Y.; Zhao, Y.; Zhou, K. L. *Green Chem.* **2003**, *5*, 618. (c) Rodriguez, H.; Brennecke, J. F. *J. Chem. Engg. Data* **2006**, *51*, 2145. (d) Widegren, J. A.; Laesecke, A.; Magee, J. W. *Chem. Commun.* **2005**, 1610.
2. (a) Baker, S. N.; Baker, G. A.; Bright, F. V. *Green Chem.* **2002**, *4*, 165. (b) Fletcher, K. A.; Pandey, S. *J. Phys. Chem. B* **2003**, *107*, 13532. (c) Fletcher, K. A.; Pandey, S. *Appl. Spectrosc.* **2002**, *56*, 1498. (d) Fletcher, K. A.; Baker, S. N.; Baker, G. A.; Pandey, S. *New J. Chem.* **2003**, *27*, 1706.
3. Harifi-Mood, A. R.; Habibi-Yangjeh, A.; Gholami, M. R. *J. Phys. Chem. B* **2006**, *100*, 7073.
4. Mellein, B. R.; Aki, S. N. V. K.; Ladewski, R. L.; Brennecke, J. F. *J. Phys. Chem. B* **2007,** *111,* 6452.
5. (a) Zhang, J.; Wu, W.; Jiang, T.; Gao, H.; Liu, Z.; He, J.; Han, B. *J. Chem. Engg. Data* **2003**, *48*, 1315. (b) Jarosik, A.; Krajewski, S. R.; Lewandowski, A.; Radzimski, P. *J. Mol. Liq.* **2006**, *123*, 43. (c) Comminges, C.; Barhdadi, R.; Laurent, M.; Troupel, M. *J. Chem. Engg. Data* **2006**, *51*, 680.
6. Li, W.; Zhang, Z.; Han, B.; Hu, S.; Xie, Y.; Yang G. *J. Phys. Chem. B* **2007,** *111,* 6452.
7. Tokuda, H.; Baek, S. J.; Watanabe, M. *Electrochemistry* **2005**, *73*, 620.
8. (a) Chakrabarty, D.; Seth, D.; Chakraborty, A.; Sarkar, N. *J. Phys. Chem. B.* **2005**, *109*, 5753. (b) Seth, D.; Chakraborty, A.; Setua, P.; Sarkar, N *J. Phys. Chem. B* **2007**, *111*, 4781. (c) Adhikari, A.; Sahu, K.; Dey, S.; Ghosh, S.; Mandal, U.; Bhattacharyya, K. *J. Phys. Chem. B.* **2007**, *111*, 12809.
9. (a) Chakrabarty, D.; Chakraborty, A.; Seth, D.; Hazra, P.; Sarkar, N. *Chem. Phys. Lett.* **2004**, *397*, 469. (b) Baker, S. N.; Baker, G. A.; Munson, C. A.; Chen, F.; Bukowski, E. J.; Cartwright, A. N.; Bright, F. V. *Ind. Eng. Chem. Res.* **2003**, *42*, 6457. (c) Chakrabarty, D.; Chakraborty, A.; Seth, D.; Sarkar, N. *J. Phys. Chem. A* **2005**, *109*, 1764.
10. Reichardt, C. *Green Chem.* **2005**, *7*, 339.
11. Reichardt, C. *Solvents and Solvent Effects in Organic Chemistry*; VCH: Weinheim, Germany, 1988.
12. Wakai, C.; Oleinikova, A.; Ott, M.; Weingartner, H. *J. Phys. Chem. B* **2005**, *109*, 17028.
13. Chakrabarty, D.; Hazra, P.; Chakraborty, A.; Seth, D.; Sarkar, N. *Chem. Phys. Lett.* **2003**, *381*, 697.
14. Ito, N.; Arzhantsev, S.; Maroncelli, M. *Chem. Phys. Lett.* **2004**, *396*, 83.
15. Horng, M.-L.; Gardecki, J.; Maroncelli, M. *J. Phys. Chem.* **1997**, *101*, 1030.
16. Fee, R. S.; Maroncelli, M. *Chem. Phys.* **1994**, *183*, 235.

17. (a) Karmakar, R.; Samanta, A. *J. Phys. Chem. A* **2002**, *106*, 4447. (b) Karmakar, R.; Samanta, A. *J. Phys. Chem. A* **2002**, *106*, 6670. (c) Karmakar, R.; Samanta, A. *J. Phys. Chem. A.* **2003**, *107*, 7340.
18. Mandal, P. K.; Samanta, A. *J. Phys. Chem. B* **2005**, *109*, 15172.
19. (a) Ito, N.; Arzhantsev, S.; Heitz, M.; Maroncelli, M. *J. Phys. Chem. B* **2004**, *108*, 5771. (b) Arzhantsev, S.; Ito, N.; Heitz, M.; Maroncelli, M. *Chem. Phys. Lett.* **2003**, *381*, 278. (c) Ingram, J. A.; Moog, R. S.; Ito, N.; Biswas, R.; Maroncelli, M. *J. Phys. Chem. B* **2003**, *107*, 5926.
20. (a) Samanta, A. *J. Phys. Chem. B* **2006**, *110*, 13704. (b) Jin, H.; Baker, G. A.; Arzhantsev, S.; Dong, J.; Maroncelli, M. *J. Phys. Chem. B* **2007**, *111*, 7291.
21. See Chapter 5 of this thesis.
22. Hanke, C. G.; Johansson, A.; Harper, J. B.; Lynden-Bell, R. M. *Chem. Phys. Lett.* **2003**, *374*, 85.

Chapter 7

Photophysical Behavior of a Microviscosity Probe in RTILs

In this chapter, the photophysical behavior of a *molecular rotor* probe, namely, 9-(dicyanovinyl)julolidine (DCVJ) has been studied in seven imidazolium RTILs of varying viscosity in order to understand the factors that contribute to the microviscosity and related parameters. Also, the correlation between the micro- and bulk viscosity of the media has been discussed in this chapter.

7.1. Introduction

Measurement of microviscosity of different organized assemblies using various fluorescence techniques has been briefly introduced in Chapter 1. One of the well-known fluorescent microviscosity probe is 9-(dicyanovinyl)julolidine (DCVJ, in Chart 7.1) whose fluorescence efficiency increases with increasing viscosity of the media.[1-3] The molecule is rather weakly fluorescent (quantum yield, $\Phi_f \approx 10^{-3}$) in conventional less viscous (<2 cP) solvents,[1] whereas in highly viscous glycerol, Φ_f is as high as 0.1.[3] The first excited singlet (S_1) state of this molecule is a π,π^* intramolecular charge-transfer state. Nonradiative deactivation of this excited state is controlled by rapid internal torsional motion, which is substantially restricted in viscous media.[2,3] Loutfy and Arnold[3] have shown that for a series of malononitrile derivatives, there is an excellent agreement between the experimentally determined quantum yield and the solvent viscosity as predicted by the Förster-Hoffmann equation.[4] This viscosity-dependent

fluorescence behavior of DCVJ has been exploited in a wide variety of applications, both in chemical and biological systems.[5-7] In a recent study, the photophysical behavior of DCVJ has been studied in an ionic liquid. In this work, the authors have shown that the activation energy of nonradiative decay of the excited state is much less than the viscosity activation energy, indicating a free volume-controlled deactivation process.[8] However, this study lacks a detail investigation on the relationship between viscosity and free volume parameters.

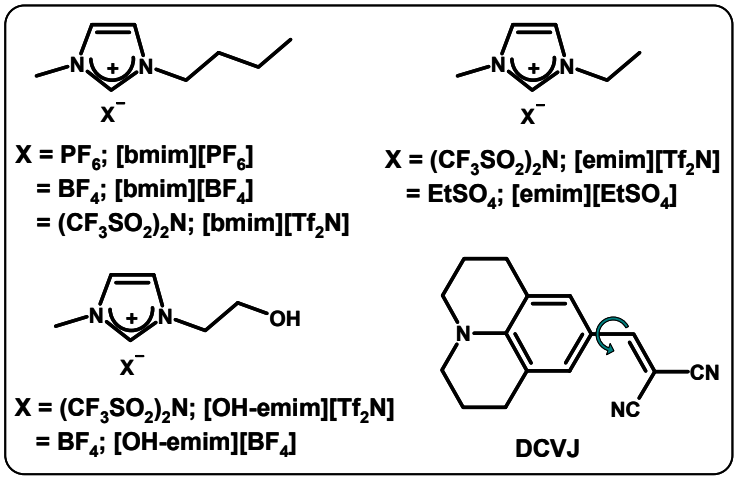

Chart 7.1. Structure and abbreviation of the RTILs and the probe molecule (DCVJ) employed in this study. emim ≡ 1-ethyl-3-methylimidazolium, bmim ≡ 1-butyl-3-methylimidazolium, OH-emim ≡ 1-hydroxyethyl-3-methylimidazolium. Tf_2N ≡ bis(trifluoromethanesulfonyl)imide. The arrow in DCVJ indicates the internal torsional motion responsible fast nonradiative decay of photoexcited molecule.

In recent years, heterogeneous nature of the RTILs have been indicated in many experimental and simulation studies.[9-12] Although a complete picture is yet to emerge, these studies have indicated nanoscale ordering or association in liquid structure of RTILs. To understand the heterogeneity in RTILs, a knowledge of the

microviscosities of the various domains of RTILs is necessary, but, only a little effort has been made in this direction.[8,13] In the present work, the absorption and fluorescence behavior of DCVJ in seven RTILs of varying viscosity has been studied in order to understand the microviscosity and free volume criteria of RTILs in greater detail. We have measured the viscosity of the media and fluorescence quantum yield of DCVJ in RTILs at different temperatures (typically in the range of 10-60°C) to achieve the aforesaid goal. The structure and abbreviation of the RTILs employed in this study have been depicted in Chart 7.1.

7.2. Steady-state absorption and fluorescence

The steady-state absorption spectra of DCVJ in various RTILs are very similar with the absorption maxima (λ_{max}^{abs}) appearing between 462 and 468 nm (Table 7.1). Fig. 7.1(a) depicts representative absorption spectra of DCVJ in three RTILs. As can be seen, there is a small but monotonic red shift of the absorption maxima from [bmim][Tf_2N] (λ_{max}^{abs} = 462 nm) to [OH-emim][Tf_2N] (λ_{max}^{abs} = 465 nm) to [emim][$EtSO_4$] (λ_{max}^{abs} = 468 nm). This shift presumably reflects increasing polarity of these media. The fluorescence spectra of DCVJ in the RTILs, however, do not follow the same trend (Table 7.1). The fluorescence maxima (λ_{max}^{ems}) in alcohol-functionalized RTILs, namely, [OH-emim][Tf_2N] and [OH-emim][BF_4] are found to be red-shifted compared to their alkyl-functionalized analogues. However, the λ_{max}^{ems} values of DCVJ in the RTILs also lie within a small range of 499-507 nm (Table 7.1). The fluorescence spectra of DCVJ in three RTILs are shown in Fig. 7.1(b).

Table 7.1. Viscosity and steady-state absorption and fluorescence behavior of DCVJ in RTILs at 25°C.

	RTILs/Normal solvents	Viscosity (cP)	λ_{max}^{abs} (nm)	λ_{max}^{ems} (nm)[a]	Φ_f
1.	[emim][Tf_2N]	31.5	462	500	0.013
2.	[bmim][Tf_2N]	49	462	500	0.019
3.	[emim][$EtSO_4$]	76	468	504	0.022
4.	[OH-emim][Tf_2N]	83.5	465	502.5	0.019
5.	[bmim][BF_4]	92	465	501	0.023
6.	[OH-emim][BF_4]	117	466.5	507	0.028
7.	[bmim][PF_6]	260	464	499	0.024
8.	acetonitrile	0.34	457[b]	502[b]	0.0022[b]
9.	methanol	0.054	454.7[b]	495[b]	0.0015[b]
10.	glycerol	954[c]	469[c]	508[c]	0.1[c]

[a]λ_{exc} = 430 nm for RTILs, [b]from ref. 1, [c]from ref. 3.

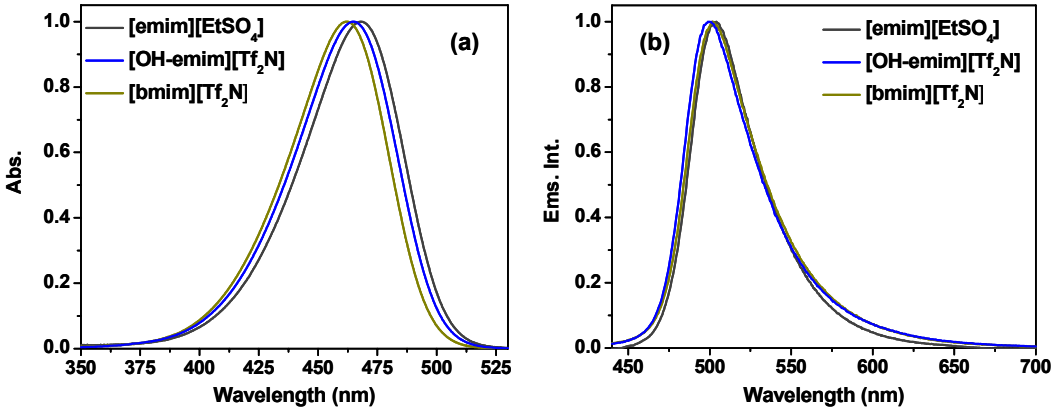

Fig. 7.1. Steady-state (a) Absorption and (b) Emission spectra of DCVJ in three RTILs.

A comparison of the spectral data of DCVJ in RTILs and in conventional solvents reveals that the λ_{max}^{abs} and λ_{max}^{ems} values in RTILs lie between those in

acetonitrile and glycerol. This observation is consistent with the literature that the RTILs are at least as polar as acetonitrile, if not more.

7.3. Relationship between viscosity and quantum yield

For molecular rotors like DCVJ, fluorescence quantum yield, which is largely governed by torsional relaxation, is shown to be viscosity dependent.[3] According to Loutfy and Arnold,[3] in viscous media the time for internal rotation (τ_{rot}), termed as torsional relaxation time, of a molecular rotor like DCVJ does not follow simple hydrodynamic model (Debye-Stokes-Einstein model), which predicts, $\tau_{rot} \propto \eta/T$, where, η is the viscosity of the media at temperature T. Instead, the following relationship was shown to be valid:[3]

$$\tau_{rot} = C\left(\frac{\eta}{T}\right)^{x} \tag{7.1}$$

where, C is a constant and x is a fractional number. When this torsional relaxation process is the main nonradiative deactivation channel of the photoexcited probe, τ_{rot} can be equated to the nonradiative decay time (τ_{nr}) and since,

$$\frac{1}{\tau_{rot}} \approx \frac{1}{\tau_{nr}} = k_{nr} = k_r\left(\frac{1}{\Phi_f} - 1\right) \tag{7.2}$$

where, k_{nr} and k_r are the nonradiative and radiative rate constants, respectively, and Φ_f is the fluorescence quantum yield, one can write

$$\Phi_f = B\left(\frac{\eta}{T}\right)^{x} \tag{7.3}$$

for $\Phi_f << 1$, which is the case with DCVJ in normal solvents and RTILs (Table 7.1). Eqn. 7.3 is shown to be valid for moderate-to-high viscosity solvents, where,

'x' is the *free volume parameter*.[2,3] It was observed that the higher the viscosity, the greater is the free volume dependence and larger is the value of x.[3] At constant temperature, eqn. 7.3 can be written as,

$$\log \Phi_f = \text{Const} + x\ (\log \eta) \qquad (7.4)$$

which is known to be the Förster-Hoffmann expression.[4] This equation is widely used for microviscosity measurements of many microheterogeneous systems or organized assemblies.[5-7] A plot of log Φ_f vs log η gives x = 2/3 for a number of triphenylmethane dyes,[4] and ~0.6 for DCVJ,[5] indicating the probe dependence of x.

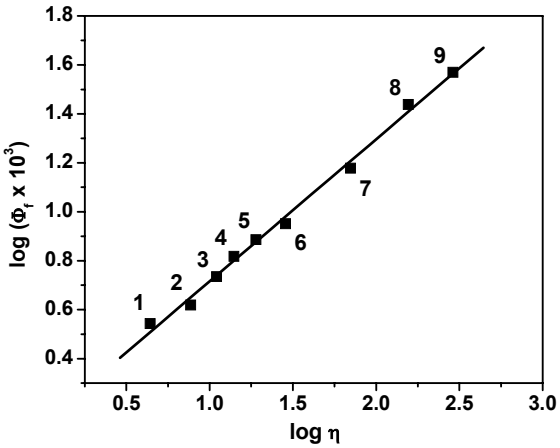

Fig 7.2. log Φ_f vs log η, at 25°C for DCVJ in solvents: 1. EG:2-propanol (1:3 v/v), 2. EG:2-propanol (1:1 v/v), 3. EG:2-propanol (3:1 v/v), 4. EG (neat), 5. EG:glycerol (9:1 v/v), 6. EG:glycerol (4:1 v/v), 7. EG:glycerol (3:2 v/v), 8. EG:glycerol (2:3 v/v), 9. EG:glycerol (1:3 v/v), where, EG = ethylene glycol. The straight line shows linear fit according to eq. 7.4.

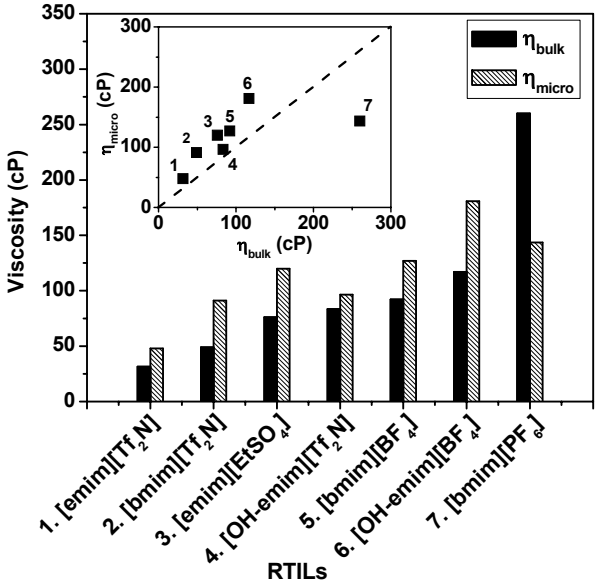

Fig. 7.3. A Bar diagram representing relative deviation of the microviscosity (η_{micro}) obtained from Fig. 7.2 and the measured bulk viscosity (η_{bulk}) of the seven RTILs used in this study (at 25°C). The inset shows the deviation from the mean regression line (dashed line).

To measure the fluorescence quantum yield (Φ_f) of DCVJ in RTILs and other solvents, the reported yield of the same compound in acetonitrile ($\Phi_f = 0.0022$, at 25°C) has been taken as standard.[1] We have measured the quantum yield (Φ_f) of DCVJ in a number of solvent mixtures of varying viscosity at constant temperature (at 25°C) and plotted log Φ_f vs. log η to produce a calibration curve (Fig. 7.2), which is similar to that already reported.[5] We have found that the slope $x = 0.58\pm0.02$ is very close to the reported value ($x = 0.6$).[5] Then the microviscosity (η_{micro}) of the RTILs at 25°C was calculated from the plot using the measured Φ_f values of DCVJ in the respective RTILs. However, the microviscosity (η_{micro}) of the RTILs measured this way differs considerably from

the bulk viscosity (η_{bulk}), and interestingly, except for highly viscous [bmim][PF_6] the former is always greater than the latter (Fig. 7.3).

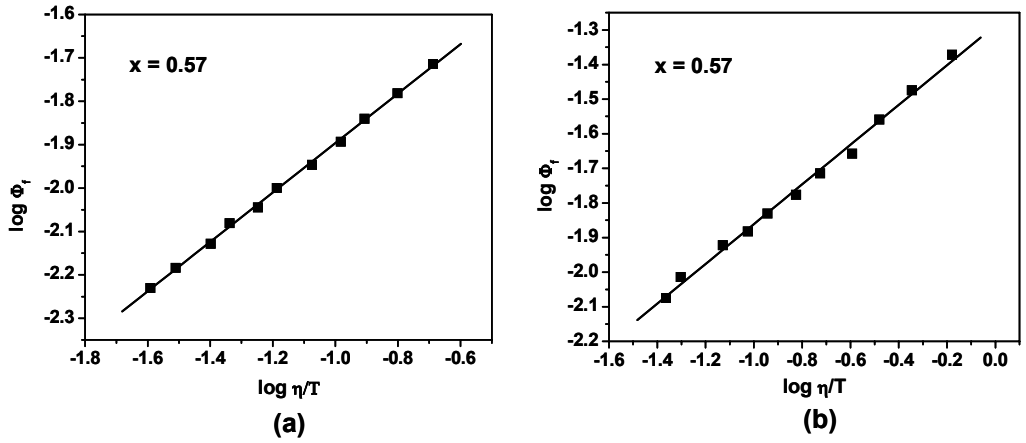

Fig. 7.4. Plots of log Φ_f vs log η/T for DCVJ in two less viscous RTILs: (a) [emim][Tf_2N] and (b) [emim][$EtSO_4$]. The values of x were obtained from respective slopes.

Lack of correlation between η_{micro} and η_{bulk} reflects the limitation of a single temperature measurement of viscosity, which gives an inappropriate description of the microscopic domain. Thus a treatment of Loutfy and Arnold[3] (eqn. 7.3) is more appropriate because then the temperature variation of viscosity (i.e., bulk viscosity) is taken into account. Therefore, log Φ_f is plotted against log η/T (here, $\eta = \eta_{bulk}$) for a temperature range of 10-60°C for all RTILs. It is found that for less viscous RTILs, namely, [emim][Tf_2N], [bmim][Tf_2N] and [emim][$EtSO_4$], this plot is linear, as shown in Fig. 7.4. The x values obtained from the slopes vary between 0.52 and 0.57 (Table 7.2). These values are not very different from those obtained in normal solvents (x = 0.58). However, for the remaining RTILs (4-7, Table 7.2), which are comparatively more viscous, a departure from linearity is

observed. In these cases, a clear break-point is noticeable around 28-30°C. The representative log Φ_f vs log η/T plots for two RTILs, namely, [bmim][PF_6] and [OH-emim][BF_4], are shown in Fig. 7.5.

Table 7.2. The value of 'x' obtained from the slopes of the log Φ_f vs log η/T plots for respective RTILs.

RTILs	Viscosity (cP) (at 25°C)	x	
1. [emim][Tf_2N]	31.5	0.57	
2. [bmim][Tf_2N]	49	0.52	
3. [emim][$EtSO_4$]	76	0.57	
4. [OH-emim][Tf_2N]	83.5	0.53	0.69
5. [bmim][BF_4]	92	0.38	0.55
6. [OH-emim][BF_4]	117	0.35	0.68
7. [bmim][PF_6]	260	0.36	0.51

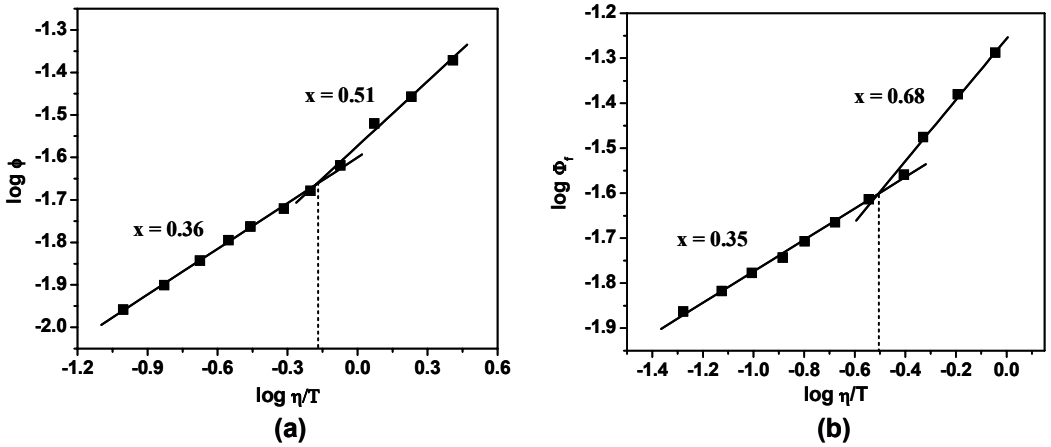

Fig. 7.5. Plots of log Φ_f vs log η/T for DCVJ in two highly viscous RTILs: (a) [bmim][PF_6] and (b) [OH-emim][BF_4]. The values of x were obtained from respective slopes.

The break in the linearity of the log Φ_f vs log η/T plots (Fig. 7.5) presumably indicates a change in the liquid structure of RTILs around certain temperatures (28-30°C) resulting in an abrupt change of the free volume dependence. A closer look at Table 7.2 reveals that the x values for more viscous RTILs (4-7, Table 7.2) lie in two distinct ranges. In the high temperature range, i.e., below the break-point (Fig 7.5), the x values are in the range of 0.35-0.38 excepting [OH-emim][Tf_2N], for which x = 0.53. In the low temperature region, i.e., above the break-point in Fig. 7.5, the x values (0.51-0.55) are comparable to the values obtained for the less viscous RTILs (0.52-0.57). However, for alcohol-functionalized RTILs, namely, [OH-emim][Tf_2N] and [OH-emim][BF_4] the x values in the low temperature region are quite high cf. 0.68-0.69, which indicate that the free volume dependence is more in case of these RTILs in this temperature range.

The appearance of this break-point within a narrow range of temperatures, 28-30°C, for *all* highly viscous RTILs is quite interesting. However, this can be understood as follows. Loutfy and Arnold[3] pointed out that the temperature dependence of viscosity of many small molecular liquids arises largely from their dependence on the available free volume,[14] much similar to the free volume concept applied to polymers.[15] It is also known that higher the viscosity, smaller is the available free volume and consequently greater is the free volume dependence.[3,5] Again, with decreasing temperature the free volume shrinks to about 2.5% at the glass transition temperature (T_g) and the predominant influence of free volume expansion upon viscosity remains from T_g to ~T_g + 100 K.[16] We note that the reported T_g values for RTILs vary rather widely (Table 7.3). For

example, two different groups have reported the T_g value [bmim][PF_6] as –61°C[17] and –77°C.[18] However, if only the closely matched values of T_g are accepted (Table 7.3) then it is observed that these values lie in a rather narrow range of –77°C to –85°C for all RTILs concerned here.[17-23] This is probably the reason for the appearance of a break-point at around a close range of temperatures (28-30°C) for more viscous RTILs (4-7, Table 7.2), because, as stated earlier, the dominant influence of free volume sustains upto ~T_g + 100 K. This explains a higher x value for low temperature region (e.g., <30°C) and a much lower x value above that temperature.

Table 7.3. Reported glass transition temperatures (T_g) of the RTILs employed in the present study.

RTILs	Glass Transition Temperature, T_g (°C)		
1. [emim][Tf_2N]	–78[a]	–92[b]	
2. [bmim][Tf_2N]	–86[b]	–87[a]	
3. [emim][$EtSO_4$]	–77[c]		
4. [OH-emim][Tf_2N]	–79[d]		
5. [bmim][BF_4]	–85[b]	–81[e]	–71[f]
6. [OH-emim][BF_4]	–84[g]		
7. [bmim][PF_6]	–77[a]	–76[b]	–61[e]

From, [a]ref. 18, [b]ref. 19, [c]ref. 20, [d]ref. 21, [e]ref. 17, [f]ref. 22, [g]ref. 23.

7.4. Activation energy of viscosity and nonradiative decay

The viscosity activation energy (E_η) of the RTILs can be measured from the following Arrhenius-type plot of the temperature-dependence of solvent mobility (η^{-1}):

$$\ln \eta^{-1} = \ln \eta_0^{-1} - \frac{E_\eta}{R} \cdot \frac{1}{T} \tag{7.5}$$

where, η_0^{-1} is the limiting solvent mobility at infinite temperature. The plot of ln η^{-1} vs 1/T is found to be reasonably linear *for all RTILs* regardless of their viscosity (Fig. 7.6) and from the slopes of the respective plots the corresponding activation energies (E_η) are obtained (see Table 7.4).

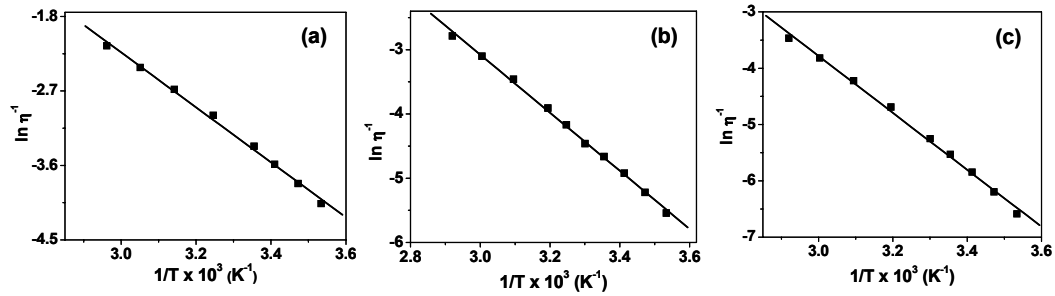

Fig. 7.6. Plots of ln η^{-1} vs 1/T for three RTILs: (a) [emim][Tf_2N], (b) [OH-emim][BF_4] and (c) [bmim][PF_6].

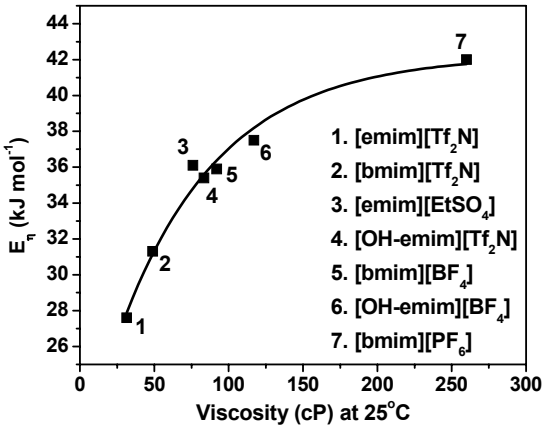

Fig. 7.7. Plot of viscosity activation energy (Eη) vs viscosity (at 25°C) for all RTILs. The solid line represents the trend line for variation of Eη with viscosity.

As can be seen from Fig. 7.7, the viscosity activation energy (E_η) for different RTILs increases with increasing viscosity of the media. The figure shows almost exponential increment of E_η with increasing viscosity of the RTILs.

The activation energy for nonradiative decay (E_{nr}), which is essentially the same for torsional relaxation, can be obtained by using the Arrhenius equation of temperature dependence of k_{nr}, the nonradiative rate constant:

$$k_{nr} = A\exp\left(-\frac{E_{nr}}{RT}\right) \tag{7.6}$$

where, A represents the preexponential factor. By combining eqn. 7.6 and 7.2, we arrive at the following relationship,

$$\left(\frac{1}{\Phi_f} - 1\right) = \frac{k_{nr}}{k_r} = \frac{A}{k_r}\exp\left(-\frac{E_{nr}}{RT}\right) \tag{7.7}$$

or,
$$\ln\left(\frac{1}{\Phi_f} - 1\right) = \ln\frac{A}{k_r} - \frac{E_{nr}}{R}.\frac{1}{T} \tag{7.8}$$

in which, k_r and Φ_f represent the raditative rate constant and quantum yield of DCVJ, respectively, in a given RTIL. The Arrhenius plot of ln $(1/\Phi_f - 1)$ vs. $1/T$ is expected to be linear whose slope is a measure of the nonradiative activation energy (E_{nr}).

Table 7.4. Activation energy for solvent viscosity and nonradiative (torsional relaxation) process.

ILs	E_η (kJ mol^{-1})	x	E_{nr} (kJ mol^{-1})	$E_{nr}^{cal} = x\ E_\eta$ (kJ mol^{-1})
1. [emim][Tf_2N]	27.6	0.57	17.5	15.7
2. [bmim][Tf_2N]	31.3	0.52	17.7	16.3
3. [emim][$EtSO_4$]	36.1	0.57	23.2	20.6
4. [OH-emim][Tf_2N]	35.4	0.53 0.69	18.6 25.0	18.9 24.6
5. [bmim][BF_4]	35.9	0.38 0.55	15.2 20.7	13.7 20.1
6. [OH-emim][BF_4]	37.5	0.35 0.68	13.3 26.3	13.1 25.1
7. [bmim][PF_6]	42.0	0.36 0.51	16.1 26.3	15.1 21.3

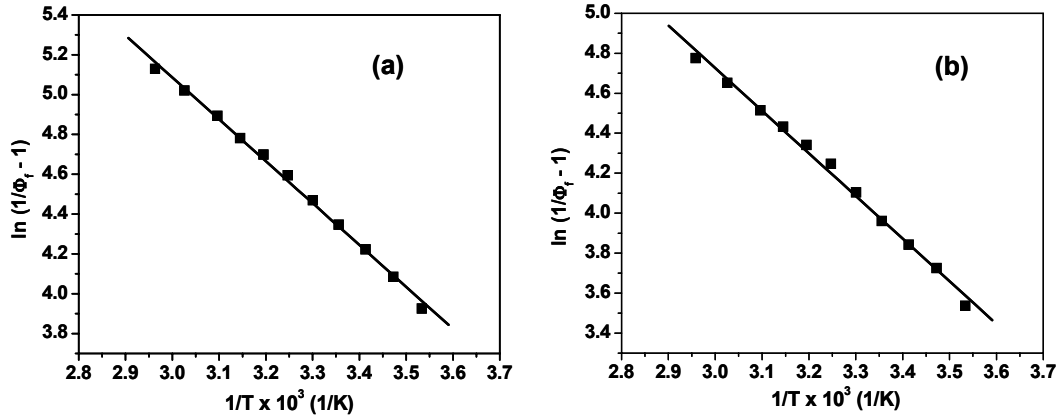

Fig. 7.8. Plots of ln ($1/\Phi_f$-1) vs 1/T for two RTILs: (a) [emim][Tf_2N] and (b) [bmim][Tf_2N].

The, ln $(1/\Phi_f - 1)$ vs 1/T plot (Arrhenius plot) is found to be a straight line (Fig. 7.8) only in case of less viscous RTILs (1-3, Table 7.4). A significant departure from linearity has been noted for other more viscous RTILs (4-7, Table 7.4), and this departure is most prominent in case of [OH-emim][BF_4] (Fig. 7.9). A similar deviation from linearity for highly viscous glycerol was also reported in the literature,[3] but then this observation was not highlighted.

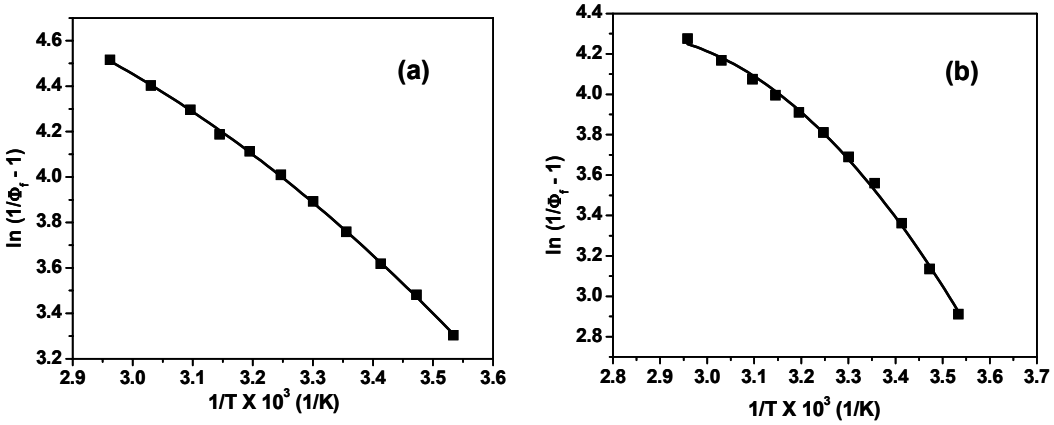

Fig. 7.9. Plots of ln $(1/\Phi_f-1)$ vs 1/T for two RTILs: (a) [bmim][BF_4] and (b) [OH-emim][BF_4]. The data in both cases were fitted with the polynomial $y = A + Bx + Cx^2$, which interprets the nonlinear behavior.[25]

A curvature in the Arrhenius plot can arise from the temperature dependence of the activation parameters, namely the preexponential factor and activation energy.[24] Since, the temperature effect is very much dominant for the exponential term of the Arrhenius equation (see eqn. 7.6),[24] the same for the preexponential factor can be neglected for the present case, given the small temperature range of the present study (10-60°C). The nonlinear Arrhenius plot can be fitted to a polynomial function,[25] as shown in Fig. 7.9. However, the significance of the use

of such function is unclear in the present case and thus, instead of polynomial fitting, the data obtained in more viscous RTILs, namely, [OH-emim][Tf_2N], [bmim][BF_4], [OH-emim][BF_4] and [bmim][PF_6] is subjected to two linear fitting in the two different temperature-range, as shown in Fig. 7.10. It can be seen that the break-point in these plots appears around the same temperatures (28-30°C) as is found in case of log Φ_f vs log η/T plots. Hence, it can be concluded that the activation energy (E_{nr}) for the two ranges of temperatures, is a measure of the free volume parameter x of the respective region. The nonradiative activation energies (E_{nr}) are given in Table 7.4.

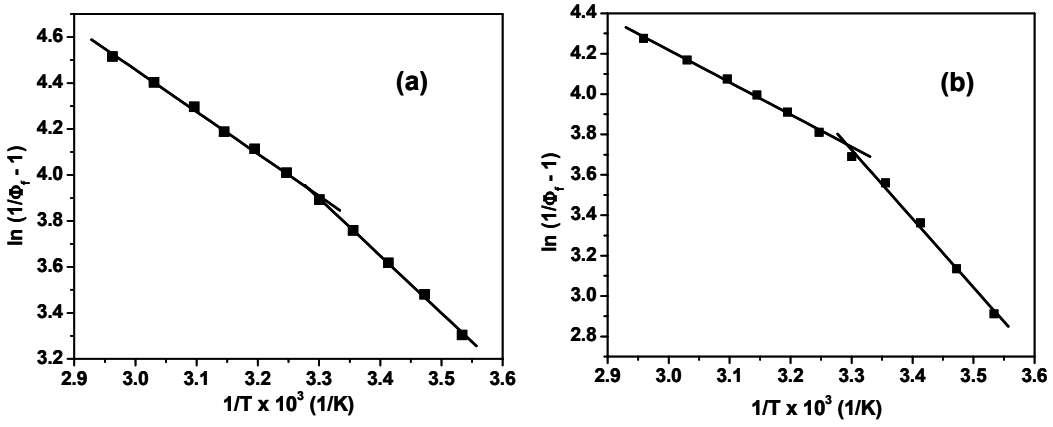

Fig. 7.10. Plots of ln ($1/\Phi_f$-1) vs 1/T for two RTILs, namely, (a) [bmim][BF_4] and (b) [OH-emim][BF_4] with the appropriate bilinear fit.

A relationship of x and E_{nr} can be derived from the following consideration: Rearranging eqn. 7.1 and using $\tau_{rot} = \tau_{nr} = 1/k_{nr}$ we can obtain the following equation,

$$\frac{1}{\tau_{rot}} = k_{nr} = \frac{T^x}{C}\left(\frac{1}{\eta}\right)^x . \quad (7.9)$$

By introducing the expression for $1/\eta$ one can get, after suitable rearrangement,

$$k_{nr} = \frac{T^x}{C\eta_0^x}\exp\left(-\frac{xE_\eta}{RT}\right). \quad (7.10)$$

By comparing eqn. 7.6 and 7.10, we can arrive at the following relationship:

$$E_{nr} = x\, E_\eta \quad (7.11)$$

by assuming the temperature dependence (T^x) of the preexponential factor of eqn. 7.10 to be far less than that of the exponential term. The calculated nonradiative activation energy (E_{nr}^{cal}) values, obtained from respective values of x and E_η for different RTILs (by using eqn. 7.11) in the two different regions (below and above the break-point), have been tabulated in Table 7.4. A comparison of the respective E_{nr} and E_{nr}^{cal} values for all the RTILs (see Table 7.4) reveals an excellent agreement between the two, thus validating the relationship delineated in eqn. 7.11. A plot of E_{nr}^{cal} vs. measured E_{nr} has been depicted in of Fig. 7.11. One can see that most of the data points in Fig. 7.11 fall within 1 kJ mol^{-1} of the mean regression line. This is an excellent demonstration of the validity of the aforementioned relationship. In other word, the activation energy for the nonradiative process or torsional relaxation is closely related to the free volume of RTILs.

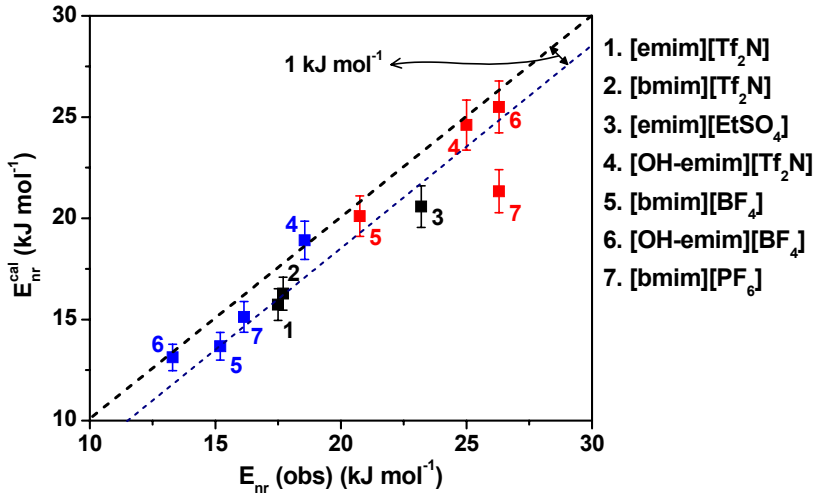

Fig. 7.11. Plot of E_{nr} (obs), i.e., obtained from Arrhenius plot, versus E_{nr}^{cal}, where, $E_{nr}^{cal} = xE_{\eta}$. The black points correspond to the three less viscous RTILs (1-3) and the colored points (red or blue) represent more viscous RTILs (4-7). The red points corresponds to the high activation energy values (therefore, high x values), whereas blue points corresponds to low activation energy values (i.e., low x values).

The most interesting feature of this study is that while the temperature variation of bulk viscosity (or mobility) shows linearity to a satisfactory extent, the nonlinear behavior is apparent in case of Arrhenius plots of the nonradiative process for more viscous RTILs (4-7, in Table 7.4). The break-point in these Arrhenius plots corresponds to that obtained previously for log Φ_f vs log η/T plots, and the validity of eqn. 7.11 justifies the fact. A different temperature dependence of bulk viscosity and nonradiative rate constant suggests that the microviscosity of the RTILs, which is correlated to the quantum yield of DCVJ, shows an entirely different temperature dependence from the bulk viscosity.

For less viscous RTILs (1-3, Table 7.4), the bulk viscosity and microviscosity are directly correlated (through the x term) throughout the whole temperature range studied (10-60°C). However, for more viscous RTILs (4-7, Table 7.4), the occurrence of a break-point in the Arrhenius plot suggests that the microviscosity is different above and below this point, owing to the difference in free volume dependence (different x values). As mentioned earlier, this is indicative of some change in the liquid structure of RTILs at the break-point. At lower temperatures (above break-point) when the viscosity is quite high and thus free volume is less, the free volume dependence of viscosity is more. One can then see that microviscosity is strongly correlated to the bulk one, and this feature is reflected in the high E_{nr} values, 21-26 kJ mol^{-1} (Table 7.4) in the low temperature regime. E_{nr} values of the alcohol-functionalized RTILs, [OH-emim][Tf_2N] and [OH-emim][BF_4] above the break-point (25.0 & 26.3 kJ mol^{-1}, respectively) are as high as that of [bmim][PF_6] (26.3 kJ mol^{-1}) even though the latter is much more viscous than the formers (see Table 7.1). This indicates a significant role of close range interaction like hydrogen bonding on the microviscosity, at least in the low temperature domain. At higher temperatures, the free volume is more and so the free volume dependence is less, which is reflected by the smaller x values. Therefore, the microviscosity becomes weakly correlated with the bulk viscosity, which is indicated by the smaller E_{nr} values, 13-15 kJ mol^{-1} for more viscous RTILs, except for [OH-emim][Tf_2N]. Interestingly, for [emim][Tf_2N] and [bmim][Tf_2N], two less viscous RTILs, the E_{nr} is also similar (~17 kJ mol^{-1}). This observation may be linked to the alkyl chain motions in RTILs. The activation

energy for hydrocarbon chain mobility, as measured from microviscosity using DCVJ, in the gel state of vesicle was found to be ~15 kJ mol^{-1}.[5] NMR study of vesicles also indicated a similar value for activation energy for acyl chain trans-gauche isomerization.[26] By analogy, it can be said that the alkyl chain mobility may have a significant influence on the microviscosity of the highly viscous RTILs at high temperature and of less viscous RTILs throughout the whole temperature range.

7.5. Conclusion

In summary, we have studied the fluorescence efficiency of a 'molecular rotor' probe, DCVJ in seven RTILs of varying viscosity at different temperatures, focusing mainly on the relationships between these parameters. The microviscosity of the RTILs estimated using the Förster-Hoffmann equation at a single temperature (room temperature) was found unsuitable for proper understanding of the viscosity criterion in the microscopic domain. Hence, variation of viscosity with temperature was also taken into account (see eqn. 7.3). The log Φ_f vs. log η/T plots for more viscous RTILs were found to be bilinear with a break around 28-30°C. A similar break-point was noted in case of Arrhenius plots corresponding to nonradiative or torsional relaxation of DCVJ in these RTILs. However, in case of less viscous RTILs, the log Φ_f vs. log η/T plots and the above-mentioned Arrhenius plots are simply linear. These observations are rationalized by introducing the free volume concept in the relation of microviscosity and bulk viscosity. Higher the bulk viscosity (at low temperature), greater is the free volume dependence and stronger is the correlation between bulk and microviscosity. At high temperature, sufficiently above the glass transition

temperature, free volume influence is less and so the microviscosity is less influenced by it. In this case, the alkyl chain motions of RTILs' cation can be an important factor for microviscosity, as indicated by the activation energy values.

References

1. Loutfy, R. O.; Law, K. Y. *J. Phys. Chem.* **1980**, *84*, 2803.
2. Law, K. Y. *Chem. Phys. Lett.* **1980**, *75*, 545.
3. Loutfy, R. O.; Arnold, B. A. *J. Phys. Chem.* **1982**, *86*, 4205.
4. Förster, Th.; Hoffmann, G. *Z. Phys. Chem. (Weisbaden)* **1971**,*75*, 63.
5. Kung C. E.; Reed J. K. *Biochemistry* **1986**, *25*, 6114.
6. (a) Loutfy, R. O. *Pure Appl. Chem.* **1986**, *58*, 1239. (b) Law, K. Y.; Loutfy, R. O. *Macromolecules* **1981**, *14,* (c) Law, K. Y., & Loutfy, R. 0. (1983) *Polymer* **1983**, *24*, 439. (d) Lu, J.; Liotta, C. L.; Eckert, C. A. *J. Phys. Chem. A* **2003**, *107*, 3995.
7. (a) Haidekker, M.A.; Heureux, N. L.; Frangos, *J. A. Am. J. Physiol. Heart Circ. Physiol.* **2000**, *278*, H1401. (c) Kung C. E.; Reed J. K. *Biochemistry* **1989**, *28*, 6678.
8. Gutkowski, K. I.; Japas, M. L.; Aramendía, P. F. *Chem. Phys. Lett.* **2006**, *426*, 329.
9. Mandal, P. K.; Sarkar, M.; Samanta, A. *J. Phys. Chem. A* **2004**, *108*, 9048.
10. (a) Triolo, A.; Russina, O.; Bleif, H.-J.; Di Cola, E. *J. Phys. Chem. B* **2007**, *111*, 4641. (b) Moutiers, B. G.; Labet, A.; Azzi A. E.; Gaillard, C.; Mariet, C.; Lutzenkirchen, K. *Inorg. Chem.* **2003**, *42*, 1726. (c) Iwata, K.; Okazima, H.; Saha, S.; Hamaguchi, H. *Acc. Chem. Res.* **2007,** *40,* 1174. (d) Dupont, J.; Suarez, P. A. Z., de Suza, R. F.; Burrow, R. A.; Kintzinger, J. *Chem. Eur. J.* **2000**, *6*, 2377.
11. (a) Hu, Z.; Margulis, C. J. *Proc. Natl. Acad. Sci.* **2006**, *103*, 831. (c) Hu, Z.; Margulis, C. *Acc. Chem. Res.* **2007**, 1097.
12. (a) Popolo, M.; Kohanoff, J.; Lynden-Bell, R. M.; Pinilla, C. *Acc. Chem. Res.* **2007**, 40, 1156. (b) Padua, A. A. H.; Costa Gomes, M. F.; Canongia Lopes, J. N. A. *Acc. Chem. Res.* **2007**, *40*, 1087. (c) Jin, H.; Li, X.; Maroncelli, M. *J. Phys. Chem. B* **2007**, *111*, 13473.
13. Lu, J.; Liotta, C. L.; Eckert, C. A. *J. Phys. Chem. A* **2003**, *107*, 3995.
14. (a) Doolittle, A. K. *J. Appl. Phys.*, 22, 1951, 1471. (b) Doolittle, A. K. *J. Appl. Phys.*, **1952**, *23*, 236. (c) Williams, M. L.; Landel, R. F.; Ferry, J. D. *J. Am. Chem.* Soc., **1955**, *77*, 3701. (d) Hildebrand J. H.; Lamoreaux, R. H. *J. Phys. Chem.,* 77, 1471
15. (a) Bondi, A. *Physical Properties of Molecular Crystals, Liquids and Glasses*; Wiley: New York, 1968. (b) J. D. Ferry, *Viscoelastic Properties of Polymers*; Wiley: New York, 1970, 2nd Ed.
16. Soesanto, T.; Williams, M. C. *J. Phys. Chem.*, **1981**, *86*, 3338.
17. Suarez, S. E. P. A. Z.; Dullius, J. E. L.; de Souza, R. F.; Dupont, J. *J. Chim. Phys. Phys.-Chim. Biol.* **1998**, *95*, 1626.
18. Dzyuba, S.; Bartsch, R. A. *Chem. Phys. Chem.* **2002**. *3*, 161.
19. Fredlake, C. P.; Crosthwaite, J. M.; Hert, D. G.; Aki, S. N. V. K.; Brennecke, J. F. *J. Chem. Engg. Data* **2004**, *49*, 954.

20. Holbrey, J. D.; Reichert, W. M.; Swatloski, R. P.; Broker, G. A.; Pitner, W. R.; Seddon, K. R.; Rogers, R. D. *Green Chem.* **2002**, *4*, 407.
21. Dzyuba, S. V.; Bartsch, R. A. *Tetrahedron Lett.* **2002**, *43*, 4657.
22. Holbray, J. D.; Seddon, K. R. *J. Chem. Soc., Dalton Trans.* **1999**, 2133.
23. Branco, L. C.; Rosa, J. N.; Ramos, J. J. M.; Afonso, C. A. M. *Chem. Eur. J.* **2002**, *8*, 3671.
24. Connors, K. A. *Chemical Kinetics: The Study of Reaction Rates in Solution*; VCH: New York, 1990, p 251.
25. Wold, S. *Acta Chem. Scand.* **1970**, *24*, 2321.
26. Brown, M. F.; Seelig, J. *J. Chem. Phys.* **1979**, *70*, 5045.

Chapter 8

Concluding Remarks

This chapter summarizes the results of the investigations delineated in this thesis. The scope of further studies based on the findings of the present work and the challenges ahead have also been outlined.

8.1. Overview

The work embodied in the thesis had been undertaken with the primary objective to explore the horizon of RTILs as media for photophysical studies. Before taking up this investigation, the optical properties of RTILs based on the imidazolium cation have been carefully examined with a view to understand the applicability and limitation of the RTILs as media for studying photophysical processes. A variety of photoprocesses like photoinduced electron transfer reaction, solvation and rotational dynamics etc have been subsequently studied in these RTILs with a two-dimensional objective. Firstly, to find out whether or to what extent these processes differ from those occurring in conventional solvents, and secondly, to determine the specific role of the RTILs, if any, in such differential characteristics of the aforementioned photoprocesses. Several instrumental techniques and methodologies, namely, NMR and IR spectroscopy for characterization, cone and plate viscometer, UV-visible absorption, steady-state and time-resolved fluorescence and laser flash photolysis techniques have been employed to carry out this work. The results obtained from the investigations are outlined below.

While optical studies on dissolved probe molecules in RTILs are reported, those focusing on the optical properties of RTILs are scarce. A few literatures that are available on the related topic have given an impression that imidazolium RTILs are optically transparent liquid as far as UV-visible spectroscopy is concerned. In order to have a definite understanding, we have made a careful scrutiny of this subject by choosing a few well-known members of the family. Our investigation revealed that these RTILs do possess non-negligible absorption in the UV region with a long tail extending to the visible region. These RTILs also exhibit an interesting wavelength-dependent fluorescence (though weak) behavior which covers a large portion of the visible region. The observations have been interpreted in terms of selective excitation of various energetically-different associated species and inefficient energy transfer between these species.

Photoinduced electron transfer reaction between pyrene and N,N-dimethylaniline has been studied in a number of RTILs of varying viscosity using steady-state and time-resolved fluorescence and laser flash photolysis techniques. Unlike in conventional media, exciplex emission for this well-known pair could not be observed in RTILs. This absence of exciplex is a consequence of high polarity of RTILs, as indicated by the microscopic polarity parameters, but indicated otherwise by the low dielectric constant of RTILs. The yield of the radical ions produced from the PET reaction found to be significantly lower in RTILs. In highly viscous RTILs, the yield was so low that the transient absorption due to the free ions could not be detected. The results have been quantitatively analyzed in terms of the formulation based upon the Onsager dielectric continuum model and the calculations show that low escape efficiency of the constituents of

the geminate ion pair and efficient back electron transfer are responsible for such behavior.

In order to understand certain unresolved issues of solvation dynamics in RTILs, especially those related to local effect and its contribution towards the early part of the dynamics (ultrafast or missing component), we have studied dynamic solvation in an alcohol-functionalized protic ionic liquid based on imidazolium moiety using popular solvation probes, namely, C153, AP and prodan, focusing on the influence of hydrogen bonding interaction on the aforementioned aspects. Steady-state absorption and emission of the probe molecules have indicated a higher polarity of this RTIL compared to common alkylimidazolium RTILs and a significant hydrogen bonding interaction with AP in particular. The rotational anisotropy study also revealed a significant hydrogen bonding interaction between RTIL cation and AP. However, most interesting feature of this study is the retardation of ultrafast or missing dynamics, leading to a net reduction of missing component by 15-20% as compared to that in alkylimidazolium RTILs. This finding is attributed to specific hydrogen bonding interaction between the probe and RTIL cation in the first solvation shell, though, the cation-anion hydrogen bonding interaction may also have some influence on it.

Since the addition of conventional solvent broadens the scope of application of RTILs, many physicochemical studies in the mixture of RTILs with these solvents have been carried out in recent days. However, these studies have been restricted to mixed solvents comprising RTILs and polar conventional solvents and no such studies have been done with the mixture of RTILs and nonpolar

solvents. We, therefore, have chosen to study the dynamics of solvation in the mixture of an RTIL with nonpolar solvents like toluene and 1,4-dioxane. The steady-state behavior of the probe, C153 in RTILs, was not affected by the addition of these nonpolar solvents and the time-resolved anisotropy study demonstrated merely the effect of dilution on rotational correlation time. However, a continuous blue shift of the time-zero emission spectra of C153 with gradual addition of toluene is observed. The time-infinity spectra, which recognize the end of dynamic solvation, however, was affected to lesser extent. This observation has been attributed to a change of the polarity of the surrounding environment of C153 during its lifetime. The observable dynamics is found to be biphasic and an interpretation based on the weighted time-constants of the observable part has been put forward to explain the biphasic dynamics. Finally, the various aspects of dynamical phenomenon of RTIL-toluene and RTIL-dioxane have been compared. It is shown that a low concentration of toluene compared to dioxane is sufficient to bring about the same changes because of favorable interactions between toluene and the imidazolium ring system leading to a more effective solubilization of toluene in the cybotactic region of the probe.

The photophysical studies of a molecular rotor probe, DCVJ have been carried out in seven RTILs of different viscosity in order to understand the free volume parameters and the correlation between microviscosity and bulk viscosity of the media. Since, a single-temperature measurement of microviscosity using a standard calibration curve is an inadequate description of this parameter, the temperature dependence of viscosity is taken into account. The plot of log Φ_f vs. log η/T and the Arrhenius plot of nonradiative decay constants show a break-point

around certain temperatures (28-30°C) for high-viscosity RTILs. For less viscous RTILs, these plots are linear. Interestingly, the Arrhenius plot of viscosity activation energy for *all* RTILs is linear. This suggests that while the correlation between microviscosity and bulk viscosity is straightforward in the case of less viscous RTILs, it is dependent on temperature and/or viscosity for more viscous RTILs. This apparent temperature dependence is attributed to a significant change in the free volume at around certain temperatures, leading to an abrupt change of the free volume dependence of microviscosity and giving rise to a break-point in the aforementioned plots.

8.2. Future scope and challenges

In the present work we have probed the optical transparency of the imidazolium RTILs. The non-negligible absorption in the UV-visible region of these RTILs, which suggests that these substances are not as optically transparent media as commonly believed, is consistent with the chemical formulae of these substances and the optical properties of the constituent ions and their various associated forms. These liquids also display weak but highly interesting fluorescence covering a large part of the visible region. Nonetheless, the weak absorption and fluorescence due to imidazolium RTILs may not be a matter of concern while studying strongly fluorescent samples in these media. On the other hand, this can be a serious problem for weakly emitting species, and extreme care is required while carrying out such measurements.

Care should be taken while estimating the polarity of an RTIL from the measured fluorescence maxima of dipolar probes. Since dynamic solvation in RTILs is slow, only those probe molecules having fluorescence lifetime

appreciably larger than the solvation time can perhaps ensure that the frequency corresponding to the maximum represents the equilibrium solvation energy and qualify as polarity indicator. However, we believe that the potential of RTILs as media for photophysical studies is quite high and the number of such studies will continue to grow in the coming years.

The polarity of RTILs reported by solvatochromic probe molecules is as high as acetoinitrile, whereas the dielectric constant values are as low as pyridine. It is not clear from these conflicting findings how a PET reaction would proceed in these media. While our study have thrown some light into this topic, further studies are necessary to obtain a clear understanding of the role of the microscopic polarity and overall polarity of these media in deciding the course of a PET reaction. Also, many aspects of the PET reactions have remained unexplored and detailed study of the mechanistic details of such processes for different donor-acceptor pairs in a variety of RTILs will be an interesting project to pursue. In this context, the study of PET processes in the mixed solvent systems containing RTILs and a series of conventional solvents of varying polarity may also be useful.

The dynamical Stokes shift of the fluorescence spectra of dipolar molecules in the ps-ns time-scale is a reflection of slow solvation in these media. The solvation dynamics in RTILs is characterized by a long average solvation time, a significant portion of missing (ultrafast) component and its probe-dependent behavior. While these features of the dynamics are known with certainty, the mechanism of the solvation process is far from clear. As far as the ultrafast component of the dynamics is concerned, its physical origin or exact time-scale is still under

considerable speculation, even though it is clear that local effect, arising from the various interactions of the ions with the probe molecule in the first solvation shell and small amplitude motion of these ions, play an important role in the ultrafast dynamics. The dynamical study in the protic ionic liquid has revealed that the hydrogen bonding interaction between ion(s) and probe molecule can retard the ultrafast dynamics. Again, while the average solvation time roughly correlates to viscosity of the media, the significance of the individual components of the biphasic dynamics is under cloud. Although recent molecular dynamics simulation studies have shed light on the time-scales of motions of the constituent ions in the vicinity of the probe molecules, the physical motions that contribute to the different components of the dynamics are not yet identified. Therefore, further investigations focusing on these aspects are necessary to have a clear understanding of the mechanism of dynamic solvation in RTILs.

Solvation dynamics in the mixture of an RTIL with nonpolar solvents have revealed many interesting features like blue-shift of the time-zero spectra or the polarity shift in the course of dynamics. This study has been performed with only two nonpolar solvents and one probe molecule. In order to have a complete picture it is necessary that the scope of this investigation is broadened by taking up several other conventional solvents and RTILs. This will perhaps improve our understanding of the interpretation of biphasic dynamics in terms of the weighted time-components.

We have studied the microviscosity in a series of RTILs using a single probe. Many interesting aspects that have come out in our study can be verified or improved upon by further studies of this nature. In fact, since microviscosity of

the microheterogeneous systems or organized assemblies is found to be dependent on reporter molecules, different microviscosity probes are required to fully understand the nature of free volume criterion and microviscosity of RTILs.